VOLUME 46, NUMBER 3, SEPTEMBER 2023

HADRONIC JOURNAL Volume 46, Number 3, September 2023

HADRONIC JOURNAL

Founded in 1978 by Prof. R. M. Santilli at Harvard University. Some of the past Editors include Professors S. L. Adler, A. 0. Barut, L. C. Biedenharn, N. N. Bogoliubov, M. Froissart, J.Lohmus, S. Okubo, Nobel Laureate Ilya Prigogine, M. L. Tomber, J. P.Vigier, J. Wess, Nobel Laureate Chen Ning Yang.

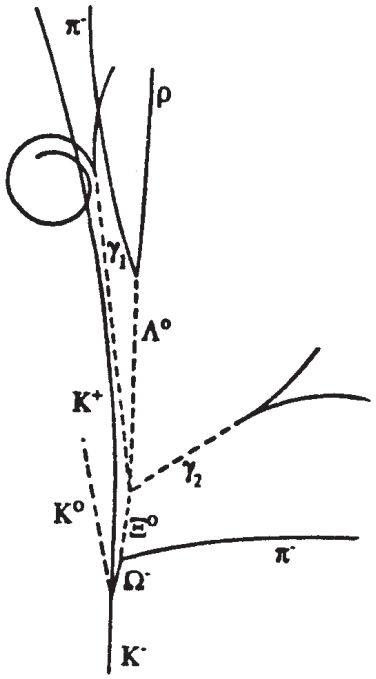

HADRONIC PRESS, INC.

HADRONIC JOURNAL

Established in 1978 by Prof. R. M. Santilli at Harvard University Hadronic Journal and Algebras, Groups and Geometries have been regularly published since 1978 without publication charges and are among the few remaining independent refereed journals.

This Journal publishes advances research papers and Ph. D. theses in any field of mathematics without publication charges.

For subscription, format and any other information please visit the website
http://www.hadronicpress.com

HADRONIC PRESS INC.
35246 U. S. 19 North Suite 215
Palm Harbor, FL 34684, U.S.A.
http://www.hadronicpress.com
Email: info@hadronicpress.com
Phone: +1-727-946-0427

HADRONIC JOURNAL

Founder and Editor in Chief
RUGGERO MARIA SANTILLI
The Institute for Basic Research
35246 U. S. 19 North Suite 215, Palm Harbor, FL 34684, U.S.A.
Email: resarch@i-b-r.org; TEL: +1-727-688-3992

ISSN: 0162-5519

Established in 1978 by Prof. R. M. Santilli at Harvard University Hadronic Journal and Algebras, Groups and Geometries have been regularly published since 1978 without publication charges and are among the few remaining independent refereed journals.

This Journal publishes advances research papers and Ph. D. theses in any field of mathematics without publication charges.

For subscription, format and any other information please visit the website http://www.hadronicpress.com

HADRONIC PRESS INC.
35246 U. S. 19 North Suite 215
Palm Harbor, FL 34684, U.S.A.
http://www.hadronicpress.com
Email: info@hadronicpress.com
Phone: +1-727-946-0427

HADRONIC JOURNAL Volume 46, Number 3, September 2023

HADRONIC PRESS, INC.

HADRONIC JOURNAL

VOLUME 46, NUMBER 3, SEPTEMBER 2023

HADRONIC JOURNAL 46, 231 - 248 (2023)
DOI 10.29083/HJ.46.03.2023/SC231

HADRONIC-TIME RELATIVITY: 28X28 METRIC TENSOR FORM OF CALENDAR (DAY/MONTH/YEAR) REPRESENTATION OF EVERYTHING

Alexander O.E. Animalu
Department Physics & Astronomy
University of Nigeria
Nsukka, Enugu State, Nigeria
nascience@aol.com

Received February 27, 2023
Revised June 3, 2023

Abstract

Recent mathematical, theoretical and experimental studies have confirmed the exact validity of quantum mechanics for point-like particles in vacuum under linear, local and potential interactions, as occurring for electromagnetic interactions. The same studies have established a progressive generalization of Heisenberg's uncertainties according to the 1935 Einstein-Podolsky-Rosen (EPR) argument, with a corresponding recovering of Einstein's determinism for extended particles in deep mutual entanglement with ensuing non-linear, non-local and non-potential interactions, as occurring for extended hadrons under strong interactions. In a recent paper we indicated, one of novel advances in condensed matter physics and chemistry that are expected from the "completion" of quantum into hadronic mechanics according to the EPR argument. In particular, we presented an apparently new form of superconductivity, submitted for the first time under the name of "Hadronic Conductivity" consisting in the propagation of electron pairs (rather than individual electrons) in singlet coupling with "attractive" EPR entanglement. and ensuring the Meissner effect (null magnetic field with consequential reduction of the resistance). In this follow-up paper , we present , under the name "Hadronic-Time Relativity" : 28x28 metric tensor Form of Calendar (Day/Month/Year) Representation of Everything. An example is provided by a (cube-hexagon) quasi-crystal system of a vibrating helix of (curl and loop) geometry of a membrane(~M-branes) of the cubic box, like Schrodinger "cat" of gravity(g~7)mass(~52)=59="branes(59)",and the implications for such a system is discussed..

KEY WORDS: EPR arguments with respect to "determinism" in quantum mechanics, condensed matter physics and chemistry and the "completion" in "hadronic" mechanics; unified geometry of matter, anti-matter and light, string theory of everything. SO(2N) algebraic projective geometry and tensors.

OUTLINE

1. INTRODUCTION AND REVIEW
2. METHODOLOGY OF ANALOGUE/DIGITAL CONSTRUCTION OF CALENDAR (DAY/MONTH/YEAR) HADRONIC-TIME RELATIVITY METRIC TENSOR
3. AB/CD/TXYZ ~DAY/MONTH/YEAR ON EARTH AS WARPED R3xSO(3) TIME-SPACE
4. DISCUSSION & CONCLUSION
5. REFERENCES

1. INTRODUCTION AND REVIEW

Despite Advances with Unitary Scattering Theory of Point-Particles in Conventional Quantum Mechanics, a number of fundamental Problems have long been identified & partially tackled:

- Replacement of Infinities in quantum scattering formalism *ab initio* by convergence (Dirac 1981 [1]) & tackling imaginary potentials in Dissipative Nuclear Models by non-unitary theory.
- Need to replace Linear Character of quantum mechanics by Nonlinear character of nature (W. Heisenberg cited by R.M. Santilli 1978 [2])
- Einstein, Podolsky and Rosen (EPR) 1935[3] expression of doubts about "lack of completion of quantum mechanics" which underscores the motivation for this paper.
- Suggestions by R.M. Santilli 1978 [2] for construction of Nonunitary Covering of Quantum Mechanics under the name Hadronic Mechanics (HM)
- Non-unitary Lie-isotopic & Lie-admissible scattering theory of HM (Santilli & Animalu 2011[4])
- A.O.E. Animalu 2019 [5] -Lie-Admissible Approach to "Extended Relativity": Non-Linear Velocity, Mass and Charge Transformations in *African Journal of Phys. Vol.12, p.2-27 (2019) [reformatted from Hadronic J. Vol.10, 321-330(1987]*
- Due to the dimension and diversification of the existing literature in the EPR argument , prior this paper, interested colleagues should view Nine minutes video on EPR verifications,
  http://www.world-lecture-series.org/legacy-of-einstein-for-new-clean-energies
  Tutoring Lecture I: Isomathematics **http://www.world-lecture-series.org/santilli-tutoring-i**
  Tutoring Lecture II: Verifications of the EPR argument
  http://www.world-lecture-series.org/santilli-tutoring-ii
  Primary references on recent verifications of the EPR argument
  http://www.santilli-foundation.org/docs/references-epr-verifications.pdf
- A.O.E. Animalu 2022 [6] Hadronic Conductivity: A New Form of Superconductivity, Hadronic J. Vol.45,333-355(2022)

- Albert Einstein (1999) [7] celebration as *"PERSON OF THE CENTURY" (in Time Magazine , Dec 31,1999) & in trending (www.thejourney.com) Einstein's equation (Energy = Love x square of speed of light)*

In a previous paper [6] we have, on the strength of the EPR Argument, developed in the framework of hadronic mechanics, both a theoretical physics (e-magnetodyamics framework of current loops) and linguistic (analogue/digital) SO(10) realizations of a principle of trichotomy between the three objects (points, lines, planes) of projective geometry of space-time and the three elements (particles, fields, currents) of gauge principles of classical and quantum mechanics. The most important aspect was the implication of trichotomy of "time-relativity" in real R3xSO(3), therein called T-symmetry, namely that it is discretely positive but non-linear and irreversible *vis-à-vis "Energy=Love x Square of Speed of Light(c)"* unified theory of energy generation in everything in Einstein's Secret 1938 Letter to his daughter(Lieseri) released in 1980 and reported by Brandon Bays www.thejourney.com [7] as "God is Love" ; "Love is the quintessence of universal energy generation ..."; etc. The significance of T-symmetry was correlated in [6] with the trichotomy of world war dates (DAY/MONTH/YEAR) in analogue/digital SO(10) linguistics which we shall elaborate as a methodology for a vibrating helix of (curl and loop) geometry of a membrane(~M-branes) of a cubic box in Sec.2 of this paper consistent with Einstein's secret letter by going beyond 4-dimensional space-time and the M-theory [8] of an 11-dimensional world filled with weird objects called "branes" inasmuch as *"M stands for many things including matrix, mystery and magic"* and in this paper "branes(59)" is cognate to "e-love(59)" and to "g-mass(59)" in SO(10) linguistic geometry.

To further underscore the question that led to the above scenario of 28x28 metric tensor in this era of search for the string theory of supergravity, called the M-theory, as well as unified field theory of gravity and its further development into the superstring theory of everything[9], let me recall an interaction in 1968 with P.A.M. Dirac 1970[10] while he was searching for a Maxwell-like (dual) gauge principle to relate electric charge and magnetic charge in projective geometric terms.

Following treatment of the Lorentz force and the linear Dirac (negative) energy relativistic wave equation for electric charge on the same footing as a corresponding dual of Lorentz force and a positive energy relativistic wave equation for magnetic charge and non-negative mass (represented by a current loop), Dirac's way of thinking led (as summarized below) to a correspondence principle:

Particle ⟷ Point, Field ⟷ Line, Current ⟷ Plane,

Such a correspondence principle implies geometric characterization of conventional electrodynamics and an analogous so-called e-magnetodynamics of current loop and to the Feynman space-time diagrammatic approach based on 10x10 representations of the dynamical group unifying strong interaction with electromagnetism and space-time geometry and violations of the discrete symmetries – parity(P), charge(C) conjugation, time-reversal(T) and spin-parity to point-plane dual interchange,

$$SU^{>}(3)\times SU^{<}(3)\times U^{>}(1)U^{<}(1)\times O^{>}(4,2)\times O^{<}(4,2)$$

This defined our SO(2N)xSO(2N) group-theoretic approach to scattering of N-particle (N=5) systems presented[11] in http://doi.org/10.52202/059404-0001 which we have elaborated and distinguished from the "trichotomy" of Minkowski space of "extended relativity" R3xSO(3) and

U(2)xSU(2) of elementary particles in Dirac's 1971 [1] SO(2N) second quantization scheme for condensed matter physics and chemistry with SO(10) linguistic geometry of two liquid water[12] molecules ($2H_2O$) as reactant "hydroxil ion" in oxonium(H_3O^+)+ hydroxide(OH^-) states.

To gain familiarity with the SO(10) group theoretic structure of metric tensor we summarise (in table 1 below) the conventional magic square representation of the metric tensor in O(4,2)xSU(3)xU(1) ~ SO(10) Lattice gauge theory.

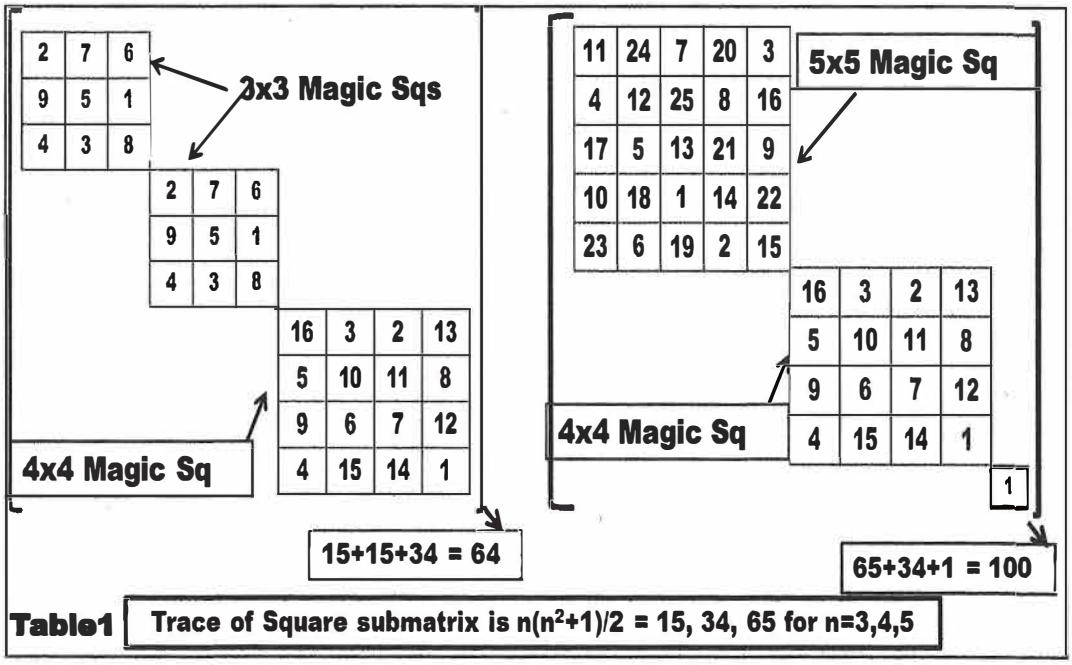

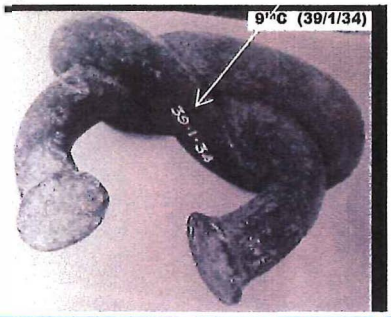

Fig.1(a): Manilla-shaped ("M-Branes") with 9th C date (39/1/34)

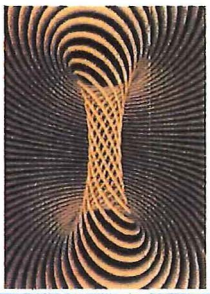

Fig. (1b) N-Helix

Accordingly, in this paper, we shall construct a 28x28 metric tensor that characterizes a Manilla-shaped artifact with 9th C date 39/1/34 (in Fig1a) which is here called "M-Branes(72)"cognate to "Hadronic(72)" ~ "N-Helix(72)" ~ "Lover(72)" in SO(10) linguistics of Calendar (Day/Month/Year) ~ (AB/CD/TXYZ) geometry and requires a generalization of the space-time metric tensor correspondence with Maxwell's 4x4 tensors

$$\left\| R^{k}_{\mu\nu} \right\| \equiv \begin{pmatrix} 0 & t_1 & t_2 & t_3 \\ -t_1 & 0 & z & -y \\ -t_2 & -z & 0 & x \\ -t_3 & y & -x & 0 \end{pmatrix} \longleftrightarrow \begin{pmatrix} 0 & E_x & E_y & E_z \\ -E_x & 0 & B_z & -B_2 \\ -E_y & -B_z & 0 & B_x \\ -E_z & B_y & -B_x & 0 \end{pmatrix} = \left\| F^{k}_{\mu\nu} \right\|$$

of electromagnetism and e-magnetodynamics

Conventional Electrodynamics

$$\left\|\mathbf{F}_{\mu\nu}\right\| \equiv \begin{pmatrix} \mathbf{0} & \mathbf{E}_1 & \mathbf{E}_2 & \mathbf{E}_3 \\ -\mathbf{E}_1 & \mathbf{0} & \mathbf{B}_3 & -\mathbf{B}_2 \\ -\mathbf{E}_2 & -\mathbf{B}_3 & \mathbf{0} & \mathbf{B}_1 \\ -\mathbf{E}_3 & \mathbf{B}_2 & -\mathbf{B}_1 & \mathbf{0} \end{pmatrix}$$

Maxwell's eqn & Lorentz force

$$\partial^{\nu} F_{\mu\nu} = J^{e}_{\mu}; \mathbf{f}^{e} = e\mathbf{E} + \mathbf{J}^{e} \times \mathbf{B}.$$

$$\mathbf{E} \to \mathbf{B},\ \mathbf{B} \to \text{-}\mathbf{E}.\ \mathbf{J}^{e} \to \mathbf{J}^{m}$$

E-magnetodynamics of Current Loop

$$\left\|G_{\mu\nu}\right\| \equiv \begin{pmatrix} \mathbf{0} & \mathbf{J}_1 & \mathbf{J}_2 & \mathbf{J}_3 \\ -\mathbf{J}_1 & \mathbf{0} & \mathbf{B}_3 & -\mathbf{B}_2 \\ -\mathbf{J}_2 & -\mathbf{B}_3 & \mathbf{0} & \mathbf{B}_1 \\ -\mathbf{J}_3 & \mathbf{B}_2 & -\mathbf{B}_1 & \mathbf{0} \end{pmatrix}$$

$$(\mathbf{J}^{m} \to \mathbf{B},\ \mathbf{B} \to -\mathbf{J}^{m})$$

$$\mathbf{J}^{m} = -(2e\hbar/mc)\mathbf{A},\quad \mathbf{B} = \text{curl}\mathbf{A} \equiv \text{curl}(\zeta \mathbf{J}^{m}),$$

$$\zeta = (mc/2|e|\hbar)$$

$$\text{Det}\left\|F_{\mu\nu} - \lambda\eta_{\mu\nu}\right\| \equiv \lambda^4 - (R_{\mu\nu\rho\sigma}F^{\mu\rho}F^{\nu\sigma})\lambda^2 + (\in_{\mu\nu\rho\sigma}F^{\mu\rho}F^{\nu\sigma})^2 = 0,$$

$$\text{Det}\left\|G_{\mu\nu} - \lambda\eta_{\mu\nu}\right\| \equiv \lambda^4 - (R_{\mu\nu\rho\sigma}G^{\mu\rho}G^{\nu\sigma})\lambda^2 + (\in_{\mu\nu\rho\sigma}G^{\mu\rho}G^{\nu\sigma})^2 = 0,$$

$$\left\|\eta_{\mu\nu}\right\| \equiv diag(+1,-1,-1,-1), R_{\mu\nu\rho\sigma} \equiv (\eta_{\mu\nu}\eta_{\rho\sigma} - \eta_{\mu\rho}\eta_{\sigma\nu}),$$

$$R_{\mu\nu\rho\sigma}F^{\mu\rho}F^{\nu\sigma} - 2 \in_{\mu\nu\rho\sigma} F^{\mu\rho}F^{\nu\sigma} = \begin{cases} \mathbf{E}^2 \\ \mathbf{B}^2 \end{cases} \Rightarrow \begin{cases} \mathbf{E}^2 - \mathbf{B}^2 \pm 2\mathbf{B}.\mathbf{E} = 0 \\ \mathbf{B}^2 - \mathbf{E}^2 \pm 2\mathbf{E}.\mathbf{B} = 0 \end{cases}$$

$$R_{\mu\nu\rho\sigma}G^{\mu\rho}G^{\nu\sigma} - 2 \in_{\mu\nu\rho\sigma} G^{\mu\rho}G^{\nu\sigma} = \begin{cases} \mathbf{J}^{m2} \\ B^2 \end{cases} \Rightarrow \begin{cases} \mathbf{J}^{m2} - \mathbf{B}^2 \pm 2\mathbf{B}.\mathbf{J}^{m} = 0 \\ \mathbf{B}^2 - \mathbf{J}^{m2} \pm 2\mathbf{J}^{m}.\mathbf{B} = 0 \end{cases}$$

Note that the **current loop** J^m, involves **e/m**, and this insures the **Meissner effect** ($J^m.B \neq 0$)

This will led to the following digital/analog relations in SO(10) Linguistic geometry:
N-helix(72) Loops(77) ~ M-branes(72)Loops(77) ~ Hadronic(72)power(77) ~Environment(149) as realized in Figs.2, 3 & 4 below;

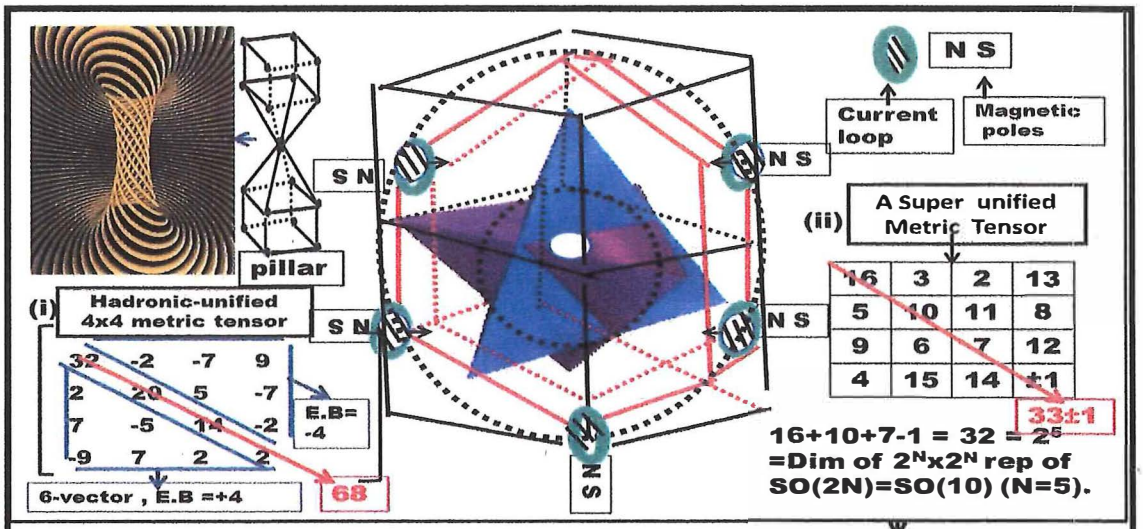

Fig.2(i) Realization of hadronic-unified 4x4 metric tensor as given by electric (E=2,-7,9) & magnetic (B=2,-7,5) 6-vector components, such that E.B=±4 animated as "pillar of water" ; (ii)A Super array of magnetic poles & pivoted slab of soft iron in e-magnetodynamics machine (Animalu *et al* 2013) [12] animated as array of magnetic poles with pivoted slab replaced by Kepler's 6-star vortex ; (iii) Generalization of Durer's 4x4 magic square by the replacement of ±1 by 26 ±1, so that trace(16+10+7 +26±1) =59 ±1 is 60 ~Word(60) or 58~Helix(58), and the Word(60)Power(77) = 137 can be associate with helical current loop on a membrane of the pillar of water with a magnetic charge, hc/e^2 = 137 =Lover(72)Music(65). Similarly hadronic(72)power(77)=149 and super(79)power(77)=156 .

Generalized Durer's 4x4 Magic Square

16	3	2	13	34
5	10	11	8	34
9	6	7	12	34
4	15	14	26±1	59±1
34	34	34	59±1	59±1

34+34+34+59±1+59±1=220±2;
Elaboration of 4x4 Magic Square

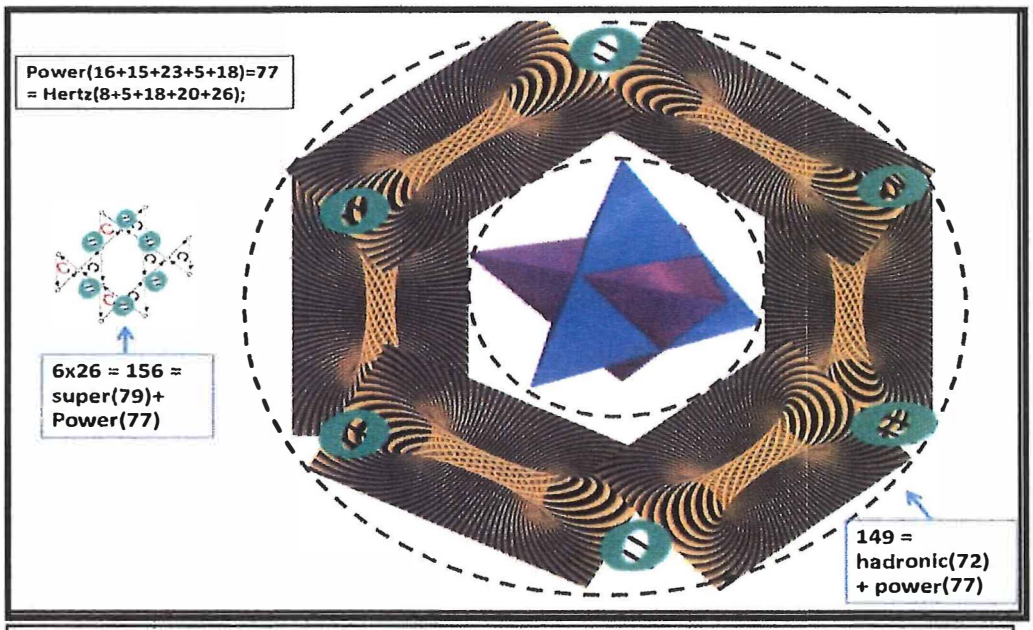

Fig. 3: Realization of Hadronic and Super-Power Geometry of e-magnetodynamics

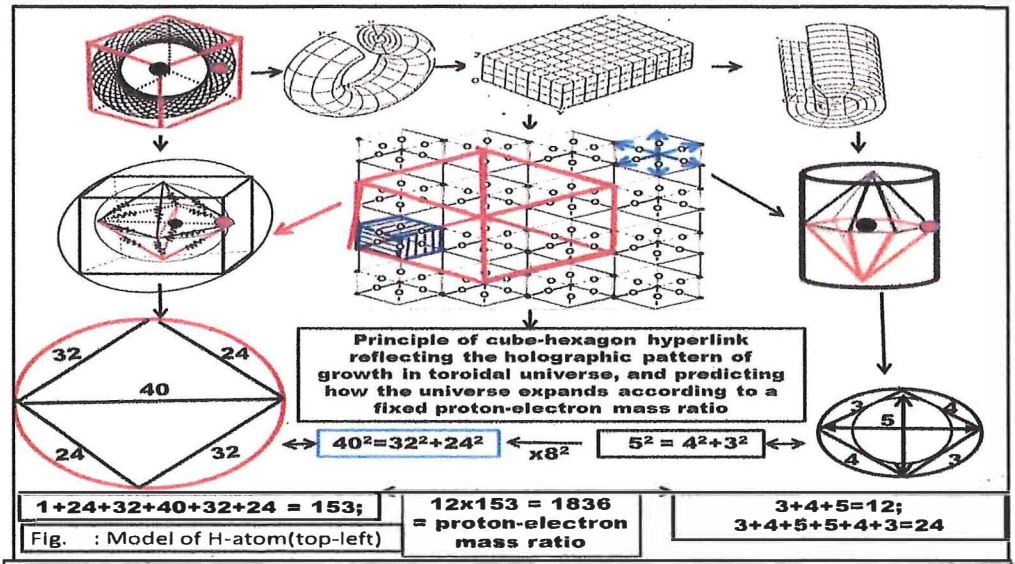

Fig. 4: **The introduction of mass ratio in geometry is reflected by ref.[13]: A.O.E.Animalu, Samuel Edeagu, Godfrey Akpojotor & Erik Trell, Electromagnetism of Atomic Structural Constitution in Deformable Real R3xSO(3) Configuration Space. Afr. J. Phys. 11. 2 (2018).**

2. METHODOLOGY OF ANALOGUE/DIGITAL CONSTRUCTION OF CALENDAR (DAY/MONTH/YR) TIME RELATIVITY METRIC TENSOR

If AB/CD/TXYZ ~ Day/Month/Year on spherical Earth Surface, then as shown in Fig.5,

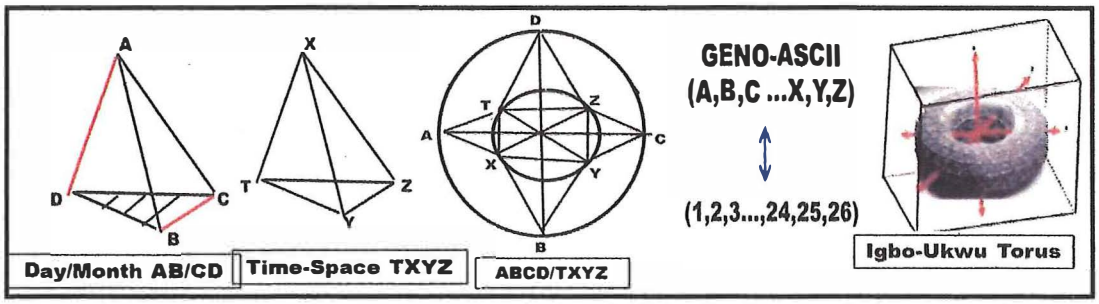

then ABC, ACD, ABD are projective "plane coordinates" & BCD is the "timeless" plane on Earth with "cyclic" radius(T) such that,

$$T^2 = c^2 (t_1^2 + t_2^2 + t_3^2)$$

form a 6-vector (T,R), and (T,R) ~ (E,B) of electromagnetism. Such a 6-vector space-time, referred to as R3xSO(3) symmetry, has a "Warped (Cube-Hexagon) Time-Space geometry" , represented by 3-dimensional grid map (Fig.6).

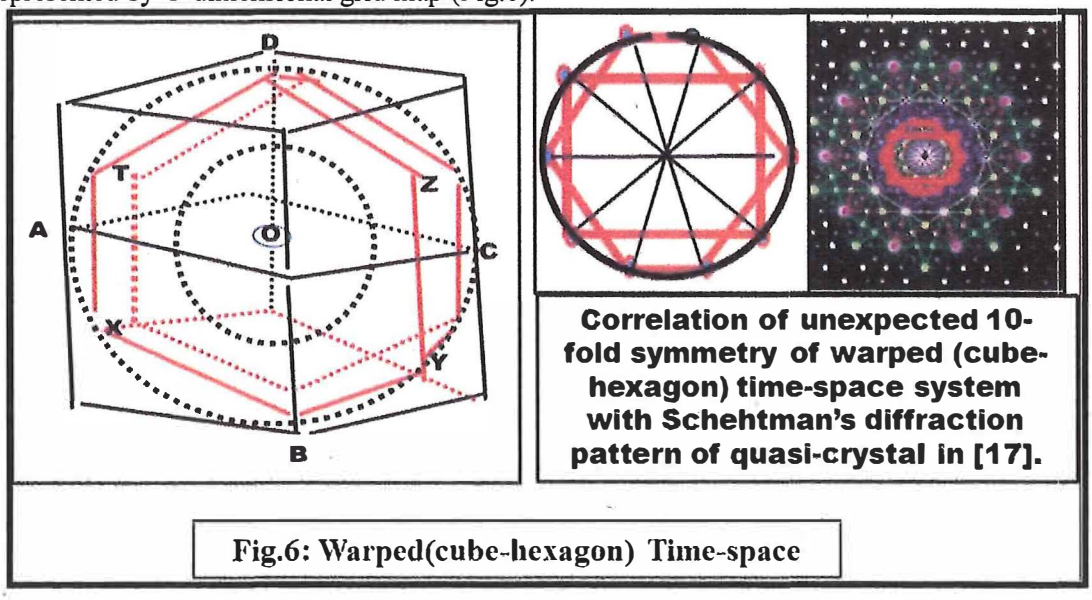

Fig.6: Warped(cube-hexagon) Time-space

The warping geometry of the quasi-crystal diffraction pattern is like the Igbo-Ukwu bronze torus and Manilla-shaped artifact of 9thC date (39/1/34) and step-pyramid fly-shaped pattern correlated in the realization of step-pyramid definition of R3xSO(3) Linguistics as presented next.in Fig.7

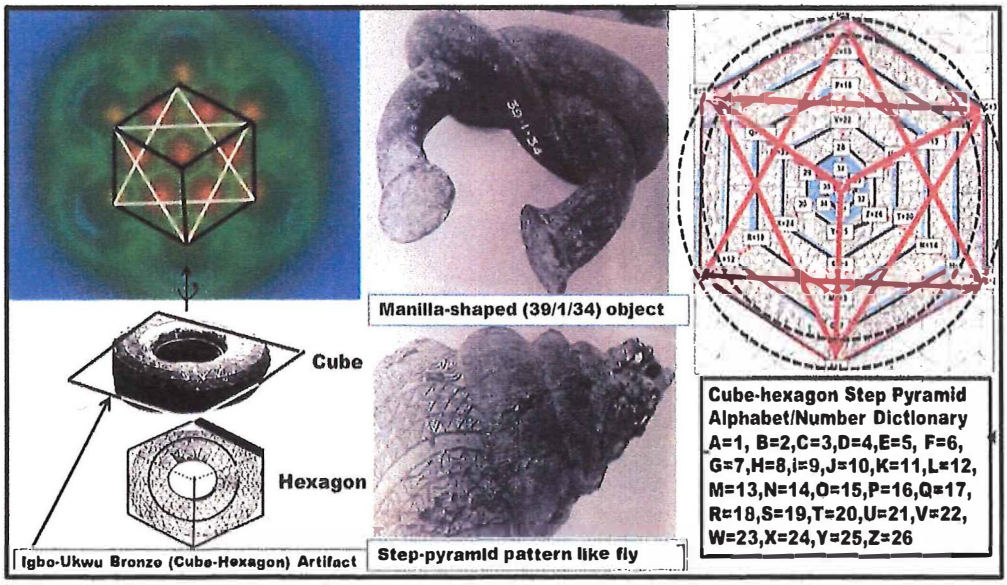

Fig.7: The quasi-crystal diffraction pattern (top left) transcends the bronze Torus (cube-hexagon)artifact (bottom left) alongside the 9thC Manilla-shaped object dated (39/1/34) and step-pyramid fly pattern which are Igbo-Ukwu artifacts in Elizabeth Isichei[14] *A History of the Igbo People*(1976). These lead to the Cube-hexagon pyramid Alphabet/Number dictionary of GENO-ASCII Code given by A.O.E. Animalu & A.V.Animalu[15] in Afr. J. Physics Vol. 5, 122-140(2012).

The interest of the 9thC Calendar Date (39-1-34) on the Manila-shaped object lies in providing a motivation for the digital aspect of the step-pyramid-alphabet number dictionary of the GENO-ASCII Code,(A=a=1, B=b=2, … , Z=z=26) and 1+2+3+…+36=666 for closure in SO(10) linguistic geometry in which "Word ~ W+o+r+d=23+15+18+4=60 can be written as "Word(60)" and "A membrane" = "M-branes(72)". Consequently, just as Einstein's cosmic religious aphorism contained in his secret letter on "*Energy=Love x square of the speed of light(c)*" linked war date Calendar (Day/Month/Year) to Life(32)Language(68)=100 as well as War(42)date(30)chaos(46) =118 (as in the table below), the 9thC date (39/1/34) on the Manilla-shaped membrane that folds and curls links the corresponding numbers 39+1+34=74 and 39+1+3+4=47 to Energy(74)Time(47) =121 =11x11 metric tensor of 11-dimensioonal world filled with weird objects, called branes(59) = e(5)-love(54) which one can associate with current loop on a membrane with a magnetic charge, g = hc/e^2 = 137 = lover(72)music(65).

Date of 1st World War
28 / 7 / 1914
28 + 7 + 19 + 14 = 68
2+8+7+1+9+1+4= 32
28 + 7 + 1 + 9+ 1 + 4 = 50;
68+32=100
68+50=118

The Second World War date
1 / 9 / 1939
1 + 9 + 19 + 39= 68
1 + 9 + 1+ 9 + 3 + 9= 32 ; 68+32=100

Date of Ukraine war
24 / 2 / 2022
24 + 2 + 20 + 22= 68
24 + 2 + 2 + 0 + 2 + 2= 32 ; 68+32=100
2 + 4 + 2 + 20 + 22=50; 68+50=118

Date on 9th C Igbo-Ukwu Manilla-shaped object 39/1/34:

39+1+34=74, 39+1+3+4=47, 3+9+1+1+3+4=21, 21+47=68, 74+47=121.

Further correlation of metric tensor with Calendar dates and linguistic geometry is given here for the date 1/11/2022 and the generalized Durer's 4x4 matrix introduced earlier in Fig.2(iii) for characterizing the relations, 888=666+22 corresponding to an update of Einstein's aphorism.

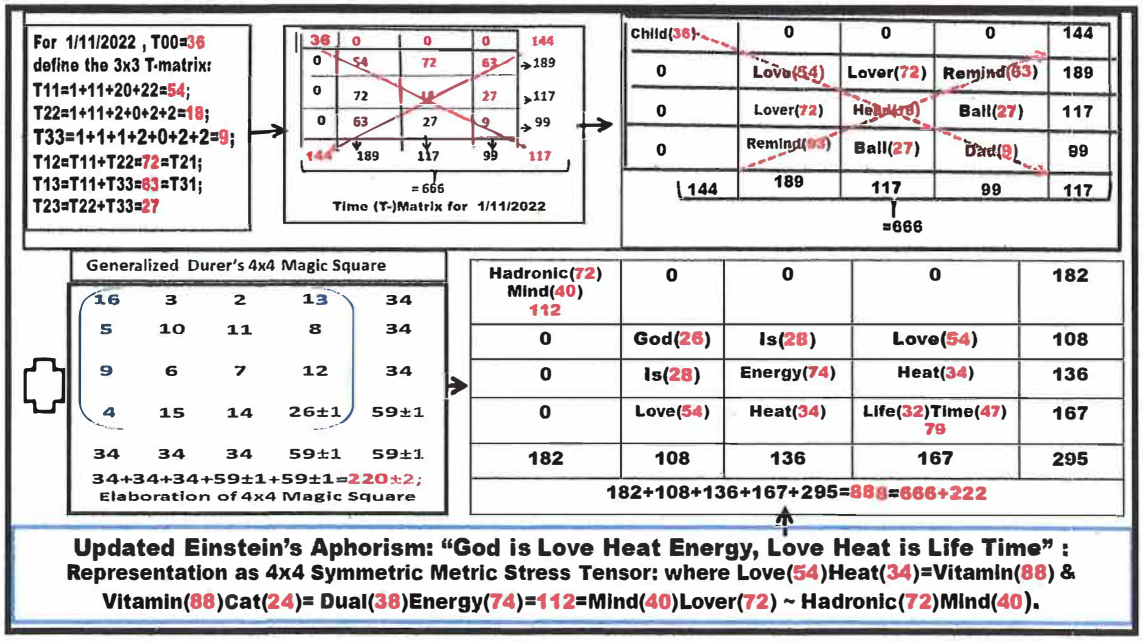

The impressive result of this "magic square" correlation is that it gives the Judeo-Christian "sacred" number (666) for predicted catastrophic change of human consciousness called "Rapture(99)" and 882=216+666 correlates it with 216=6x6x6 = 20+56+70+70* related to the fundamental representation of the SU(6) symmetry of constituent quarks of the proton(three-quark) building blocks of matter in the universe while 10x216=2160 is the cycle (in years) of the cross-road predicted by ancient cultures for the same catastrophe. 888=666+216+6=666+222 Moreover, 882+666=666+216+666=1548 is the date of publication of the book *Revolutions*, written by Nicholas Copernicus that gave birth to *Renaissance* in 16th C Europe. By combining such correlation with Biblical(Exod.3v14) record of human consciousness of daily rest energy(74), and weakly,7x74=518, we have achieved an elaboration of step-by-step construction of 28x28 matrix from seven 4x4 symmetric metric tensors for "hadronic" time relativity as follows:

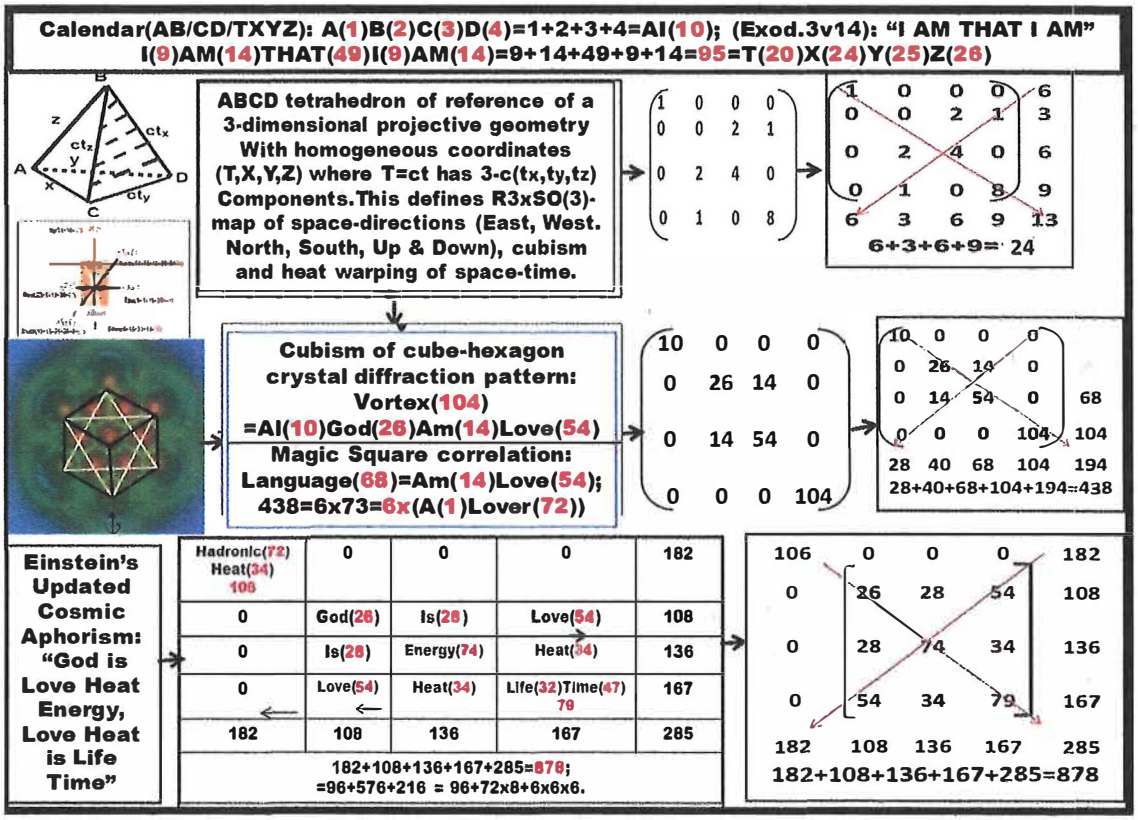

Updated Einstein's Aphorism: "God is Love Heat Energy, Love Heat is Life Time"
Representation as 4x4 Symmetric Metric Stress Tensor :
where "Life(32)Energy(74)=106~Heat(34)Lover(72) ~ Hadronic(72)Heat(34);
& Corresponding Warping of time-space.

Hadronic(72) Heat(34) 106	0	0	0	182
0	God(26)	Is(28)	Love(54)	108
0	Is(28)	Energy(74)	Heat(34)	136
0	Love(54)	Heat(34)	Life(32)Time(47) 79	167
182	108	136	167	285

182+108+136+167+285=878
=96+576+216 = 96+72x8+6x6x6.

106	0	0	0	182
0	26	28	54	108
0	28	74	34	136
0	54	34	79	167
182	108	136	167	285

182+108+136+167+285=878

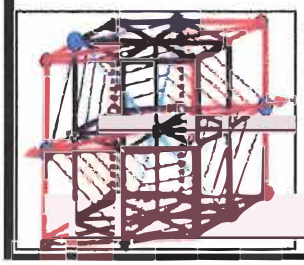

Warping Projection of 3D hadronic cube-hexagon lattice onto 2D plane.

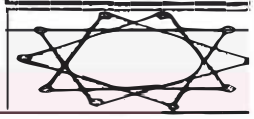

18	0	0	0	222
0	66	78	96	240
0	78	30	42	150
0	96	42	12	150
222	240	150	150	126

222+240+150+150+126=888

For 21/2/2023 ; T00=18
Define 3x3 T-matrix
T11 =21+2+20+23=66
T22 =21+2+2+0+2+3=30
T33 =2+1+2+2+0+3+3=12
T12 = T11 + T22=78
T13 = T11 + T33=96=T31
T23 = T22 + T33=42=T32

Proceeding in this way, we have constructed the 28x28 symmetric metric tensor consisting of positive numbers from a selection of seven 4x4 matrices arranged in **the same manner as the "magic square" representation of the metric tensor in O(4,2)xSU(3)xU(1) ~ SO(10) Lattice gauge theory presented earlier. The primary interest is to** correlate various dated (archival) materials with geometry so as to endow the methodology with predictive capacity in the ranges from 0 to 170 (Ancient Egypt) and 170 to 2075 (Judeo-Christian till 2012 New Age cross-over to the "Hadronic(72) ~ COVID-19 era and beyond). Quantum mechanics will demand characterization of End-Time(70)Stress(100) on Schrodinger "Cat" consciousness from the **trace** of the 28x28 metric tensor arranged and elaborated below as seven 4x4 matrices so that the 4th in the sequence characterizes the (888=666+222) warping of (cube-hexagon) time-space as follows:

Trace(5256) of 28x28 Matrix + 222 (cross diagonal)=5478= 78+5400 =
Nano(44)Heat(34) + Love(54)xStress(100);
& adding to this number 5256, a weekly rest, 7x Energy(74)=518 gives:
5478+518= 5996 = 96+5900 = Hadronic(72)Cat(24) + Stress(100)xBranes(59)

This is the result we are after, as summarized in the two complementary tables below:

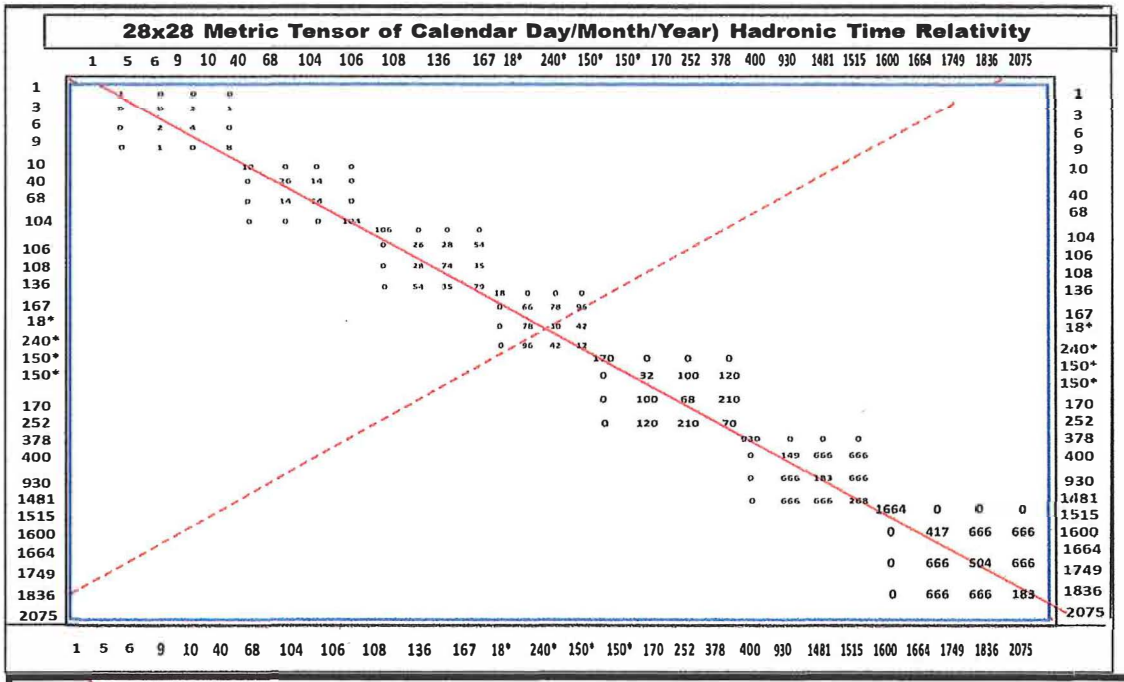
28x28 Metric Tensor of Calendar Day/Month/Year) Hadronic Time Relativity
1 5 6 9 10 40 68 104 106 108 136 167 18* 240* 150* 150* 170 252 378 400 930 1481 1515 1600 1664 1749 1836 2075

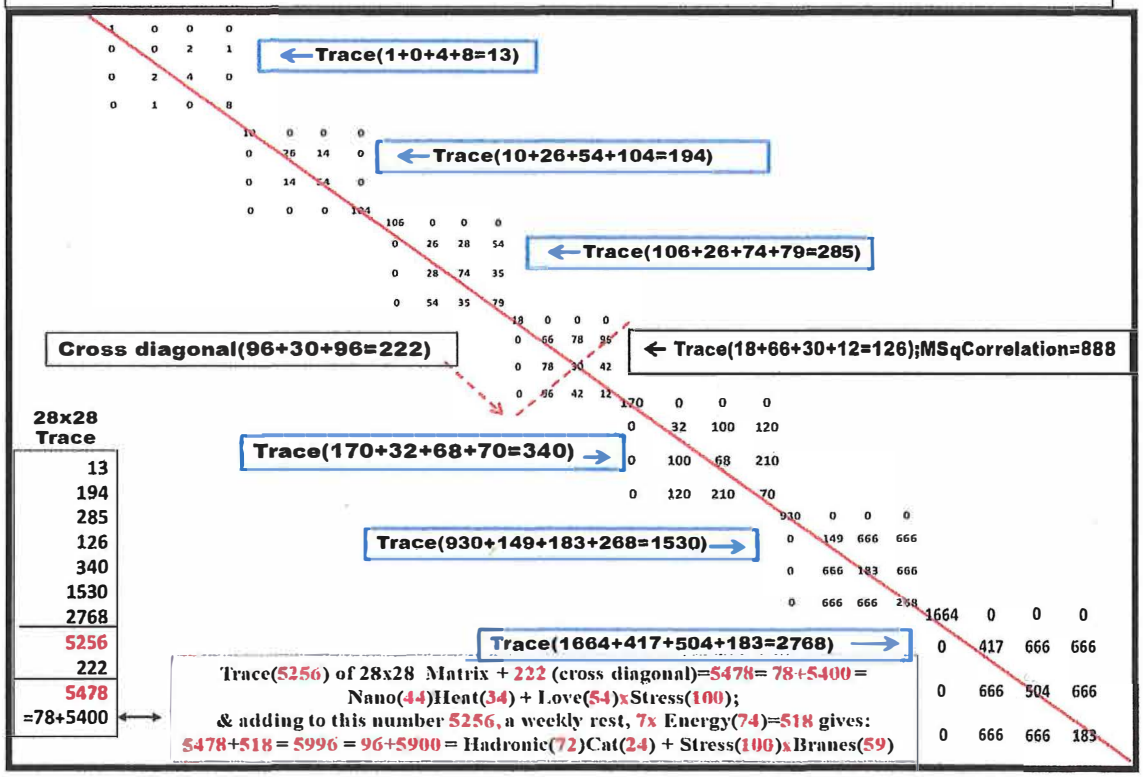
Trace(1+0+4+8=13)
Trace(10+26+54+104=194)
Trace(106+26+74+79=285)
Cross diagonal(96+30+96=222)
Trace(18+66+30+12=126);MSqCorrelation=888
Trace(170+32+68+70=340)
Trace(930+149+183+268=1530)
Trace(1664+417+504+183=2768)
28x28 Trace
13
194
285
126
340
1530
2768
5256
222
5478
=78+5400
Trace(5256) of 28x28 Matrix + 222 (cross diagonal)=5478= 78+5400 =
Nano(44)Heat(34) + Love(54)xStress(100);
& adding to this number 5256, a weekly rest, 7x Energy(74)=518 gives:
5478+518 = 5996 = 96+5900 = Hadronic(72)Cat(24) + Stress(100)xBranes(59)

The primary features of the correlation are, firstly the addition of the Nano(44)Heat(34) to Love(54)xStress(100), where

Nano(44)Heat(34)=78=e(5)lover(72)~e(5)Hadronic(72)= Anti(44)Hate(34)

by noting that "Heat(34)=34" is cognate to "Hate(34)".and Nano(44) is cognate to Anti(44). Secondly, it underscores the reliance on seven symmetric and positive definite 4x4-metrices for calendar(AB/CD/TXYZ) correlating Day/Month/Year on Earth and dual linguistic geometric elements (ab/cd/txyz) of lattice gauge theory so that pairing(p~16) is associated with the geometric element (A+a,B+b,C+c,D+d)/(T+t,X+x,Y+y,Z+z) in the transition from ASCII to GENO-ASCII Code and hence rest Energy(74)=p(16)Asleep(58).has mass(52)=p(16)field(36). Thirdly, the necessity of updating Einstein's cosmic aphorism to include the time in the "secret equation, "Energy = Love x square of the speed of light" has permitted inclusion of the weekly rest(t=0) energy(74) of 7x74=518 as the trace of seven rest frame diagonal 4x4 metric tensors. ..

The primary interest of the range 170 to 2075 is that it defines a sub-group of three 4x4 matrices forming a 12x12 metric tensor beyond the M-theory of 11-dimenions of interest to experiments at giant particle colliders in the US and Europe.

	170	252	378	400	600	1481	1515	1600	1664	1749	1836	2075
170	170	0	0	0								
252	0	32	100	120								
378	0	100	68	210								
400	0	120	210	70								
600					600	0	0	0				
1481					0	149	666	666				
1515					0	666	183	666				
1600					0	666	666	268				
1664									1664	0	0	0
1749									0	417	666	666
1836									0	666	504	666
2075									0	666	666	743
	170	252	378	400	600	1481	1515	1600	1664	1749	1836	2075

To underscore the interest of the range 170 to 2075, the correlation of the Digital Signal Processing (DSP) maps of the 12x12 metric tensor with various archival artifacts have been assembled as displayed below

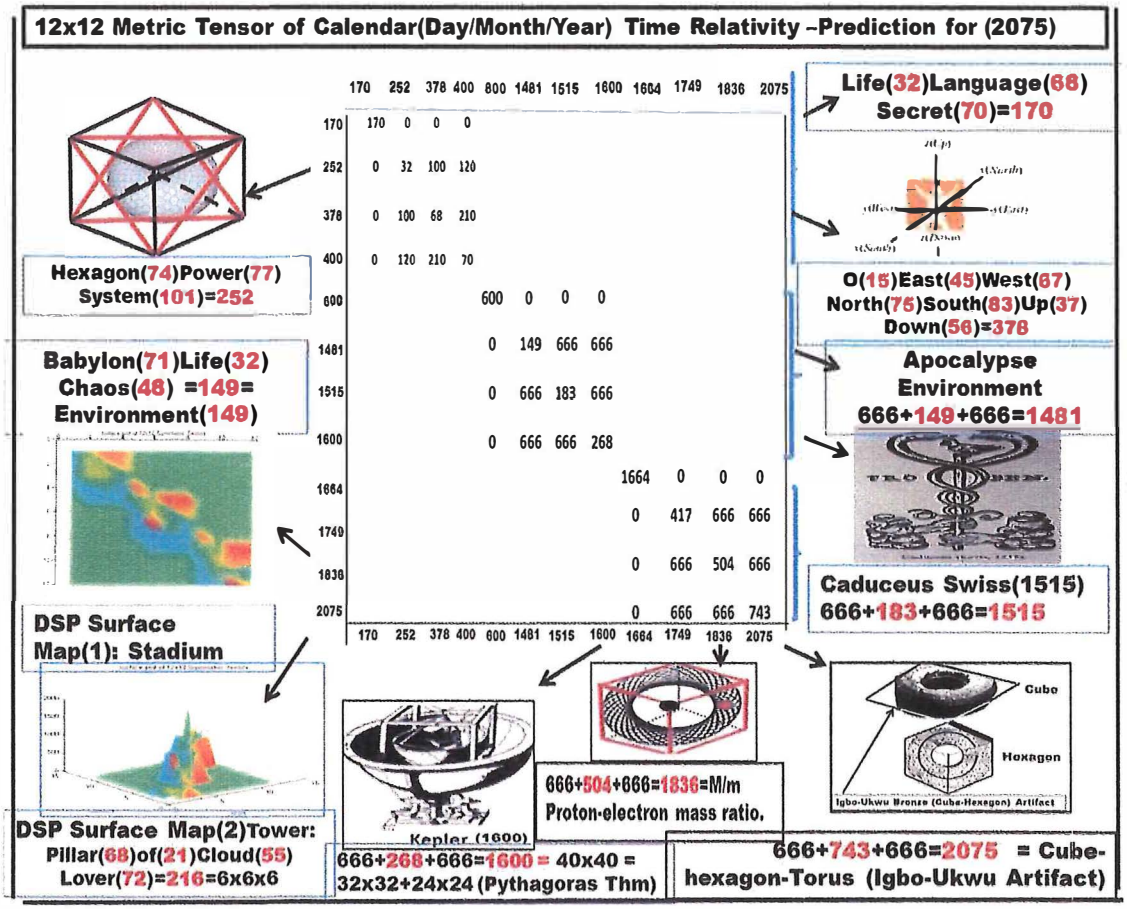

4. DISCUSSION & CONCLUSION

Having shown how the unification of electromagnetism with e-magnetodynamics was realized[6] in the hadronic unified 4x4 metric tensor, we finally proceed to discuss the challenges of how the demands for secrecy of the higher dimensional 28x28 metric tensor for everything demands the use of artificial intelligence and communication technology of the digital age paradigm shift linking

"Environment(149)=N-helix(72)Loops(77)=M-branes(72)Loops(77)=Hadronic(72)Power(77)"
to "Hadronic(72)Cat(24) + Stress(100) xBranes(59)" and to End-time(70)Stress(100)

on Hadronic Cat(24) consciousness defined by the trace of our 28x28 metric tensor. The famous Schrodinger Cat(24) experiment in which *the cat always responds according to the expectation*

of the observer has led to the conclusion that the cat is conscious and aware of the mind(40)-set(43) ~ wisdom(83) of the observer, and responds in consonance with that mindset as if it has its own "mind" that resides in the "wave(51)field(36)" ~ "the(33)love(54)" associated with the motion of its parts. It is no wonder then that, as illustrated below, a quantum of rhythm energy of breathing is associated with an extended (non-pointlike) living body

"asleep(58)in(23)cubic(38)cell(30)" = "a(1)w(23)w(23)w(23)dot(39)mind(40)"
= "environment(149)" = hadronic(72)power(77)

of a periodic lattice, as displayed below.

The quantum of rhythm energy of breathing of an extended (non-pointlike) living body asleep(58) in a cubic cell of a periodic lattice shown below relates "g-mass(59)" to "branes(59)"

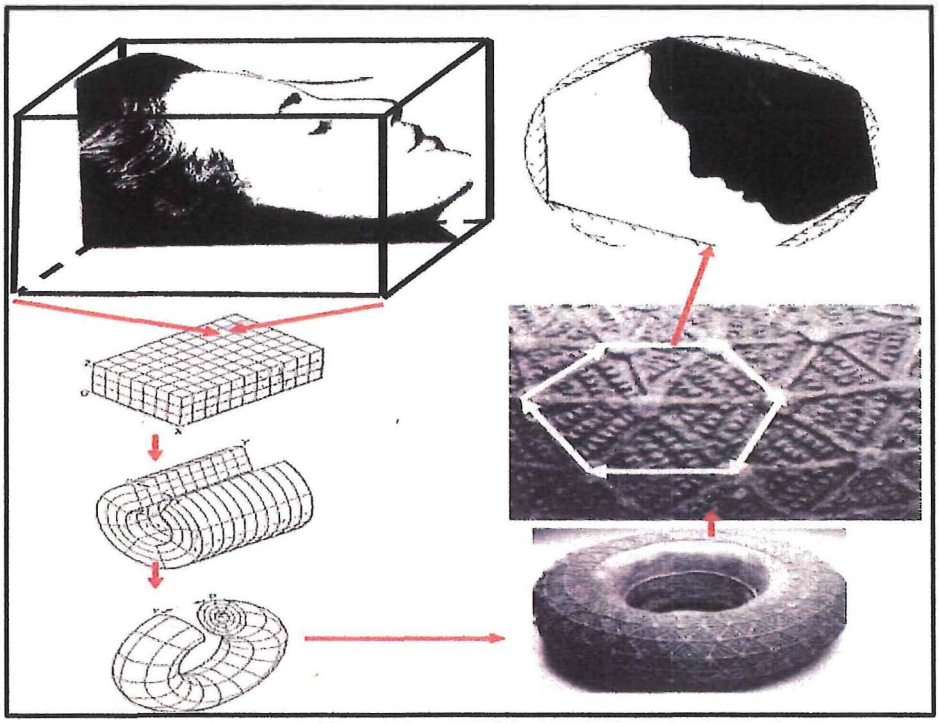

This is because in time of falling asleep in the (top left) cubic cell of a lattice that gets curved under one's weight, (i.e.by gravity), into a curved cylindrical hadronic space (bottom left), one becomes conscious or dreams (top right) of one's spiritual self gone out of a torus (bottom right) whose surface is covered by cells of a reciprocal lattice hexagrams (middle right) as crafted on ancient African (Igbo-Ukwu) bronze "enigmatic tyre"(a torus) from Catherine Acholonu[16], *They Lived Before Adam* p.447 (2009).

We conclude, therefore, that the analogue/digital correlation of SO(10) linguistics and 28x28 metric tensor of hadronic time relativity have given enlightenment in this era of global warming environment the complementarity of love and nano-heat ~ anti-hate and challenges of COVID-19(72) pandemic. It has accordingly strengthened the realization of hadronic power and superpower as predicted in ref.[6] from 4x4 metric tensor of e-magnetodynamics.

5. REFERENCES

[1] P.A.M. Dirac 1971 Proc. Roy. Soc. 322A, 435 (1971).

[2] R.M. Santilli 1978 *Hadronic J.* 1, 574

[3] A. Einstein, B. Podolsky and N. Rosen (EPR), (1935)"Can quantum-mechanical description of physical reality be considered complete?" Phys. Rev., Vol. 47, p. 777 (1935),
www.eprdebates.org/docs/epr-argument.pdf
Nine minutes video on EPR , verifications,
http://www.world-lecture-series.org/legacy-of-einstein-for-new-clean-energies
Tutoring Lecture I: Isomathematics
http://www.world-lecture-series.org/santilli-tutoring-i
Tutoring Lecture II: Verifications of the EPR argument
http://www.world-lecture-series.org/santilli-tutoring-ii
Primary references on recent verifications of the EPR argument
http://www.santilli-foundation.org/docs/references-epr-verifications.pdf

[4] R. M. Santilli & A.O.E. Animalu *2011 Non-unitary Lie-isotopic & Lie-admissible scattering theory of HM* (2 011); Also Papers I, II, III, IV and V, in the *Proceedings of the Third International Conference on Lie-Admissible Treatments of Irreversible Processes,* C. Corda, Editor, Kathmandu University (2011) published in *Hadronic J.* Vol. 34, Nos.5 & 6 (2011) with the links
http://www.santilli-foundation.org/docs/Isoscattering-I.pdf
http://www.santilli-foundation.org/docs/Isoscattering-II.pdf
http://www.santilli-foundation.org/docs/Isoscattering-III.pdf

[5] A.O.E. Animalu 2019 -Lie-Admissible Approach to "Extended Relativity": Non-Linear Velocity, Mass and Charge Transformations in *African Journal of Phys. Vol.12, p.2-27 (2019) [reformatted from Hadronic J. Vol.10, 321-330(1987]*

[6] A.O.E. Animalu, Hadronic Conductivity: A New Form of Superconductivity, Hadronic J. Vol.45,333-355(2022)

[7] Albert Einstein(1879-1955) has been celebrated as *"PERSON OF THE CENTURY" (in Time Magazine Dec. 31, 1999) on the trending* (by Brandon Bays *www.thejourney.com) Einstein's equation (Energy = Love x square of speed of light) delivered in a Letter to his daughter (Lieseri) in 1938, a year before the outbreak of the 2nd World War date (1/09/1939)* released in 1980

.[8] **J. Madeleine Nash, Unfinished Symphony p.49 of *"PERSON OF THE CENTURY" (Time Magazine Dec. 31, 1999) citing Witten on Superstring M-theory(1995) that "M stands for many things including matrix, mystery and magic".***

[9] ***A.O.E. Animalu and N.C. Animalu, (2020) "Space-time Geometry of a torus for a Lorentz- and Conformal-Invariant String Theory without divergencies", African J. Phys. Vol.13, 1-36 (2020).***

[10] **P.A.M. Dirac (1970) *Can Equation=of-motion method be used in High Energy Physics?* In Appendix Physics Today April 1970, p. 29.**

[11] **A.O.E. Animalu and R.M. Santilli SO(2N)xSO(2N) group-theoretic approach to scattering of N-particle (N=5) systems, http://doi.org/10.52202/059404-0001**

[12] **A.O.E.Animalu, Nwakanma & Akpojotor (2013) Afr. J. Physics Vol. 6 1-18,(2013).**

[13] **A.O.E. Animalu, Samuel Edeagu, Godfrey Akpojotor & Erik Trell, Electromagnetism of Atomic Structural Constitution in Deformable Real R3xSO(3) Configuration Space, Afr. J. Phys. 11, 2 (2018).**

[14] **Elizabeth Isichei[13] *A History of the Igbo People*(1976).**

[15] **A.O.E. Animalu & A. V. Animalu (2012)*GENO-ASCII Code for Translation of Alphabets into Natural Numbers Equivalents and Geometry* African Journal Of Physics Vol.5, 122-140)(2012).**

[16] **C. Acholonu (2009): They Lived Before Adam p.447.**

[17] **A.O.E. Animalu, Geno-Bragg's Law, Geno-Higg's Function and 10*x10 Representation of SU(3) Symmetry for Quasi-Crystal Structures, Afr. J. Phys. 4, 14-42 (2011).**

ACKNOWLEDGEMENTS

The author wishes to acknowledge with deep appreciation the support of the Santilli Foundation and express gratitude to Professor R.M. Santilli for his encouragement of this research paper.

HADRONIC JOURNAL 46, 249 - 262 (2023)
DOI 10.29083/HJ.46.03.2023/SC249

QUANTIFYING THE EFFECT OF TEMPERATURE ON DIFFERENTIAL CROSS SECTION IN JOSEPHSON-JUNCTION SYSTEMS

Saraswati Chaudhary[1], Suresh Prasad Gupta[1,2], Jeevan Jyoti Nakarmi[1,2], Kishori Yadav[1,2], Saddam Husain Dhobi[2,3,4]
[1]Department of Physics, Patan Multiple Campus, Tribhuvan University, Lalitpur-44700, Nepal
[2]Innovative Ghar Nepal, Lalitpur-44700, Nepal
[3]Robotics Academy of Nepal, Lalitpur-44700, Nepal
[4]Central Department of Physics, Tribhuvan University, Kirtipur-44618, Nepal
saddam@ran.edu.np

Received June 22, 2023

Abstract

This study aims to investigate the differential cross section (DCS) across a Josephson junction in a superconductor with Kondo impurities, addressing a limitation of the previous work conducted by Goldstein et al. (2013). The DCS is derived using the Bransden and Joachain as well as the Sakurai methods, employing the Kroll Watson Approximation. The analysis focuses on examining the behavior of the DCS at both lower and higher frequencies. The results demonstrate that the DCS exhibits a linear increase at lower frequencies, while at higher frequencies, it shows an exponential increase with fluctuations. These findings provide valuable insights into the scattering phenomena in superconductors with Kondo impurities, shedding light on the interplay between the Kondo effect, impurity scattering, and Josephson coupling. Further research can explore the influence of additional factors such as temperature, impurity concentration, and lattice structure on the observed scattering dynamics. Moreover, investigations into the transport properties, proximity effects, and phase dynamics of Josephson junctions with Kondo impurities would contribute to a comprehensive understanding of these systems.

Keywords: Differential cross section, Josephson junction, Kondo impurities, Kondo effect, lower and higher frequencies

1. Introduction

This coupling occurs when quasiparticles hybridize to generate a molecular, or multi-weak link, Andreev Bound State (ABS) for two weak links separated by an order of the superconducting coherence length. The Andreev molecules with numerous channels are described by the scattering matrix formalism. Introduce new terms to the problem formulation to account for part Andreev reflection at the finite central superconductor in the scenario of two weak links coupled to three superconductors. ABS hybridization is caused by the microscopic scattering mechanisms called crossed Andreev reflection and elastic tunneling. A system of sparsely spaced superconducting weak links that can accommodate overlapping Andreev Bound States is known as an Andreev molecule. Recent theoretical studies have taken into account one-dimensional Andreev molecules having a single conduction channel and using the scattering formalism to expand the investigation to multiple conduction channels, a condition present in epitaxial superconductor/semiconductor weak junctions [1]. Quantum condensed-matter physics has long been interested in how impurities affect superconductivity. Nonmagnetic impurities shouldn't have much of an impact on the superconducting transition temperature, according to Anderson's theorem. Magnetic impurities make conduction electrons scatter in the spin-fip direction, which has a significant impact on the Cooper pairing in a superconductor. According to Anderson, a magnetic impurity ion's ability to preserve its magnetic moment depends on the host metal's density of states at the Fermi energy EF. Because Nb has a higher density of state at EF than molybdenum, the Anderson model explains why Fe in molybdenum is magnetic and can induce a Kondo effect but Fe in Nb cannot [2-4].

A fascinating phenomenon in quantum many-body physics is the Kondo effect. A common superconductor that is essential for many applications using superconducting devices is niobium (Nb). It has long been believed that Nb cannot detect the Kondo effect because Nb would have quenched the magnetic moment of a magnetic impurity, such as iron (Fe). When the annealing temperature is higher, the Kondo effect is more noticeable. Even though the system never becomes superconducting, the temperature relationship of the resistance points to the possibility of remnant superconductivity at low temperatures. The Hamann analysis produces a Kondo temperature for this Nb-Fe system of about 16 K, which is much higher than the beginning Nb flm's 9 K superconducting transition onset temperature, indicating that the impurity spins' screening is effective in allowing Cooper pairs to form at low temperatures [5]. The pair breaking and the successful repulsive interaction between s-electrons are included as

impurity effects in the interpolation theory, which is the foundation upon which the s- and d-electrons in superconductors are derived. Differently from that of Muller-Hartmann and Zittartz, the order parameter, the critical magnetic field at zero temperature despite the presence of impurities, its initial decline, and the localized excited state in the gap 1s were identified and demonstrated to be doublet [6].

Gapless unconventional superconductors have a self-consistent Kondo impurity theory that holds true in the Fermi-liquid domain. The large-N slave-boson method is used to treat the impurity degrees of freedom, producing tractable equations that describe how the Kondo effect and superconductivity interact [7]. There are various techniques to introduce magnetic moments into graphene, such as via defects or adatom deposition. Theoretically, effective Anderson or Kondo impurity models coupled with the Dirac electrons of graphene describe dilute moments. The physics of these models, particularly the impact of carrier doping and associated quantum phase transitions. Finally, draw parallels to other quantum impurity concerns, such as those in topological insulators, quantum spin liquids, and unconventional superconductors [8]. The extensive phenomena connected with spin-flip dynamics can be revealed through the electrons' interactions with nearby magnetic moments. In the study of condensed matter, the Kondo effect is crucial. Recent quasiparticle-interference experiments have shown that novel phenomena, such as heavy-fermion phases, emerge when Kondo correlations and spin systems of increasing complexity are utilized. We examine recent findings that demonstrate the connection between atomic spin entanglement and the emergence of Kondo correlations. Non-equilibrium Although the Kondo effect in the tunneling regime is mostly accounted for by its equilibrium qualities, Kondo nonetheless adds its unique peculiarities. Explored concepts include Kondo peaks, inelastic electron tunneling spectroscopy, and electron paramagnetic resonance of single atoms, molecules, and atomic objects [9].

Quantum interference is one of the key components of mesoscopic physics; it produces phenomena like weak localization, Aharonov-Bohm interference, universal conductance fluctuations, and fluctuations in the mesoscopic local density of states. The phase coherence of the conduction electrons is a prerequisite for all of these occurrences. However, inelastic scattering events, when an excitation is generated in the surroundings, break this phase coherence. After the so-called dephasing time, also referred to as the inelastic scattering time, these inelastic processes decrease quantum interference. The excitations produced during an inelastic scattering process can be electromagnetic radiation, phonons, magnons, or just electron-hole

excitations. A quantum impurity in a Josephson-Junction array was the subject of a 2013 study by Goldstein et al. that shed light on the inelastic microwave photon scattering off it. They looked at the design Hamiltonian, the Kondo temperature, the transition matrix, and the likelihood of scattering photons across the junction. Despite the fact that their work greatly advanced our understanding of these events, a huge research hole remained unfilled. The work by Goldstein et al. found a research gap in the absence of study into Direct Cooper Pair Scattering (DCS) caused by impurity potential form across the junction. Despite studying photon scattering, the study avoided going into detail about how impurities specifically affect Cooper pair behavior, which is a crucial quasiparticle in superconductivity. It is crucial to comprehend the DCS of Cooper pairs across the junction caused by impurity potential for a number of reasons. Impurities can, in the first place, interfere with the coherence of Cooper pairs, which can result in the loss of superconducting characteristics. Understanding the processes for the loss of superconductivity in these systems can be gained by looking into the scattering of Cooper pairs. Second, the Cooper pairs-based DCS method can result in unique phenomena and effects. Studying the scattering characteristics of Cooper pairs may make it feasible to identify particular quantum phenomena that arise as a result of impurity-induced scattering, potentially paving the way for the identification of novel physical phenomena or the creation of novel device functions. For practical applications, it is important to comprehend the DCS across the junction caused by contaminants. Platforms for quantum computing and quantum information processing that use Josephson-Junction arrays appear promising. In order to develop and optimize these devices, it is therefore beneficial to study the scattering of Cooper pairs since it sheds light on the negative impacts of contaminants and suggests ways to mitigate them. The undiscovered feature of the DCS of Cooper pairs due to impurities' possible development across the Josephson-Junction array is addressed in this work in light of the aforementioned research gap. By examining this phenomenon, we hope to learn more about how Cooper pairs behave when impurity scattering is present, gaining new knowledge about the physics of superconducting systems and their applications.

2. Methods and Materials

2.1 Differential cross section across the junction

Only the appropriate degrees of freedom are the total number of Cooper pairs n_i on island i and the associated superconducting phase φ_i, obeying $[\varphi_i, n_j]$,

assuming that the superconducting gap is bigger than any other energy scale and the Hamiltonian of the array is given as

$$H = \sum_{ij}\left[2e^2(n_i - n_i^0)(C^{-1})_{ij}\left(n_j - n_j^0\right) - E_J^{ij}\cos(\varphi_i - \varphi_j)\right] \qquad (1)$$

where E_J^{ij} and C_{ij} are the matrices of Josephson couplings and capacitances, respectively. And $n_i^0 = \frac{C_i^g V_i^g}{2e}$ with V_i^g and C_i^g being the gate voltage and capacitance to the ground, respectively. The Hamiltonian of noninteracting spin-1/2 fermions is derived by Goldstein et al. in 2013 as,

$$\hat{H}_K = \sum_{k,\sigma=\uparrow,\downarrow} vk c_{k,\sigma}^{\dagger} c_{k,\sigma} + \frac{I_z S_z}{2L}\sum_{k,\sigma,k',\sigma'} c_{k,\sigma}^{\dagger}\tau_{\sigma,\sigma'}^{z} c_{k',\sigma'} + \frac{I_{xy} S_-}{4L}\sum_{k,\sigma,k',\sigma'} c_{k,\sigma}^{\dagger}\tau_{\sigma,\sigma'}^{+} c_{k',\sigma'} + H.c - B_z S_z \qquad (2)$$

Where $\tau_{\sigma,\sigma'}^{i}$ is pauli matrices, $I_z = 2\pi v\left(1 - \frac{\alpha}{\sqrt{2}}\right)$, and $I_{xy} = 2\pi a E_J^{LR}$. Incoming microwave photons scatter elastically and inelastically due to the quantum impurity. The elastic T-matrix $\hat{T}_{\ell'|\ell}^{el'}(\omega)$, which is typical determined by the relationship between the single photon propagators in the presence and absence of the impurity [10],

$$-2\pi i\hat{T}_{\ell'|\ell}^{el'}(\omega) = \begin{pmatrix} r_L(\omega) - 1 & t_R(\omega) \\ t_L(\omega) & r_R(\omega) - 1 \end{pmatrix} \qquad (3)$$

where $t_\ell(\omega)$ and $[r_\ell(\omega)]$ is the transmission and reflection amplitude for a photon of frequency ω incoming, respectively and T matrixed is derived as

$$\hat{T}_{\ell'|\ell}^{el'}(\omega) = (-1)^{\delta_{\ell,\ell'}-1}\omega\alpha_\ell\alpha_{\ell'}\chi_{zz}(\omega) \qquad (4)$$

In equation (7) of Goldstein et al. (2013), all components of the elastic $\hat{T}$matrix and the local dynamic differential spin susceptibility of the Kondo problem are described in further depth. The coupling parameter and the parameters ($\alpha_{\{L,R\}}$) are provided by $\alpha_L = \alpha_R = \frac{1}{g}(1 - \lambda_{LR})$, $\alpha^2 = \alpha_L^2 + \alpha_R^2$ and $\lambda_{LR} = \frac{C_L C_R}{(C_L + C_R)C_{LR}} \sim \sqrt{\frac{C_g}{C}} \ll 1$. At low frequency $\omega \ll T_K$ the arbitrary susceptibility is approaches [11] as,

$$\chi_{zz}(\omega) = \chi_0\left(\alpha, \frac{B_z}{T_K}\right)\left[1 + i\pi\alpha^2\omega\chi_0\left(\alpha, \frac{B_z}{T_K}\right)\right] \quad (5)$$

where $\chi_0\left(\alpha, \frac{B_z}{T_K}\right) \equiv \frac{\partial\langle S_z\rangle}{\partial B_z}$ represent static local differential susceptibility. At high frequencies, $\omega \gg T_K$, the arbitrary susceptibility is approaches [12] as,

$$\chi_{zz}(\omega) = i\frac{\pi}{4}\frac{f(\alpha)}{\omega}\left(\frac{T_K}{i\omega}\right)^{2-\alpha^2}, \alpha > 1 \quad (6)$$

Where $f(\alpha) = -2\sin\left(\frac{\pi\alpha^2}{2}\right)\frac{\Gamma(1-\alpha^2)}{\{\pi[c(\alpha)]^{2-\alpha^2}\}}$. The array is uniform outside of the quantum impurity: all Josephson couplings, with the exception of the islands of the quantum impurity, are E_J, and all capacitances to the ground and junction capacitances, respectively, are C_g and C. Two ratios E_J/E_{C_g} and $E_J = E_C$, as well as two charging energies $E_C = \frac{(2e)^2}{2C}$and $E_{C_g} = \frac{(2e)^2}{2C_g}$ control the uniform array's properties. [10]. The many-body S-matrix defined by the overlap of the entering and outgoing scattering states is used to define the inelastic scattering problem as follows,

$$_{out}\langle f|i\rangle_{in} = {}_{in}\langle f|\hat{S}|i\rangle_{in} \quad (7)$$

The asymptotically free incoming and outgoing scattering states, $|i\rangle_{in}$and $|i\rangle_{out}$, may have several excitations, making them genuine many-body states. The identity operator $\hat{I}$ is used to define the many-body T-matrix as the'scattering part' of the S-matrix, which is defined as $\hat{S} = \hat{I} + i\hat{T}$.

$$_{out}\langle f|\hat{T}|i\rangle_{in} = 2\pi\delta(E_f - E_i)\langle f|T|i\rangle \quad (8)$$

A huge plateau develops above the Kondo scale, where the inelastic scattering rate's energy-dependence turns out to be remarkably small [13]. The inelastic scattering rate is nearly linear between 0.5 $T_K < \omega < 0.5T_K$. The well-known phrase provides the explicit form of the S matrix in the interaction representation $\hat{S} = Texp\{-i\int_{-\infty}^{\infty} H_{int}(t)dt\}$, where T is the time ordering operator (matrix elements of the T matrix) [14]. The scattering cross-section in terms of the tran-sition matrix according to Bransden & Joachain and Sakurai using Kroll Watson Approximation [15] is given by

$$\frac{d\sigma}{d\Omega} = \frac{k_f}{k_i}\left(\frac{m^*(2\pi)^2}{\hbar^2}\right)^2 |T_{fi}|^2 \qquad (9)$$

Where T is transition matrix m is mass of coopers pair $m^* = 2m$ and k_f and k_i is final and initial momentum of cooper pairs. On substituting the value from equation (4) in (9) and solving for $\ell = \ell'$ and $\ell \neq \ell'$

$$\frac{d\sigma}{d\Omega} = \frac{k_f}{k_i}\left(\frac{m(2\pi)^3}{(2\pi)\hbar^2}\right)^2 \left|\omega\left(\frac{1}{g}(1-\lambda_{LR})\right)^2 \chi_{zz}(\omega)\right|^2 \qquad (10)$$

For both cases, $\ell = \ell'$ and $\ell \neq \ell'$ the T-matrix is same so the DCS is same. Now at low frequency $\omega \ll T_K$, the DCS from (10) and (5) is obtained as

$$\frac{d\sigma}{d\Omega} = \frac{k_f}{16k_i}\left(\frac{m(2\pi)^3}{(2\pi)\hbar^2}\right)^2 \left|\omega\left(\frac{1}{g}(1-\lambda_{LR})\right)^2 [2 + i\pi\alpha^2\omega]\right|^2 \qquad (11)$$

Since we have $\chi_0\left(\alpha, \frac{B_z}{T_K}\right) = \frac{\partial <S_z>}{\partial B_z}$, $S_Z = \frac{n_L - n_R}{2} = \pm\frac{1}{2}$ and n_L is cooper pairs in left and n_L is cooper pairs in right. Also using $\alpha^2 = 2$ and $g = 1$, $\lambda_{LR} \ll 1$, when $I_{xy} = I_z$, the DCS is

$$\frac{d\sigma}{d\Omega} = \frac{m^{*2}\pi^4 k_f}{\hbar^4 k_i}|\omega(1-\lambda_{LR})^2[2 + 2i\pi\omega]|^2 \qquad (12)$$

This equation (12) DCS for lower frequency. For higher frequency $\omega \gg T_K$, from (10) and (6) with $\alpha > 1$, g=1, $T_K = c(\alpha)\omega_0\left(\frac{I_{xy}}{2\pi\alpha\omega_0}\right)^{\frac{2}{2-\alpha^2}}$, $c(\alpha)\sim 1$ is obtained as

$$\frac{d\sigma}{d\Omega} = \frac{k_f}{k_i}\left(\frac{m(2\pi)^3}{(2\pi)\hbar^2}\right)^2 \left|(1 - \lambda_{LR})^2 \frac{1}{16}\left(2\sin\left(\frac{\pi\alpha^2}{2}\right)\frac{\Gamma(1-\alpha^2)}{\{\pi[1]^{2-\alpha^2}\}}\right)\frac{I_{xy}^2}{\pi\alpha^2\omega\omega_0}\right|^2 \qquad (13)$$

Since we have, $I_{xy} = I_z = 2\pi v(1 - \alpha/\sqrt{2})$ and $\pi[z] = \frac{1}{\Pi[z]}$, $\Rightarrow \Pi(z) = \Gamma(z+1) = z!$ Therefore equation (13) become

$$\frac{d\sigma}{d\Omega} = \frac{16m^{*2}\pi^4 k_f}{\hbar^4 k_i}\left|(1-\lambda_{LR})^2\left(\frac{\pi v^2}{2\alpha^2\omega\omega_0}\right)\sin\left(\frac{\pi\alpha^2}{2}\right)\left(\frac{\Gamma(1-\alpha^2)}{\left[\frac{1}{2}\right]^{2-\alpha^2}}\right)\left(1-\frac{\alpha}{\sqrt{2}}\right)^2\right|^2 \quad (14)$$

This is equation for high frequency.

2.2 Thermodynamic properties coopers' pairs across junction

Use the quantum mechanical canonical ensemble partition function, which Chester established as the trace of the Boltzmann factor in 1954, to examine the thermodynamic characteristics represented as

$$Z = tr\left(e^{\beta\hat{H}_K}\right) \quad (15)$$

where $\beta = \frac{1}{k_B T}$ and $\hat{H}_K$ is the Hamiltonian operator of to the single-channel Kondo model, describing a confined spin exchange connected to a bath of spin-1/2 fermions that are not interacting, as evidenced by the bandwidth _0 in equation (2). The thermodynamic energy/internal energy of the coopers pair across connection is studied using the chosen Hamiltonian of equation (2), described [16] as

$$\langle E\rangle = -\frac{\partial \ln Z}{\partial\beta} = H_K - \frac{3}{2\beta} \quad (16)$$

The entropy is obtained with the help of equation (2) as

$$S = -k_B(\ln Z + \beta\langle E\rangle) = \frac{3}{2}k_B \quad (17)$$

The Helmholtz free energy is defined as $A = U - TS$, where U = ⟨E⟩ is the total energy and S is the entropy of coopers pairs,

$$A = H_K - 3k_B T \quad (18)$$

The thermal potential [17-18] of cooper pairs across the junction is defined as

$$\Omega = -\frac{1}{\beta V}\ln Z \tag{19}$$

3. Results and Discussion

3.1 Differential cross section at low frequency

According to figure 1, the DCS at low frequency increases as cooper pair frequency and momentum rise. Kondo impurities interact with the Cooper pairs and have an impact on the charge dynamics when they are added to a superconducting system. The Kondo effect results from the interaction of the system's itinerant electrons and localized spins linked to the impurities. Through this interaction, a many-body entangled state is created, where the surrounding electrons screen the impurities' spins.

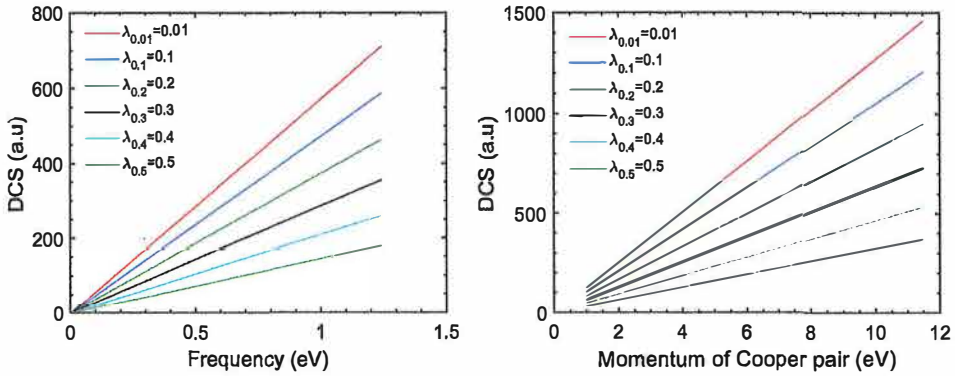

Figure 1: DCS with frequency and Momentum of cooper pairs

Cooper pair dynamics are impacted by Kondo impurities due to their interaction with the localized spins. At low frequencies, the differential cross section may be raised as a result of this interaction's modification of the scattering processes. Cooper pairs scatter more readily with Kondo impurities due to their increased frequency and momentum, which results in a bigger DCS. In this case, a number of factors could play a role in the precise process underpinning the improvement of the DCS. The system's overall scattering processes are aided by the Kondo effect, which can generate new scattering channels and resonances. The amount of charge excitations and their cross-sectional area can be efficiently augmented by these extra scattering processes, leading to an increased DCS at low frequencies. It is crucial to keep in mind that the precise behavior of the DCS when Kondo impurities are introduced can vary depending on the particulars of the system, such as the impurity concentration, lattice structure, and other characteristics. In

order to completely comprehend the underlying mechanisms and establish a thorough grasp of the interaction between the DCS, Cooper pairs, and Kondo impurities in your particular study, additional research and analysis are therefore required.

3.2 Differential cross section at high frequency

As demonstrated in figure 2, the DCS decreases abruptly in the lower energy range and gradually in the higher energy range. Figure 2 illustrates how the DCS grows exponentially as the momentum of the cooper couples increases. The study of scattering events in superconducting systems with Kondo impurities was based on the observation of a dramatic fall in the DCS at lower energies. In addition, our research shows that the DCS declines more slowly at higher energies. This pattern suggests that incoherent scattering processes become more prevalent as energy levels rise. Notably, we discovered that the DCS exhibits an exponential growth with Cooper pair momentum. Greater momentum Cooper pairs have larger kinetic and momentum energies, which raises the probability of scattering and, as a result, the DCS. In summary, our research shows that the DCS rapidly decreases at low energies, then gradually decreases at high energies, and then exponentially increases when the momentum of Cooper pairs increases in superconductors with Kondo impurities. These results contribute to a better understanding of these systems by offering insightful information on the scattering dynamics and momentum dependence of Cooper pairs in the presence of Kondo impurities.

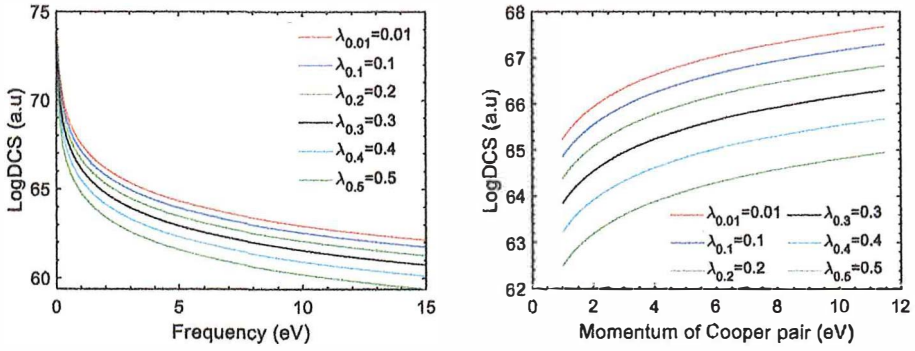

Figure 2: DCS with Frequency and momentum of cooper pair at high frequency

Cooper pair coherent tunneling between two superconducting electrodes through a tiny barrier is the basis for Josephson junctions. In the barrier area, the existence of Kondo impurities can bring about scattering processes that

prevent coherent tunneling. The scattering events may result in a suppression of the Josephson interaction between the superconducting electrodes at high frequencies. Through theoretical models that take into account the interaction between impurity scattering, Cooper pair tunneling, and the Kondo effect, this effect can be explored. Current-voltage characteristics may exhibit nonlinearities as a result of scattering by Kondo impurities in the Josephson junction. High frequency impurity scattering processes have the potential to increase junction resistance and alter current flow. The interaction between Kondo physics, Cooper pair tunneling, and the Josephson effect can be taken into consideration in theoretical modeling and experimental observations to further understand this behavior. The presence of scattering processes can affect the dynamics of the superconducting phase difference across Josephson junctions with Kondo impurities. At high frequencies, the stability and coherence of the phase dynamics may be impacted by scattering-induced dissipation. Both experimental research and theoretical analysis can be used to study how impurity scattering, phase dynamics, and dissipation interact. High frequency scattering can affect how Andreev bound states arise in the Josephson junction when Kondo impurities are present. The reflection of electrons as electron-hole pairs at the superconducting interfaces causes these bound states to form. The energy spectrum and spatial distribution of these bound states may be altered by impurity scattering, which may have an effect on the junction's transport characteristics and proximity effects.

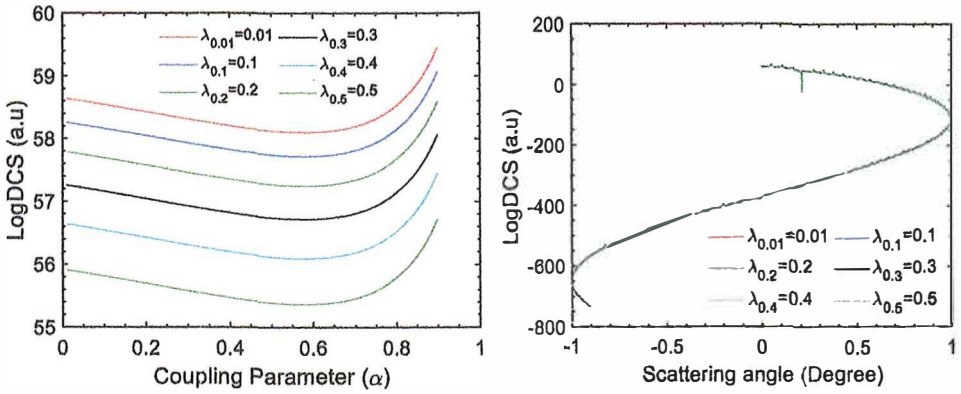

Figure 3: DCS with Coupling parameters and scattering angle at high frequency

Figure 3 illustrates how the DCS increases exponentially with Josephson junction coupling parameters after a minor drop with those parameters up to a certain number. As seen in figure 3, the DCS with scattering angle increases and reaches its maximum with a certain fluctuation. The interplay between

the Kondo effect, impurity scattering, and Josephson coupling can be used to explain the behavior of the scattering/differential cross section (DCS) with the coupling parameter of the Josephson junction in superconductors when Kondo impurities are present. The Kondo effect initially predominates when the coupling parameter of the Josephson junction rises. The localized spins of the impurities interact with the conduction electrons to produce the Kondo effect. The Kondo effect causes the creation of a Kondo singlet state in this regime, which effectively screens the impurities' spins. This screening lessens the contaminants' ability to deflect conduction electrons, which lowers the DCS. The Josephson coupling, which competes with the Kondo effect, becomes more prominent when the coupling parameter of the Josephson junction increases over a specific threshold. Cooper pair coherent tunneling between the junction's superconducting electrodes is made possible by the Josephson coupling. In this regime, the Kondo effect starts to give way to the Josephson coupling. At this moment, the Kondo screening of the impurity spins is being undermined by the enhanced Josephson coupling. As a result, the impurity dispersion is more prominent, increasing the DCS exponentially. Because of the higher influence of the Josephson coupling, the Kondo screening mechanism breaks down, resulting in increased impurity dispersion. Theoretical models and computations that take into account the interaction between the Josephson coupling, impurity scattering, and Kondo effect can help us understand the precise specifics of this mechanism. To capture the intricate behavior of the system, these models often include solving the proper quantum mechanical equations, such as the Anderson model or the Kondo lattice model. It is important to keep in mind that a number of variables, such as the impurity concentration, temperature, and material parameters, might affect how precisely the DCS with the coupling parameter of the Josephson junction behaves when Kondo impurities are present. Therefore, in order to confirm and further understand this mechanism, thorough theoretical research and experimental experiments are required.

Conclusion

In conclusion, the findings of our study provide some key insights into how scattering events affect superconductors containing Kondo impurities. First off, as Cooper pair frequency and momentum increase, the differential cross section (DCS) at low frequency increases, indicating intensified scattering processes. This finding suggests that Kondo impurities alter the charge dynamics in the system and have an impact on Cooper pair dynamics. Furthermore, our research shows that at high frequency, the DCS shows a fast decline in the lower energy range and a slower decrease in the higher

energy range. The interaction of the Kondo effect and incoherent scattering processes is responsible for this phenomenon. Higher energies result in more pronounced incoherent scattering, which slows down the DCS drop. Additionally, the DCS exhibits an exponential growth with Cooper pair momentum, representing the elevated scattering likelihood connected to higher momentum states. Kondo impurities in Josephson junctions cause the DCS with the coupling parameter to behave differently. The Kondo effect takes over initially, which causes the DCS to drop. Beyond a certain point, the Josephson coupling, which competes with the Kondo effect, becomes more relevant. The Kondo filtering breaks down as a result of this competition, while the DCS increases exponentially.

Acknowledgement

We would like to thanks all the faculties' member of Department of Physics, Tribhuvan University, Nepal; Innovative Ghar Nepal and Robotics Academy of Nepal for their support during this work.

References

[1] J.D. Pillet, V. Benzoni, J. Griesmar, J.L. Smirr, and Ç.O. Girit, SciPost Phys. Core. 2 (2020).

[2] A. V. Balatsky, I. Vekhter, and J.X. Zhu, Rev. Mod. Phys. 78 (2006).

[3] P.W. Anderson, J. Phys. Chem. Solids. 11 (1959).

[4] B.T. Matthias, M. Peter, H.J. Williams, A.M. Clogston, E. Corenzwit, and R.C. Sherwood, Phys. Rev. Lett. 5 (1960).

[5] H. Zeng, D. Zhou, G. Liang, R. Tang, Z.H. Hang, Z. Hu, Z. Pei, and X. S. Ling, Scientifc Reports. 11 (2021).

[6] T. Matsuura, Prog. Theor. Phys. 57 (1977).

[7] L.S. Borkowski, and P. J. Hirschfeld, Phys. Rev. B. 46 (1992).

[8] L. Fritz, and M. Vojta, The Physics of Kondo Impurities in Graphene, arXiv. (2013).

[9] D.J. Choi, and N. Lorente, Magnetic Impurities on Surfaces: Kondo and Inelastic Scattering. Handbook of Materials Modeling. Springer, Cham. (2018).

[10] M. Goldstein, M.H. Devoret, M. Houzet, and L.I. Glazman, Phys. Rev. Lett., 110 (2013).

[11] U. Weiss, Quantum Dissipative Systems, World Scientific, Singapore, (1999).

[12] A. C. Hewson, The Kondo Problem to Heavy Fermions, Cambridge University Press, Cambridge, England, (1993).

[13] G. Zaránd, and L. Borda, Physica. 40 (2007).

[14] G. Zaránd, L. Borda, J. von Delft, and N. Andrei, Phys. Rev. Lett. 93 (2004).

[15] B.N. Kim, Angular Distribution of Electron-Helium Scattering in the Presence of a 1.17 eV Laser Field, Theses and Dissertations--Physics and Astronomy. 95 (2022).

[16] A.K. Pradhan, S.N. Nahar, Atomic Astrophysics and Spectroscopy, Cambridge University Press, New York, NY, USA, (2011).

[17] N. Bralic, D. Cabra, and F.A. Schaposnik, Thermodynamics of Relativistic Fermions with Chern-Simons Coupling, ArXiv. (2019).

[18] K. K Singh, Ann. Phys. 75 (1973).

HADRONIC JOURNAL 46, 269 - 292 (2023)
DOI 10.29083/HJ.46.03.2023/SC269

It is the asymmetry that creates the phenomenon. Pierre Curie (1894)

SERIES OF INTEGER PRIMES AND EVOLUTIONARY CLASSIFICATION OF GALAXIES

Peter Matveevich Mazurkin
Volga State University of Technology
Yoshkar-Ola, the Republic of Mari El, Russia
kaf_po@mail.ru
Researcher ID: H-7464-2014; Orchid ID: 0000-0003-0177-5521

Received July 4, 2022

Abstract

To model the parameters of galaxies by classes of evolutionary morphology, it is proposed to use series of integer prime numbers. As among spiral galaxies in the direction of rotation, in nature there are only two types of integer primes: right-handed and left-handed asymmetries. This similarity made it possible to prove that the arms of spiral galaxies are sources of gravitational waves. In the plane of a galaxy of the SBd type, it is necessary to measure the coordinates of large stars in the spiral arms, which will provide statistical material for identifying finite-dimensional series of integer primes. An evolutionary classification scheme for galaxies that change their average density from a cloud of hydrogen to a void is proposed. The transitions between classes occur according to two processes: growth according to the exponential law of the average density of visible matter and dissipation of the same matter according to the Mandelbrot law with an additional damped oscillation. For a hydrogen cloud (class 0), dissipation of matter occurs in helium. The helium concentration becomes a quantitative characteristic for different primary clouds of hydrogen. For the first class (spiral galaxies with network arms in gas and dust clouds with stars), the detector is chlorine. For galaxies of the second class (existing types SBd, SBc, SBb, SBa), nitrogen is clearly distinguished as a detector. In classes 3-11 of the evolution of galaxies, the average density refers not to chemical elements, but to sets of chemical elements of space objects.

Keywords: series of integer primes, similarity, asymmetry of galaxies, classes, network arms, evolution, average density, class transitions, patterns.

PACS: 95.30.-k MSG: 11A41

1. INTRODUCTION

In the string theory of mathematical physics, there are five fundamental interactions in our Universe of a type I cosmic string (URL: https://new-science.ru/pochemu-astronomy-zainteresovany-v-gravitacionnyh-volnah/).

In this article, instead of the open first fundamental cosmic string, it is proposed to use series of integer primes [15] of different cardinality (the number of negative and positive primes, as well as additionally zero). Such a replacement makes it possible to carry out a physical (according to the chiral asymmetry of life in space) classification of galaxies. We have created this classification based on the nonlinear evolution of galaxies, in the direction of rotation belonging to the right-sided asymmetry of galaxies.

In the future, by measuring the parameters of specific spiral galaxies, it is possible to identify the distribution of large stars in the arms, and then to identify the set of regularities of the cosmic string, which contains the main linear law and additionally the equations of asymmetric wavelets. Apparently, these asymmetric wavelets are formulas for the oscillatory adaptation of galaxies in the course of their evolution in the Cosmos in the form of a series of gravitational waves of different amplitudes and oscillation periods.

2. MATERIALS AND METHODS

In mathematical physics, we adhere to the concept of Rene Descartes on the need for a direct application of the general algebraic additive equation as the final mathematical solution of unknown differential and integral equations. Generalizing the set of examples, including in the form of a list (space) of space objects [7, 8, 13, 18, 19] located in the same section of time, we proposed a new class of wave functions [11, 12, 20] in the form of asymmetric oscillations having variable amplitudes and periods of oscillatory perturbation.

An asymmetric wavelet signal, as a rule, of any nature (object of study) is mathematically written according to the wave formula [12] of the form

$$y = \sum_{i=1}^{m} y_i\ ,\ y_i = A_i \cos(\pi x / p_i - a_{8i})\ ,$$

$$A_i = a_{1i} x^{a_{2i}} \exp(-a_{3i} x^{a_{4i}})\ ,\ p_i = a_{5i} + a_{6i} x^{a_{7i}}\ , \qquad (1)$$

where y – is the indicator (dependent factor), i – is the number of the component in the model (1), m – is the number of components in the model (1), x – is the explanatory variable (influencing factor), $a_1 ... a_8$ – are the model parameters that take numerical values in the process of structural and parametric identification according to statistical data measurements of galaxies in the CurveExpert-1.40 software environment [2] (URL: http://www.curveexpert.net/), A_i – is the amplitude (half) of the asymmetric wavelet (axis y), p_i – is the oscillation half-period (axis x).

According to formula (1) with two ***fundamental physical constants*** e (the Napier number or the number of time) and π (the Archimedes number or the number of space), a series of ***quantized asymmetric wavelet signals*** is formed.

In our example, these are the quanta of the behavior of a spiral galaxy from the moment a stretched comic string arises (over time, during evolution, loosening of the arms appears in the form of oscillations with increasing amplitude, and then the amplitude of oscillations decreases to form a spherical shape and the gradual scattering of this spherical galaxy in the Cosmos to void density).

The concept of an asymmetric wavelet, which differs from the known classical symmetric wavelets, allows one to abstract from the physical meaning of statistical series and consider their additive decomposition into components (behavior quanta). The general equation (1) is obtained as a sum of wavelets, and all components of this general model are sequentially distributed in the form of non-multiple fractals according to the Mandelbrot law.

Relationships between the fundamental laws of physics and series of prime numbers were considered by us in the article [16]. As a result, following the remarks of Stephen Hawking [5] about the need to predominate the description of the physical entity over mathematical calculations, in this article only the formulas of the series of integer primes necessary for astrophysics have been given. Details about integer primes are given in the book [15].

Galaxies are peculiar signals that astrophysicists have not yet learned to fully decipher. A signal is a material carrier of information. And we understand information as a measure of interaction between physical objects. The signal can be generated, for example, by galaxies, but it is not necessary for a person to receive it.

A signal can be any physical process (or an object in the form of a phenomenon) or part of it. It turns out that the change in the set of unknown signals has long been known, for example, through the series of measurements of galaxies according to the classification of Edwin Hubble (the Hubble sequence). According to the measurement results, even atlases have been created [1, 6]. However, there are still no models for the distribution of large stars inside the arms of spiral galaxies, although a system of celestial coordinates has long been created.

In essence, the loosening of the arms of galaxies due to a change in the location of large stars becomes a source of gravitational waves. This is proved by the fact that the series of integer primes [9, 10] have a linear basic law of the cosmic string and additionally asymmetric oscillations of gravitational waves, which determine the block structure of the series of primes. Moreover, it turned out that with an increase in the power of a series of prime numbers, a transition from regularity to chaos gradually occurs [10]. The expansion of prime numbers from the decimal system in the binary system relatively easily proves the Riemann hypothesis [14-16] about the real root 1/2.

Under the condition $a_5 \to \infty$, wave (1) turns into a nonlinear change in half the amplitude. The result is an asymmetric trend. The amplitude $y = A$ at $a_2 = 0$

and $a_4 = 1$ turns into the well-known law $y = a_1 \exp(-a_3 x)$ of Laplace (in mathematics), Mandelbrot (in physics), Zipf-Pearl (in biology) and Pareto (in econometrics).

It seems to us that a cosmic string [21] exists according to the Mandelbrot law: at a certain zero moment, an energy explosion occurs and a cosmic string instantly appears in the Cosmos inside a gas and dust cloud. Then, according to the exponential Mandelbrot law, the string energy slowly decreases to zero. When approaching zero, a void is formed, for example, in the form of the supervoid of Eridanus.

Under the conditions $a_2 = 0$, $a_3 = 0$ and $a_4 = 1$, a simple equation $y = ax$ is formed to describe the axis of symmetry (a cosmic string stretched along a straight line for the origin and development of a galaxy) of a spiral galaxy with two symmetrical arms. Moreover, the structure of the arms of the galaxy is formed in the form of residues from the equation $y = ax$.

These residuals are further modeled by wave equations, the number of which increases with the power of a series of integer primes. This fact will make it possible to reveal the power of a finite-dimensional series of integer primes after identifying, using measurement data, a specific spiral galaxy of the SBd type, in which the matter from the arms has not yet flowed into the bar, and then into the bulge of an already mature galaxy.

3. RESULTS AND DISCUSSION

3.1. Series of integer primes

3.1.1. Construction of two mirror-asymmetric series of integer primes. The series of integer primes [9, 10, 15] is symmetric with respect to 0 and infinite-dimensional in the negative and positive ends of the series. The study of the properties of the positive part of the full series of integer primes showed a clear geometry through the block structure and gave patterns of distribution of primes over blocks.

Then a series of integer primes can be considered as follows: $P_Z \in \mathbf{Z}$, where P_Z – a series of integer prime numbers in a set $\mathbf{Z}$ integers. In a row P_Z the abscissa is taken as a complete series of integers $Z = \{-\infty,...,-4,-3,-2,-1,0,1,2,3,4,...,\infty\}$.

If we supplement natural numbers with "+" or "-" signs, then we will get integer numbers Z with center 0 and edges $\pm\infty$ along the abscissa axis, and integer prime numbers along the ordinate axis, also with signs "+" (prime numbers) or "- "(negative prime numbers).

From Table 1 and the graphs in Figure 1, it is clear that in nature there are only two types of integer primes: ***right-handed and left-handed asymmetries***. They have a chiral character due to the fact that the direction of the abscissa axis in both types of infinite-dimensional and finite-dimensional series of integer

primes remains unchanged, and the directions of the ordinate axis become mirror opposite.

Table 1. Two types of series of integer primes

Kind A of integer primes (right-sided Rsa asymmetry)				Kind B of integer primes (right-sided Lsa asymmetry)			
Z	A	Z	A	Z	B	Z	B
$-\infty$	$-\infty$	-	-	$-\infty$	∞	-	-
...	...	1	1	...	...	1	-1
-10	-23	2	2	-10	23	2	-2
-9	-19	3	3	-9	19	3	-3
-8	-17	4	5	-8	17	4	-5
-7	-13	5	7	-7	13	5	-7
-6	-11	6	11	-6	11	6	-11
-5	-7	7	13	-5	7	7	-13
-4	-5	8	17	-4	5	8	-17
-3	-3	9	19	-3	3	9	-19
-2	-2	10	23	-2	2	10	-23
-1	-1	...	...	-1	1	...	...
0	0	∞	∞	0	0	∞	$-\infty$

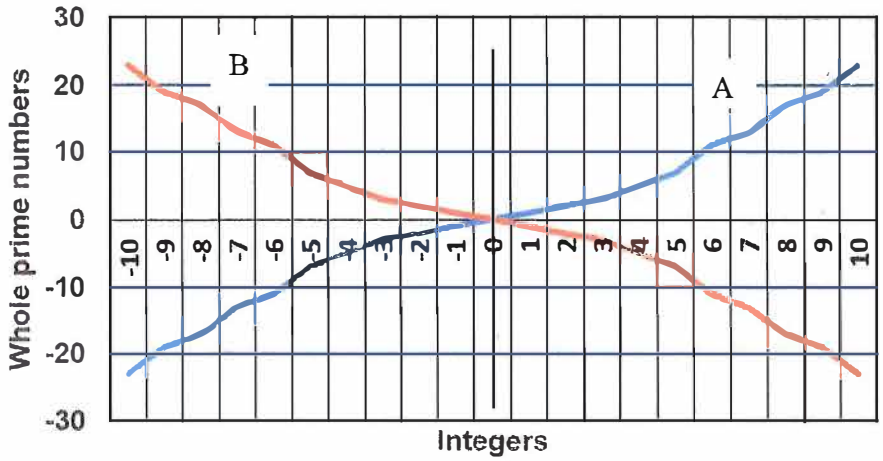

Figure 1. Graphs of two types (right A and left B) of series of integer primes

Apparently, the chirality of the living world in the Universe is characterized by an almost mirror reflection between types A and B, in Figure 1, for series of integer primes [15]. Regarding the common x-axis of integers, this property of chirality is quite simple: chirality is formed only by changing the sign (from positive to negative or vice versa) in front of an asymmetric wavelet (1).

3.1.2. Finite-dimensional right-hand series of prime integers. All galaxies in space have specific sizes and shapes. Measurements of galaxies, for example, in the plane of the galaxy, calculating the coordinates of large stars in spiral

arms, will provide statistical material for identifying finite-dimensional series of integer primes.

Next, we will study the symmetrical series of type A from Figure 1.

Consider an example of a finite symmetric series of integer primes (Table 2). This example was compiled according to the computational capabilities of the CurveExpert-1.40 software environment [2]. It can only contain a little more than 3300 lines for parameter value pairs x and y. According to these data, it becomes possible to identify the model (1).

In a series of primes, the power of a series n shows the total number of terms, and in a symmetric series of integer primes, the number of pairs of primes. Then the cardinality of a series of integer prime numbers will be equal to $2n+1$

Table 2. Finite-dimensional series of integer primes with cardinality $n = 16500$ PC. (fragment)

Left edge		Center symmetry		Right edge	
Z	P_Z	Z	P_Z	Z	P_Z
-16500	-182057	-3	-3	...	...
-16499	-182047	-2	-2	16495	182011
-16498	-182041	-1	-1	16496	182027
-16497	-182029	0	0	16497	182029
-16496	-182027	1	1	16498	182041
-16495	-182011	2	2	16499	182047
...	...	3	3	16500	182057

With the total number $2n+1$ in the example of table 2, together with zero, there is $2 \times 16500 + 1 = 33001$ a prime integer. A larger number of pairs of numbers Z and P_Z does not fit in the RAM of the CurveExpert-1.40 software environment.

The origin of coordinates is clearly defined at the point ($Z = 0$, $P_Z = 0$). This is a ***point of singularity*** due to the fact that, according to the existing definition of a prime number (the second property of dividing by itself), division 0 / 0 occurs.

At the same time, according to the first property (division by 1), it turns this point into zero.

A definition is known that a prime number is a natural number $N = \{0,1,2,3,4,5,6,...\}$ that has two natural divisors: one and itself [15]. But, when zero is included in the series of integer primes, division by itself has no physical meaning (it is required to mathematically reveal this uncertainty through the study of a singularity at the center of a black hole located approximately in the center of the galaxy).

Therefore, for series of integer prime numbers, we exclude the second condition and leave the following definition:

A prime integer is an integer that is only divisible by 1.

Table 2 also shows that the center of symmetry is determined by seven integer prime numbers. In this case, the negative semiaxis 0(-0), -1, -2 and -3 ... is

directed to the left, and the positive semiaxis 0, 1, 2 and 3 ... (for a number of prime numbers) is directed to the right.

The signs give what we believe to be Stephen Hawking's arrow of time [5] from left to right when moving from negative to positive integers. Apparently, at the same time, types A and B, for series of integer primes, determine the chirality of cosmic life. For terrestrial biological objects (we have proved the correspondence of the series of Fibonacci numbers to the series of prime numbers) in our Milky Way Galaxy, right-sided asymmetry is observed.

Then it turns out that right-handed finite-dimensional series of integer primes can describe any galaxies rotating clockwise.

We also note that, according to the results of our research, the numbers 0, 1 and 2 belong to the critical prime numbers in the series of primes. It was they who prevented mathematicians for more than 2200 years from finding the distribution law in the traditional Gauss series: 2, 3, 5, 7, 11, ... in the decimal number system. But Gauss nevertheless removed one critical number 1, but apparently did not dare to exclude the number 2. In a well-known film on the history of mathematics, one of the mathematicians known to his contemporaries said that his favorite number is 2, since this is the only even number in the series of prime numbers. But now we can say that there are even numbers in the series 0, 1, 2, 3, 5, ... even two - zero and two. And taking into account the scale of integers, even three such even numbers appear: -2, 0, 2.

A non-critical series of prime numbers begins with the number 3, and it allows you to identify highly adequate (statistical, with a correlation coefficient close to 1, that is, with some error due to real values of the ordinates) mathematical patterns.

The sign does not change the essence of the numbers themselves, but only relates them to different "worlds" (negative or positive), therefore, symmetrically on the left half-axis 0 (-0), -1, -2, -3, ..., - critical primes are also located on the left numbers 0, -1 and -2.

Therefore, a non-critical negative series $-P_Z$ begins with the number -3.

We note here that the analog of ***the event horizon*** in front of the black hole in the center of the galaxy is located on the boundary of the sphere -1, 0, +1 from the inside (in Table 2, the ***core of the center of symmetry*** is highlighted), that is, under the condition $\pm P_Z \to 1$. And the rational number 1/2, or the real root of the Riemann zeta function [14, 16] (according to the well-known Riemann hypothesis or Hilbert's 8th problem) is through for the entire series of integer primes. This real root appears when translating prime numbers from the decimal number system to the binary system [16], and ***the critical Riemann line*** is clearly defined by the second vertical of the binary expansion.

Many spiral galaxies contain more than two arms. For example, the Milky Way contains at least three pairs of arms. Then our Galaxy can be described by at least three rows of integer primes, which are located with rotation and displacement of three systems of rectangular coordinates. For cosmology, we called each series of integer primes ***proston*** (from the Russian word "simple") - as a

unit of measurement in the general case of a set of finite-dimensional series of integer primes that are displaced from the center or rotated relative to each other.

With a parallel shift relative to each other of two finite-dimensional prostons relative to one position in two series of integer primes, an ***increment*** is determined. In our opinion, the distances between large stars in the arms of a spiral galaxy, starting from the point of docking of the arm to the bar or then to the bulge, are determined by this increment, which is equal to an even number in different groups. Moreover, each group of prime numbers on the right side of a series of integer prime numbers always begins with the number 2, which determines pairing in most developed forms of life.

3.1.3. Center of symmetry of the right-hand series of integer primes. Figure 2 shows a graph of the center of symmetry of a series of integer primes from seven points.

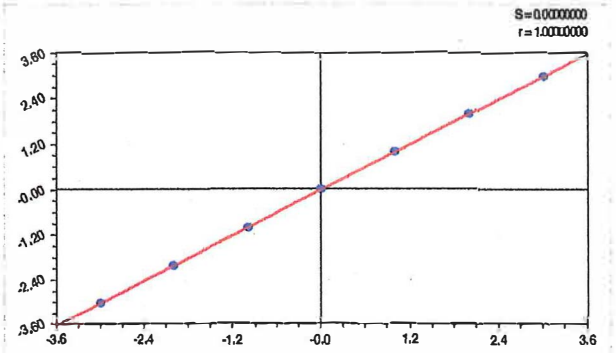

Figure 2. The center of symmetry of a series of integer prime numbers (in the upper right corner: S - standard deviation; r - correlation coefficient)

График был получен в программной среде CurveExpert-1.40 в виде формулы

$$P_Z = Z,$$
$$Z = -3,-2,-1,0,1,2,3. \quad (2)$$

The center of symmetry of a series of integer primes has remarkable mathematical and physical properties.

The same proportionality $P_Z = Z$ is observed when the power of pairs of integer primes $n = 1 \vee 2 \vee 3$ or the total number of members of a series of integer primes is $2n + 1 = 3 \vee 5 \vee 7$. Thus, at the center of symmetry, prime numbers (their numbers are also prime numbers) coincide with the values of the initial elements of the scale of integers and natural numbers.

This center of symmetry is unchanged for any power of a symmetric or asymmetric (with the inclusion of the center of symmetry) series of integer primes, including the condition $n \to \infty$ for Cantor's understanding of the types of infinity. It is a kind of start of a change in disproportion. Moreover, this start occurs from a proportionality coefficient equal to 1, and continues to infinity.

Inside the spherical ***shell of the center of symmetry*** (in Table 2, the shell is located behind the selected core of three numbers, and the sphere is formed by turning the slope of the symmetry line from an angle $\pi/4$ up to 360 degrees) there are three fundamental constants (harmony numbers - the golden and silver proportion, the number time or Napier number).

Thus, from the point of singularity 0 there is a complex and yet mathematically incomprehensible extension (within the framework of rational integers) to

the boundary of the kernel [-1, 0, +1]. Rational (fractional) prime numbers are at work here. Then in the spherical shell [-3, -2, ..., 2, 3] there is a leap of harmony [15] through the number of time or the Napier number. As a result, the properties of integer primes unite the achievements of physics and mathematics and therefore become an incentive for further in-depth complex physical and mathematical research.

In theoretical astrophysics, galaxies become objects of study.

However, paper [3] shows the existence of a runaway supermassive black hole, which was identified by impacts and star formation on its way in the medium near the galaxy. When star formation starts, a supermassive black hole is ejected from the galaxy at high speed. The reason for the ejection, in our opinion, is the very high asymmetry of star formation between the two arms of the galaxy. After the ejection, only the arms of the galaxy remain.

As a result, in space there are isolated supermassive black holes corresponding to the center of symmetry shown in Figure 2, as well as galaxies in the form of isolated arms. The latter are subject to series of non-critical primes starting from the number 3.

3.1.4. The basic law of distribution of integer prime numbers. The linearity of the basic law of distribution of a series of integer prime numbers of any cardinality of the series is geometrically interpreted as follows.

Rows of integer prime numbers of the form A (right-sided asymmetry) form a kind of core of the entire distribution structure, bypassing the special properties of the sphere -1, 0, +1 and the abrupt transition to harmony inside the shell -3, -2, ..., 2, 3.

In the triad -1, 0, +1 there are distinguishing features that are still unknown to us. In the spherical shell [-3, -2, ..., 2, 3] there is a qualitative leap from the singularity for a harmonic distribution from a prime to two (right and left) non-critical series $\pm P_{N=3,5,7,11,...}$.

t forward a hypothesis that a finite-dimensional non-critical series (without a center of symmetry) characterizes the types of galaxies in evolution after the elliptical and spherical shapes. Apparently, irregular galaxies of the **Irr** class are characterized by non-critical series of integer primes after the exclusion of the supermassive black hole from the galaxy, and then the bulge and bar. In the Hubble sequence (https://science.fandom.com/en/wiki/Hubble_Sequence), **IrrI**-type galaxies show the remnants of a spiral structure, and **IrrII** have a completely irregular shape. In our opinion, in the future there is a complete scattering of the matter of the galaxy before the void: the cycle of the emergence and existence of classes of galaxies ends.

Based on induction on a set of particular examples, one can generalize ***the law of distribution of series of symmetric integer primes*** in the form of a basic mathematical expression

$$P_Z = \alpha(n)Z \,, \tag{3}$$

where $\alpha(n)$ – is the ***slope coefficient*** (of the axis of the series as a mathematical analogue of the cosmic string [21]) of a symmetrical series with the power n of a series of pairs of integer primes.

This is the main parameter of any series of integer primes, including symmetric and asymmetric series. Asymmetric series in formula (3) have a constant term that has a clear geometric meaning (but the astrophysical meaning is not yet clear).

The ratio of an integer prime number (ordinate) to an integer (abscissa) gives the tangent of the angle ω of inclination of the axis of a series of integer prime numbers to the abscissa axis Z according to the formula

$$tg\omega = P_Z / Z = \alpha(n) . \qquad (4)$$

From expression (4) and the graph in Figure 2, we notice that the lower limit of the angle of inclination of the symmetry axis of the series will be 45^0 or $\alpha_{min} = \pi/4$. Under the mathematical condition $n \to \infty$, it will also be $P_Z \to \infty$, therefore $\alpha_{max} \to \pi/2$. Then the interval of change of the slope coefficient of the axis of the entire symmetrical series of integer primes will be equal to $a(n) = \{1, \infty\}$, and the interval of the angle of inclination of the axis of this entire series will change within $\alpha = \{\pi/4, \pi/2\}$.

3.2. Physical interpretation of series of integer primes

3.2.1. Right sided spiral galaxy. As mentioned earlier, one proton shows one cosmic string of the Universe. Many protons from the same point with different turns give many strings with the same center. And the point distribution of residuals (Fig. 3) from the linear law (3) shows similarity with one symmetrical pair of arms in spiral galaxies [17].

For a symmetrical series of integer primes with the power $n = 100$ of a series (Fig. 3) of pairs (for the measured parameters of an SBd galaxy.

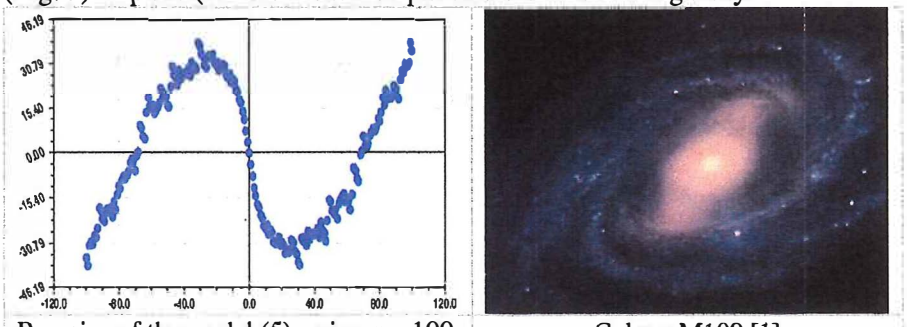

Remains of the model (5) series $n = 100$ Galaxy M109 [1]

Figure 3. Comparison of the plot of residuals from (5) and a galaxy with right-hand asymmetry

It is sufficient to register the coordinates of 100 bright stars in each arm), the equation

$$P_{Z100} = 4{,}87381Z\,. \qquad (5)$$

In the photo of the M109 galaxy, it is noticeable that the bar is gradually turning into a bulge, which is why the central part of the galaxy is moving into a new shape, moreover, due to the twisting of the arms and the flow of matter from the periphery to the center.

3.2.2. left handed spiral galaxy. In the form B of series of distributions of integer prime numbers, as shown in Figure 4 for the power of a series of pieces $n = 100$, a left-hand arrangement of arms is formed along the proston line (cosmic string)

$$P_{Z100} = -4{,}87381Z\,. \qquad (6)$$

Then we notice that the right cosmic linear string has a positive sign before the law of distribution of integer primes, and the left asymmetric linear cosmic string gets a negative sign.

As can be seen from Figure 4, the Whirlpool galaxy has a clearly defined bulge, so it is older than the M109 galaxy in Figure 3. Then a series of residues from a series of integer primes will characterize a spiral galaxy with arms oscillating gravitational waves without a bridge and a bulge. Changes in the central part of the galaxy occur in the course of evolution from the initial cloud of hydrogen to the final void.

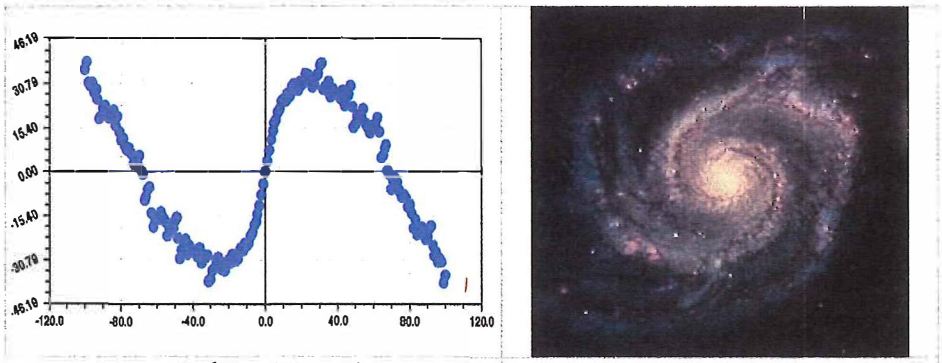

Remainders of (6) series of integer primes $n = 100$

Whirlpool Galaxy [1]

Figure 4. Remnants of the (6) axis of left-sided asymmetry and the Whirlpool Galaxy

Any symmetric series of integer primes in terms of its remainders from the main distribution law contains a pair of oppositely located arms of spiral and other types of galaxies. Apparently, in all types of galaxies there are sleeves, which, due to the lower density of stellar mass, are less noticeable in lenticular, elliptical and other types of galaxies. In our opinion, the arms of irregularly shaped galaxies are less subject to the cosmic string. It is logical to assume that

scattering galaxies are also present in voids, in which the matter mass density becomes less than 10% of the average density of the Universe.

This property of the appearance of arms from the action of a cosmic string opens up wide mathematical possibilities for statistical modeling of a set of measured parameters for specific, primarily, spiral galaxies with narrow bars of the SBd type.

At the same time, a galaxy with two arms, ideal for measurements, is formed by a single cosmic string, while the arms have a filamentous structure (in the form of a macrame with star formation nodes). Then the sleeves gradually twist and loosen, the substance from the sleeves begins to create and thicken the strip. Loan central bar goes into bulge. After the sleeves, the galaxies turn into outer rings. But a small amount of the mass of matter remains in the arms of other types of galaxies, which are barely visible to modern telescopes.

3.2.3. Right-sided asymmetry of the Milky Way. Our galaxy rotates clockwise. Due to difficulties in measurements, Figure 5 shows a modern model of the structure of the Galaxy.

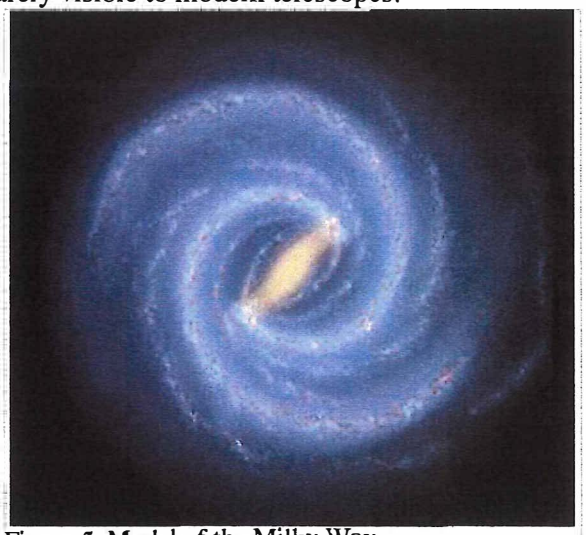

Figure 5. Model of the Milky Way

Four pairs of arms are clearly visible in this figure, indicating multiple absorptions of smaller galaxies. One gets the impression that all the absorbed galaxies also had right-sided asymmetry. As a result, a consistent and complex construction was formed, which we will not place in the classification scheme.

Figure 6 shows several candidates that have been put forward as surrogates for the Milky Way: NGC 891 (edge) and NGC 3124, NGC 3992 or NGC 2336 (face to face) are possible examples. Disputes continue about whether the Galaxy has two or four spiral arms, whether they are asymmetric or not. Even the structure of the central bar is discussed [1].

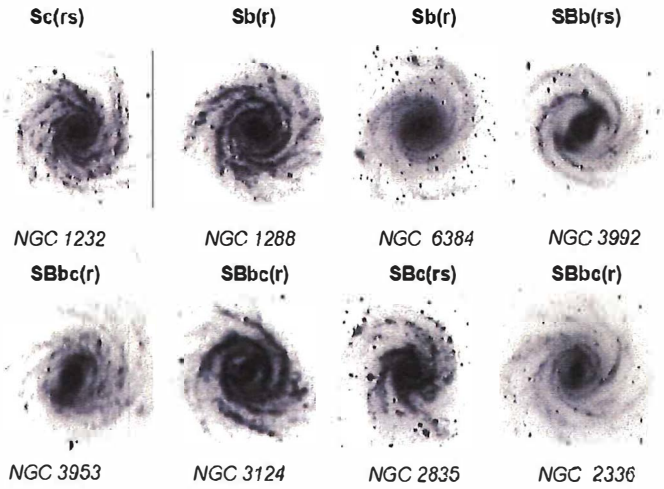

Figure 6. A selection of galaxies similar to the.Milky Way (Efremov, 2011 [4]): NGC 3992 may be closest to the Galaxy

Complex mergers of galaxies of different classes are not discussed in this article.

3.2.4. Merger of oppositely directed galaxies. Of greatest interest in future research will be the merger of two spiral galaxies that rotate in opposite directions (URL: https://zen.yandex.ru/media/id/5cadee0a906b9100b242952a/iz-chego-sostoit-nasha-vselennaia-5cff20f5fa15f800b09723c4), having right and left asymmetries (Fig. 7), and the process will be studied until their complete merging.

Figure 7. The merger of two galaxies (on the left - a galaxy of the right asymmetry, on the right - a galaxy of the left asymmetry)

In this crisis collision of galaxies rotating in different directions, due to the small size on the left, there will be a complete annihilation of this small galaxy with right-hand asymmetry.

The Milky Way and Andromeda both have right-sided asymmetry, so their merger will most likely occur smoothly, without destruction of structures in both large galaxies. It may also turn out that the same asymmetry will cause them to calmly miss each other.

3.**2.5. The fundamental law of the series and its wave complements.** Let's start statistical modeling with a small number of pairs of integer primes.

To do this, we complement the seven values of the center of symmetry in Figure 2 with two integer primes at both ends of the series (negative integer primes -5 and -7, as well as positive prime numbers 5 and 7). Then we get a finite-dimensional minimal series of integer primes with "sleeves" with the cardinality of the series $2n+1 = 11$.

For this series, we obtained (Fig. 8) the basic formula for the cosmic string

$$P_Z = 1{,}25455Z\,. \qquad (7)$$

Then, to model (7), we supplement a series of wave functions in the form of a sum of wavelet signals [7, 11, 14, 20], which can be consistently identified up to further indivisible residues of the additive expansion of a finite-dimensional series of integer primes.

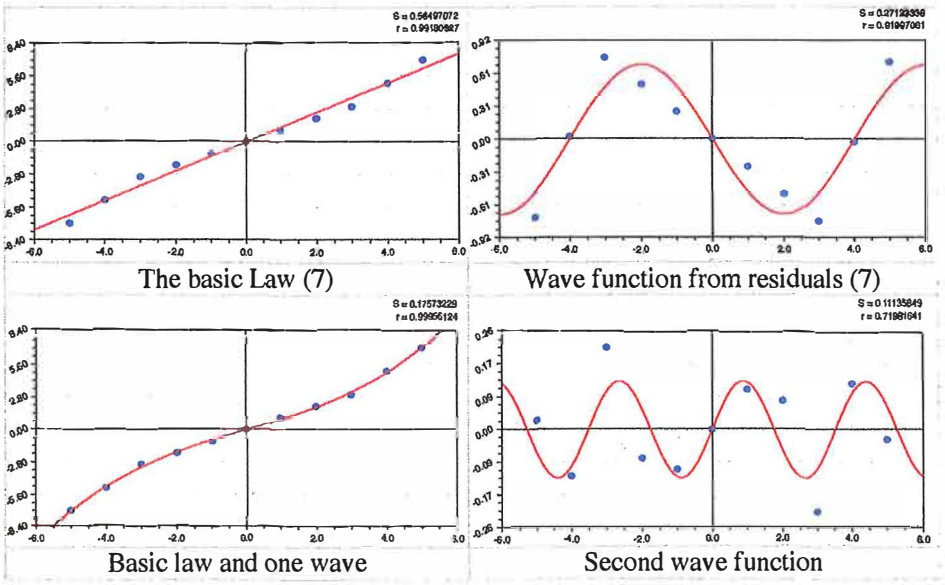

The basic Law (7) | Wave function from residuals (7)

Basic law and one wave | Second wave function

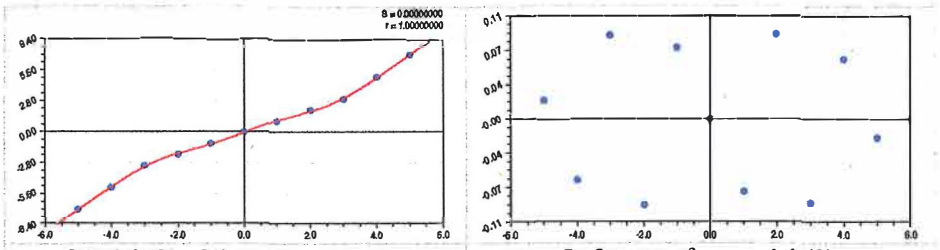

Model (8) of three components Leftovers after model (8)

Figure 8. Wavelet plots for a series of 11 integer primes

For the condition $n = 0$, we obtain the uncertainty ($Z = 0; P_Z \approx 0$) at the center of the kernel of the series of this piece of the series of integer primes.

For cases $n = 1 \vee 2 \vee 3$ near the center of symmetry of a series of integer primes, we have $a(n) = 1$. The angle of inclination of the row axis here is uniquely determined by the value $\pi / 4$. The wave shift from the linear model of the coefficient of proportionality $a(n)$ begins under the condition $n > 3$.

Due to the small number of points, the software environment [2] gives a correlation coefficient equal to one, according to the general formula (Fig. 8) with two additional wave functions (or asymmetric wavelet signals) to the main law

$$P_Z = 3{,}70951Z - 13{,}48069\exp(-0{,}00072644Z) \times$$
$$\times \cos(\pi Z / (15{,}05868 - 0{,}015492Z) - 1{,}57092) +$$
$$+ 0{,}15903\exp(-0{,}0041993Z)\cos(\pi Z / (1{,}82978 - 0{,}0023529Z) - 1{,}58502). \quad (8)$$

The introduction of two wave equations changed the value of the proportionality coefficient from 1.25455 for formula (7) to 3.70951 for equation (8). These wave equations, in our opinion, characterize gravitational waves from oscillatory disturbances from large stars in galaxy spirals. Even accounting for sleeves of two primes changes the proportionality factor by 3.70951 / 1.25455 = 2.957 times. Then it turns out that the arms have a huge fraction of the mass-energy of the entire galaxy. For example, in our Galaxy, stars were found that are up to the middle of the distance from the Milky Way to Andromeda. Then it turns out that the invisible parts of the long arms of two neighboring galaxies have been interacting in the course of evolution for a long time.

Wavelet analysis of even a short series of integer primes can be continued further along the remainders of the previous components. However, the CurveExpert-1.40 software environment does not allow simultaneously identifying a general equation with more than 11 model parameters using 11 pairs of numbers. In addition, in the series, even with 101 pairs of integer primes, the number of components of the general model (1) increases significantly, however, the CurveExpert-1.40 software environment can jointly identify components with a total number of model parameters of no more than 19. To work with all

the parameters of galaxies, a computing environment is required on supercomputers.

In both perturbation waves in model (8), from the main law of the line slope from the center of a series of integer primes, half of the amplitude decreases according to the law of exponential death (Mandelbrot's law), and the half-period decreases from some constant value. At the same time, the initial value of the slope tangent increased from 1.25455 in formula (7) to 3.70951 in formula (8), that is, almost three times.

Thus, changing the number of members of the statistical regularity also changes the values of model parameters of type (3). Therefore, a special software environment for a supercomputer is needed, which allows one to simultaneously identify a complex model containing more than 100 members and more than 1000 parameters on large series of prime numbers (at least up to a million rows).

As a result, purely speculative fundamental strings [21], now having only a hypothetical character, with the use of finite-dimensional series of integer primes in the evolutionary classification of galaxies, turn into objects of experimental research in astrophysics.

3.3. Evolutionary classification of galaxies with right-sided asymmetry

The introduction of the shape of galaxies in the form of remnants from the impact of a stretched cosmic string makes it possible to reverse the schemes of existing classifications (the Hubble sequence, the multilevel morphological classifications of Vaucouleurs, Berg, and others). We have proposed a one-level evolutionary classification of galaxies (Table 3), showing the cycle from the origin to the dissipation of galaxies.

We offer two identical (so far) classification systems:

I) Rsa - classes of right-sided asymmetry of galaxies;

II) Lsa are the classes of left-sided asymmetry of galaxies.

At the current level of astrophysics, both systems are assumed to be equal (independent nonlinear evolutions of galaxies), so let's consider the Rsa classification.

Table 3. Classes of evolutionary morphology of galaxies with right-sided asymmetry (Rsa)

Class	Class name	Existing types
0	Open cosmic strings	Clouds of hydrogen
1	Spiral galaxies with network arms	Gas and dust with stars
2	Spiral galaxies with a bar and two arms	SBd, SBc, SBb, SBa
3	Spiral galaxies with bar, bulge and two arms	SAc, SAb. SAa
4	Spiral galaxies with a bulge and two arms	Sm, Sd, Sc, Sb, Sa
5	Ring galaxies with merging arms	R
6	Lenticular galaxies	S0c, S0b, S0a
7	Nuclear galaxies (rings, bar, lenses in the core)	nr, nb, nl
8	Elliptical and globular galaxies	E7,E6,E5,E4,E3,E2,E1,F0
9	Nuclear-free galaxies (arm remnants)	AC12, AC9-AC1

10	Scattering galaxies (irregular shape)	Irr
11	Void	Supervoid Eridani

In the proposed classification, it is necessary to search for spiral galaxies with network filamentous arms that coincide in shape with the outlines of the remnants after the basic law of a finite-dimensional series of integer primes. Network wide and filamentous narrow arms are considered by us according to the catalog of images obtained by the James Webb telescope (galaxies as photographs by the James Webb telescope).

3.4. Examples of galaxies from the James Webb telescope

Astronomers have been amazed by the complex networks of gas and dust in a nearby galaxy detected by NASA's James Webb Space Telescope (Figure 9).

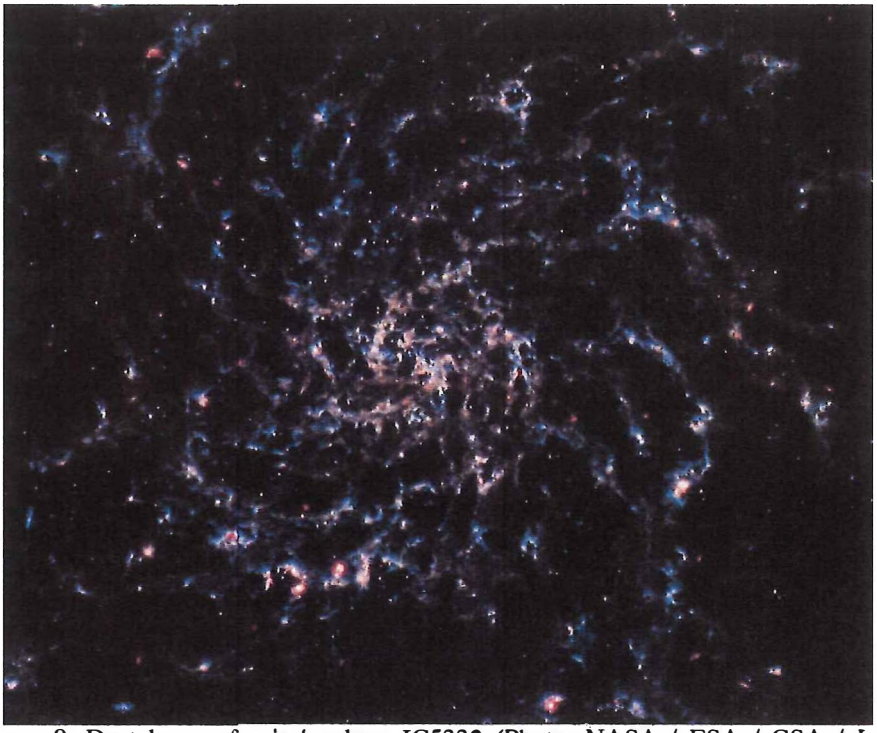

Figure 9. Dust lanes of spiral galaxy IC5332 (Photo: NASA / ESA / CSA / Judy Schmidt, CC BY 2.0, https://mymodernmet.com/james-webb-spiral-galaxies/)

This galaxy has a left-sided asymmetry, and the image shows that the dust lanes are the beginnings of spiral arms. Moreover, there are many more developing spiral arms in comparison with the two classical arms, and they do not have large angles of contact with the center. There is no bar in the center of the galaxy yet. Therefore, this construction, according to the classification scheme from Table 3, belongs to the first class of galaxies. At the same time, it belongs

to the initial types of the first class with a pronounced gas and dust cloud and a small number of stars.

Figure 10 shows two galaxies, NGC 7496 and NGC 628, located near the Milky Way Galaxy, which were imaged using raw data collected together by the James Webb Space Telescope (JWST) (ttps://in.mashable.com/science/35472/james-webb-space-telescopes-raw-data-used-by-scientist-to-form-images-of-two-spiral-galaxies).

The diagram of the construction of the galaxy is already closer to the end of the first class due to the fact that two strongly loosened arms were formed. Moreover, a relatively small bar is visible in the center, which will grow and then this galaxy will move into the second class "Spiral galaxies with a strip and two arms". The galaxy in figure 10 belongs to the right-handed asymmetry.

These two examples show that the class numbers, in fact, show the conditional time of the evolution of galaxies. However, we will not touch on the issue of galaxies of the early age of the Universe (deeper than 12.2 billion years ago), since it is clear that both considered examples refer to galaxies close to the Milky Way. Therefore, we believe that the age of the Universe, and even more so the Big Bang theory, have nothing to do with the process of evolution of individual galaxies and their clusters.

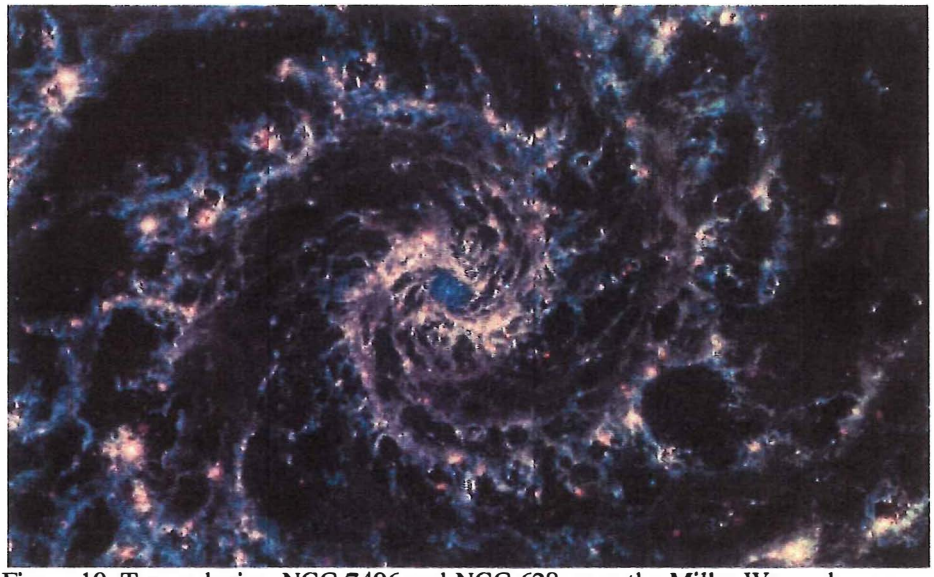

Figure 10. Two galaxies, NGC 7496 and NGC 628, near the Milky Way galaxy were captured using raw data collected by the James Webb Space Telescope (JWST)

Each galaxy is so peculiar that it develops as if on its own, independently organizing itself inside clusters and superclusters of galaxies in the Universe. Therefore, each galaxy is a kind of cosmic organism, which forms some kind of cosmic populations in the form of clusters. In physical essence, the strike of a

cosmic string in a cloud of hydrogen becomes a kind of Big Bang for each newly emerging galaxy in the Universe.

Due to the left and right asymmetry, galaxies have the property of chirality, so each galaxy is a biologically unique cosmic organism. But the asymmetry makes it possible to distinguish among all galaxies two sets Rsa and Lsa, the study of which, even in terms of their abundance in different regions of the Universe, is undoubtedly of great scientific interest.

3.5. Evolution of galaxies by transitions between classes

Let us take the galaxy class scale according to Table 3 as a conditional time scale.

Then the evolution of galaxies can be quantified by some parameters. For example, consider the classes of galaxies according to the average density of comic objects (Table 4) (URL: https://www.calc.ru/169.html https://www.calc.ru/169.html).

Table 4. Average density of space objects by galaxy classes

Space object	Average density, kg/m^3	Power of ten	Class of galaxies
Universe (estimate)	7e-26	-25.2	-
Cluster of galaxies	7e-25	-24.2	0
Interstellar medium	3e-22	-21.5	1
Galaxy (Milky Way)	2e-21	-20.7	3
Globular cluster	4e-18	-17.4	8
Void (our estimate)	1e-27	-27.0	11

According to Table 4, we will take five classes of galaxies as the abscissa, and the power of ten according to the base of the decimal logarithm as the ordinate.

First, a two-term model was obtained (Fig. 11) of the form

User-Defined Model: y=-a*exp(-b*x)-c*exp(d*x). (9)

Coefficient Data:

a = 2.36068821047E+001 b = 5.08551989924E-002 c = 6.75166043655E-003 d = 6.91012212625E-001.

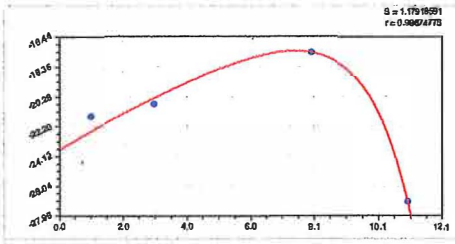

Model (9) of two components

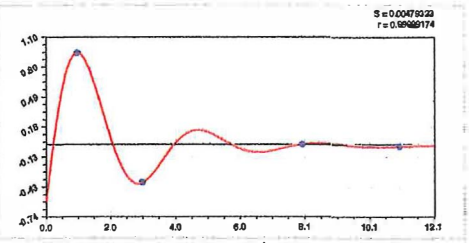

Model (10) of the third component

Figure 11. Graphs of 10y changes in the density of space objects depending on the class of galaxies (in the upper right corner: S - standard deviation; r - correlation coefficient)

Model (9) contains two physical Mandelbrot's laws and has a level of adequacy "superstrong connection" with a correlation coefficient of 0.9867, greater than the level of 0.95.

The third component of the general model (which cannot be combined due to the small amount of data) is the wave equation with a correlation coefficient of 0.99999 (almost close to 1) with an amplitude decaying according to the Mandelbrot law (Fig. 11) according to the formula

User-Defined Model: y=-a*exp(-b*x)*cos(pi*x/c+d). (10)
Coefficient Data:
a = 1.58746236411E+000 b = 4.76808028491E-001 c = 1.86990158717E+000
d = 1.19244505433E+000.

It is known that a necessary condition for the formation of galaxies is the presence of inhomogeneity in the distribution of the mass-energy density in the Universe. Galaxies could arise in those spatial regions in which there were sufficient density fluctuations.

Then equation (10) characterizes the dynamics of the conditions for the emergence of galaxies. From the graph of the third component, in Figure 11, it can be seen that in classes 0-5, the strongest oscillatory disturbances arise in amplitude (Table 5).

On the graphs of Figure 12, the first component shows an increase in the average density of a space object, that is, it characterizes the materialization process in terms of the complication of the chemical composition of visible matter in the Universe.

The second component, on the contrary, characterizes the process of decreasing the average density with increasing galaxy class code, that is, the process of dissipation and simplification of the chemical composition of visible matter. In both processes, hydrogen with a density of 0.0899 kg/m^3 can become the beginning and end.

The antilogarithm of the power -0.01 from Table 5 for the second component gives a value of 0.977 kg/m^3 of the average density for the zero class. Only two chemical elements have a lower density: neon 0.84 kg/m^3 and helium 0.17 kg/m^3. Neon is an inert gas and therefore hardly participates in the dissipation of cosmic matter.

Table 5. Degree 10y and average density of galaxy classes according to models (9) and (10)

Galaxy class	Powers of 10			Dissipation of matter			General power of ten
	y_1	y_2	y_3	$y_2 + y_3$	Density, kg/m^3	Chemical element (gas)	

0	-23.61	-0.01	-0.59	-0.59	0.26	Helium He	-24.20
1	-22.44	-0.01	0.95	0.94	8.71	Xe, Kr, Cl, Ar	-21.50
2	-21.32	-0.03	0.10	0.07	1.17	Nitrogen N	-21.25
3	-20.27	-0.05	-0.38	-0.43	0.37	-	-20.70
4	-19.26	-0.11	0.01	-0.09	0.81	-	-19.35
5	-18.31	-0.21	0.14	-0.07	0.85	-	-18.38
6	-17.40	-0.43	-0.02	-0.45	0.35	-	-17.85
7	-16.54	-0.85	-0.05	-0.90	0.13	-	-17.44
8	-15.72	-1.70	0.02	-1.68	0.02	-	**-17.40**
9	-14.94	-3.39	0.02	-3.37	4.27e-4	-	-18.31
10	-14.20	-6.77	-0.01	-6.78	1.25e-7	-	-20.97
11	-13.49	-13.51	-0.01	-13.51	3.1e-14	-	-27.00

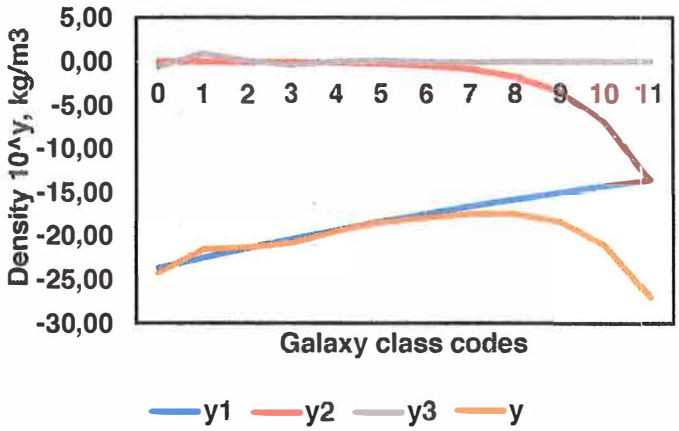

Figure 12. Graphs of changes in the density of space objects depending on the class of galaxies

Due to inhomogeneities in the average density of space objects, the dispersion of matter occurs taking into account additional fluctuations in the perturbation of the density of the first 0-5 classes of galaxies in the third component. Therefore, the dissipation of cosmic matter in the transition from class to class of galaxies is determined by the sum $y_2 + y_3$.

Table 5 shows the calculated values of the dissipation of cosmic matter in sum $y_2 + y_3$ for the power of 10 antilogarithm. This table also shows the average densities for each galaxy class. For a hydrogen cloud (class 0), it turns out that the dissipation of matter occurs only in helium. In this regard, for the zero class, we can offer an indicator - the concentration of helium in a cloud of hydrogen. This indicator becomes a quantitative characteristic for different primary and secondary clouds of hydrogen.

For the first class (spiral galaxies with network arms in gas and dust clouds with stars), four chemical elements (gases) with a density less than the critical value of 8.71 kg/m^3 can become detectors: xenon Xe 4.49; krypton Kr 3.48;

chlorine Cl 2.95 and argon Ar 1.66 kg/m^3. Three elements are inert gases, so chlorine can become a detector for the first class of galaxies. An indicator of the diversity of this class of galaxies is the concentration of chlorine in the studied gas and dust cloud.

For galaxies of the second class (existing types SBd, SBc, SBb, SBa in decreasing concentration), nitrogen N is clearly distinguished at an average density of 1.17 kg/m^3. The same number is found according to theoretical calculations of the dissipation of matter. In classes 3-11, the average density no longer refers to chemical elements, but to sets of simple and complex chemical elements in space objects.

4. CONCLUSION

In nature, there are only two kinds of integer primes: ***right-handed and left-handed asymmetries***. They have a chiral character due to the fact that the direction of the abscissa axis in both types of infinite-dimensional and finite-dimensional series of integer primes remains unchanged, and the directions of the ordinate axis become mirror opposite. All galaxies have specific dimensions. Measurements, for example, in the plane of the galaxy, calculating the coordinates of large stars in spiral arms, will provide statistical material for identifying finite-dimensional series of integer primes.

Any symmetrical series of integer primes in terms of its remainders from the main distribution law contains a pair of oppositely located arms for identifying spiral and other types of galaxies. Apparently, in all types of galaxies there are sleeves, which, due to the lower density of stellar mass, are less noticeable in lenticular, elliptical and other types of galaxies. In our opinion, the arms of irregularly shaped galaxies are less subject to the cosmic string. It is logical to assume that scattering galaxies are also present in voids, in which the matter mass density becomes less than 10% of the average density of the Universe.

This property of the initial appearance of network arms from the impact of a cosmic string opens up wide mathematical possibilities for statistical modeling of a set of measured parameters for specific, primarily spiral SBd, galaxies. At the same time, a galaxy with two arms, ideal for measurements, is formed in the form of a complex filamentary structure. Then the sleeves gradually twist and loosen, the substance from the sleeves begins to create and thicken the bar. Then the bar turns into a bulge. After the sleeves turn into outer rings. But a small amount of matter remains in the arms that are hardly visible to modern telescopes.

The introduction of the shape of galaxies in the form of remnants from the impact of a stretched cosmic string makes it possible to reverse the schemes of existing classifications (the Hubble sequence, the multilevel morphological classifications of Vaucouleurs, Berg, and others). A single-level evolutionary classification of galaxies is proposed, showing the circulation of matter from the origin to the dissipation of galaxies.

The first component of the average density of a space object, depending on the classes of galaxies, shows an increase in the amount of matter with an increase in the class number, that is, it characterizes the materialization process in terms of the complication of the chemical composition of the visible matter in the Universe.

The second component, on the contrary, characterizes the process of decreasing the average density with increasing galaxy class code, that is, the process of dissipation and simplification of the chemical composition of visible matter. Taking into account the third wave component, for a hydrogen cloud (class 0) it turns out that the dissipation of matter occurs only in helium. In this regard, an indicator is proposed - the concentration of helium in a cloud of hydrogen.

For the first class (spiral galaxies with network arms in gas and dust clouds with stars), chlorine can become a detector. Therefore, an indicator of the diversity of this class of galaxies is the concentration of chlorine in the studied gas and dust cloud.

For galaxies of the second class (existing types SBd, SBc, SBb, SBa in decreasing concentration), nitrogen is clearly distinguished at an average density of 1.17 kg/m3. The same number is found according to theoretical calculations of the dissipation of matter. In classes 3-11, the average density no longer refers to individual chemical elements, but to sets of simple and complex chemical elements in space objects.

References

[1] Bland-Hawthorn J., Freeman K., Matteucci F. The Origin of the Galaxy and Local Group // Moore B., Swiss Society for Astrophysics and Astronomy. Berlin; Heidelberg: Springer Berlin Heidelberg, 2014. 254 p. Chapter 1. Bland-Hawthorn J., Freeman K. Near Field Cosmology. Saas-Fee Advanced Course 37, pp. 3-157.

[2] CurveExpert software environment. URL: http://www.curveexpert.net/.

[3] Dokkum P., Pasha I., Buzzo M.L, etal. A Candidate Runaway Supermassive Black Hole Identified by Shocks and Star Formation in its Wake // The Astrophysical Journal Letters, 46:L50 (14pp), 2023 April 1/ URL: https://doi.org/10.3847/2041-8213/acba86.

[4] Efremov Y.N. Astron. Reports 55, 2011, pp. 108–122.

[5] Hogging S. Mathematics slows down ideas. Mathematics complicates the perception of new ideas by society. URL: http://www.gazeta.ru/science/2012/06/26_a_4640149.shtml.

[6] Jarrett T.H. Near-Infrared Galaxy Morphology Atlas // Publications of the Astronomical Society of the Pacific, Vol. 112, No. 774 (August 2000), pp. 1008-1080. URL: https://www.jstor.org/stable/10.1086/316603.

[7] Mazurkin P.M. Asymmetric Wavelet Signal of Gravitational Waves // Applied Mathematics and Physics. 2014. Vol. 2. No. 4. P. 128-134. doi: 10.12691/amp-2-4-2.

[8] Mazurkin P.M. Asymmetric wavelet signals of the cosmological redshift // SF J Astrophyzics, 2018, 1:4. 8 p.

[9] Mazurkin P.M. Block Structure of a Number of the Integers Prime // Applied Mathematics and Physics, vol. 2, no. 4 (2014): 135-145. doi: 10.12691/amp-2-4-3.

[10] Mazurkin P.M. Chaos and Order in the Integers Primes // Applied Mathematics and Physics, vol. 2, no. 4 (2014): 146-156. doi: 10.12691/amp-2-4-4.

[11] Mazurkin P.M. Invariants of the Hilbert Transform for 23-Hilbert Problem // Advances in Sciences and Humanities. 2015. Vol. 1. No. 1. P. 1-12. doi: 10.11648/j.ash.20150101.11.

[12] Mazurkin P.M. Method of identification // 14th International multidisciplinary scientific geoconferenct & SGEM2014. GeoConference jn NANO, BIO AND GREEN – TECHNOLOGIES FOR A SUSTAINABLE FUTURE. Conference proceedincs. Vol. 1. Section Advances in Biotechnology. 17-26 June 2014. Albena, Bulgaria. P. 427-434.

[13] Mazurkin P.M. Oscillatory adaptation of redshift and module of distance in group of 186 supernew MLCS2k2 // SF J Astrophyzics, 2018, 1:4. 19 p.

[14] Mazurkin P.M. Proof the Riemann Hypothesis // American Journal of Applied Mathematics and Statistics. 2014. Vol. 2. No. 1. P. 53-59. doi: 10.12691/ajams-2-2-1.

[15] Mazurkin P.M. Regularities of integer prime numbers. Influence of the x-axis of integers on the positive and negative series of primes. Germany: Palmarium Academic Publishing, 2015. 162 p. (in Russian).

[16] Mazurkin P.M. Riemann's Hypothesis and Critical Line of Prime Numbers. // Advances in Sciences and Humanities. 2015. Vol. 1. No. 1. P. 13-29. doi: 10.11648/j.ash.20150101.12.

[17] Mazurkin P.M. Stable Laws and the Number of Ordinary // Applied Mathematics and Physics. 2014. Vol. 2. No. 2. P. 27-32. doi: 10.12691/amp-2-2-1.

[18] Mazurkin P.M. Standing Wave Angular Height of the Location Of 17088 Supernovae from Azimuth according to Open Catalog for Supernova Data as a Result of the Influence of Visible and Dark Matter, Dark Energy // SF J Astrophysics, 2018, 1:3, 32 p.

[19] Mazurkin P.M. The Limit of the Acceleration and a Further Slowdown in the Expansion of the Universe According 7823 Type 1a Supernova from Open Catalog for Supernova Data // International Journal of Scientific and Innovative Mathematical Research (IJSIMR), 2018. 6(10), pp.28-42. http://dx.doi.org/10.20431/2347-3142.0610005.

[20] Mazurkin P.M. Wavelet Analysis Statistical Data // Advances in Sciences and Humanities. 2015. Vol. 1. No. 2. P. 30-44. doi: 10.11648/j.ash.20150102.11.

[21] Morozov A.Yu. String theory - what is it? // Successes of physical sciences. 1992. Volume 162, No. 8. 175 p. (in Russian).

HADRONIC JOURNAL 46, 293 - 304 (2023)
DOI 10.29083/HJ.46.03.2023/SC293

NUMBER OF PHYSICAL DEGREES OF FREEDOM OF SYSTEMS GOVERNED BY SINGULAR LAGRANGIANS

P. Lam-Estrada[1], J. Y. Montiel-Pérez[2], J. López-Bonilla[3], S. Vidal-Beltrán[3]
[1]ESFM, Instituto Politécnico Nacional, Departamento de Matemáticas,
Edif. 9, Zacatenco, Col. Lindavista 07738, CDMX, México
[2]Centro de Investigación en Computación, Instituto Politécnico Nacional,
CDMX, México
[3]ESIME-Zacatenco, Instituto Politécnico Nacional,
Edif. 4, 1er. Piso, Col. Lindavista 07738, CDMX, México
jlopezb@ipn.mx

Received March 4, 2023

Abstract

We exhibit a simple motivation of the Díaz-Higuita-Montesinos formula about the physical degrees of freedom count in terms of Lagrangian parameters. For several singular Lagrangians we illustrate the validity of this formula to obtain the number of physical degrees of freedom. Besides, we introduce one arbitrary function by each effective gauge parameter to apply the Lanczos version of the Noether theorem, and thus to show the corresponding genuine constraints and their conservation by the time evolution.

Keywords: Constrained Hamiltonian systems, Singular Lagrangians, Noether theorem.

1. Introduction

Recently in [1] was deduced the following relation to obtain the number of physical degrees of freedom (NPDF) for systems controlled by singular Lagrangians:

$$NPDF = N - \frac{1}{2}(l + g + e), \tag{1}$$

where only appear quantities from the Lagrangian scheme, in fact, N, e, l, and g are the total number of generalized coordinates $q_j(t)$, effective gauge parameters [1], genuine constraints and gauge identities [2-6], respectively. This same calculation can be realized via the Hamiltonian formula:

$$NPDF = N - N_1 - \frac{1}{2}N_2\,, \tag{2}$$

using only concepts from the Rosenfeld-Dirac-Bergmann approach [7-15], where N_1 and N_2 are the total number of first-and second-class constraints [16-18], respectively; let's remember that N_2 is an even number [11, 19] and that the number of degrees of freedom is the same for Hamiltonian and Lagrangian formalisms [20].

In Sec. 2 we indicate a simple manner to motivate the expression (1). The Sec. 3 has applications of the matrix and canonical techniques to several Lagrangians studied in [3-5], to exhibit the validity of (1)-(7). In Sec. 4 we employ the Lanczos approach [21-23] to Noether's theorem for each effective gauge parameter, and we observe that the corresponding Euler-Lagrange equations are in terms of the genuine constraints and their time evolution. To save comments and notations it will be evident when certain quantities are satisfied on shell or on the constraint surface (hence we shall eliminate the usual symbol ≈ 0).

2. Díaz-Higuita-Montesinos formula

In [20] was obtained the relation (written in our present notation):

$$l = N_1 + N_2 - N_1^{(p)}, \tag{3}$$

being $N_1^{(p)}$ the total number of first-class primary constraints. On the other hand, the total Hamiltonian H_T already contains all the information about the gauge freedom of the theory, through the first-class primary constraints included in it [20], that is, H_T is the first-class Hamiltonian plus arbitrary linear combinations of the first-class primary constraints $\psi_a = V_{(a)}^m \varphi_m$, $m = 1, \ldots, M$, where M is the amount of primary constraints, such that [12, 16]:

$$C_{(N_1+N_2)xM}\vec{V}_{(a)} \approx 0, \quad a = 1, \ldots, N_1^{(p)}, \quad C = \left(\{\varphi_j, \varphi_m\}\right), \quad j = 1, \ldots, N_1 + N_2, \tag{4}$$

hence $H_T = H_{first-class} + v^a\psi_a$ with $v^a(t)$ totally arbitrary, but we may remember that in the Lagrangian approach [2, 3, 5] the number of arbitrary functions into the gauge transformations coincides with the number of gauge identities, therefore:

$$g = N_1^{(p)} = M - rank\, C. \tag{5}$$

If we accept that the Dirac's conjecture [2, 12, 13, 16, 24-27] is valid, then the N_1 first-class constraints (primary and secondary) generate gauge symmetries into the Hamiltonian formalism and it is natural to identify this freedom with the number of effective gauge parameters in the Lagrangian process:

$$e = N_1, \tag{6}$$

thus, from (3), (5) and (6) we have that $N_1 = e$, $N_2 = l + g - e$ and $N_1^{(p)} = g$, therefore (2) implies the formula (1) obtained by Díaz-Higuita-Montesinos [1].

On the other hand, it is useful to indicate the relations:

$$M = N - rank\, W^{(0)}\,, \qquad l = J - M + rank\, C\,, \tag{7}$$

where M is the amount of primary constraints (with $M' \leq M$ independent constraints), $W_{NxN}^{(0)}$ is the Hessian matrix, $J = N_1 + N_2$ represents the total number of constraints, and $C_{JxM'} = (\{\phi_j, \phi_m\})$.

3. Applications of (1) to singular Lagrangians

Here we consider four Lagrangians whose matrix and canonical analysis allows to show the application of the expressions (1)-(7).

a). Ref. [2]: $\quad L = \frac{1}{2}\dot{q}_1^2 + \dot{q}_1 q_2 + \frac{1}{2}(q_1 - q_2)^2\,, \qquad N = 2\,. \tag{8}$

The Lagrangian method [2-5] gives the Hessian matrix $W^{(0)} = \begin{pmatrix} 1 & 0 \\ 0 & 0 \end{pmatrix}$ whose rank is 1, with only one genuine constraint and one gauge identity:

$$\varphi^{(0,1)} = -q_2 - \dot{q}_1 + q_1\,, \qquad E_1^{(0)} + E_2^{(0)} + \frac{d}{dt}E_2^{(0)} = 0\,, \tag{9}$$

hence $l = g = 1$, and the corresponding local gauge transformations have the following structure:

$$\tilde{q}_1 = q_1 + \varepsilon\,\alpha\,, \qquad \tilde{q}_2 = q_2 + \varepsilon\,(\alpha - \dot{\alpha}), \qquad \varepsilon \ll 1, \tag{10}$$

where α is an arbitrary function, then we have to α and $\dot{\alpha}$ as effective gauge parameters, therefore $e = 2$; with the above information the formula (1) given by Díaz-Higuita-Montesinos implies that $NPDF = 0$.

The Hamiltonian approach [11, 12] applied to (8) generates a total de two constraints:

$$\phi_1 = p_2 \qquad Primary\,, \qquad \phi_2 = p_1 - q_1 \qquad Secondary\,, \tag{11}$$

which are first-class, thus $M = M' = 1$, $N_1 = 2$, $N_2 = 0$, $N_1^{(p)} = 1$, $J = 2$, and $C_{2x1} \equiv O$ because all Poisson brackets [21, 28, 29] $\{\phi_j, \phi_m\}$ worth zero on the constraint region, then $rank\, C = 0$. With these canonical data the expression (2) implies that $NPDF = 0$, the same value as (1); besides, it is simple to verify the validity of (3)-(7).

b). Ref. [30]: $\quad L = \frac{1}{2}[(\dot{q}_2 - e^{q_1})^2 + (\dot{q}_3 - q_2)^2], \qquad N = 3. \tag{12}$

The matrix procedure and (12) lead to $W^{(0)} = \begin{pmatrix} 0 & 0 & 0 \\ 0 & 1 & 0 \\ 0 & 0 & 1 \end{pmatrix}$ such that $rank\, W^{(0)} = 2$, with one gauge identity and two genuine constraints:

$$\begin{aligned} &\dot{q}_1^2\, E_1^{(0)} + \dot{q}_1\, e^{q_1}\, E_2^{(0)} + e^{q_1}\, E_3^{(0)} - \dot{q}_1\, \frac{d}{dt} E_1^{(0)} \\ &\qquad + \frac{d}{dt}\left(-\dot{q}_1\, E_1^{(0)} - e^{q_1}\, E_2^{(0)} + \frac{d}{dt} E_1^{(0)}\right) = 0, \end{aligned} \tag{13}$$

$$\varphi^{(0,1)} = e^{q_1}(\dot{q}_2 - e^{q_1})\,, \qquad \varphi^{(1,1)} = e^{q_1}(q_2 - \dot{q}_3)\,,$$

therefore $l = 2$, $g = 1$, and the gauge transformations take the form:

$$\tilde{q}_1 = q_1 + \varepsilon\, \ddot{\alpha}\, e^{-q_1}\,, \qquad \tilde{q}_2 = q_2 + \varepsilon\, \dot{\alpha}\,, \qquad \tilde{q}_3 = q_3 + \varepsilon\, \alpha\,, \tag{14}$$

hence $e = 3$ because we have to $\alpha, \dot{\alpha}$ and $\ddot{\alpha}$ as effective gauge parameters; in this case the formula (1) gives $NPDF = 0$.

The Lagrangian (12) under the canonical method gives three constraints:

$$\phi_1 = p_1\,, \quad Primary, \qquad \phi_2 = p_2\,, \quad Secondary,$$
$$\phi_3 = p_3\,, \quad Tertiary, \tag{15}$$

and all are first-class, then $M = M' = 1$, $N_1 = 3$, $N_2 = 0$, $N_1^{(p)} = 1$, $J = 3$ and $C_{3x1} = O$, thus from (2) is immediate to deduce that $NPDF = 0$ in harmony with (1). The relations (3)-(7) are verified by this set of values generated by the matrix and Hamiltonian approaches.

c). Refs. [31, 32]: $\quad L = (\dot{q}_1 - q_2)\,\dot{q}_3 + q_1\,q_3\,, \qquad N = 3 \tag{16}$

Now $rank\,W^{(0)} = 2$, with two genuine constraints and one gauge identity:

$$\varphi^{(0,1)} = \dot{q}_3\,, \quad \varphi^{(1,1)} = -q_3\,, \quad E_2^{(0)} + \frac{d}{dt}\left(E_1^{(0)} - \frac{d}{dt}E_2^{(0)}\right) = 0\,, \tag{17}$$

that is, $l = 2$, $g = 1$, and the gauge transformations are given by:

$$\tilde{q}_1 = q_1 + \varepsilon\,\dot{\alpha}, \qquad \tilde{q}_2 = q_2 + \varepsilon\,(\ddot{\alpha} - \alpha), \qquad \tilde{q}_3 = q_3\,, \tag{18}$$

therefore $e = 3$ due to the presence of α and its two derivatives; here $NPDF = 0$ via the Díaz-Higuita-Montesinos formula.

For (16) the Hamiltonian formalism leads to three constraints of first-class:

$$\phi_1 = p_2\,, \quad Primary, \qquad \phi_2 = p_1\,, \quad Secondary,$$
$$\phi_3 = q_3\,, \quad Tertiary, \tag{19}$$

such that $M = M' = 1$, $N_1 = 3$, $N_2 = 0$, $N_1^{(p)} = 1$, $J = 3$, and $C_{3x1} = O$; thus (2) produces the same value as (1), and (3)-(7) are satisfied.

d). Ref. [2]: $L = \frac{1}{2}\,\dot{q}_1^2 + (q_2 - q_3)\,\dot{q}_1 + \frac{1}{2}\,(q_1 - q_2 + q_3)^2\,,\ N = 3$ (20)

Here $rank\,W^{(0)} = 1$, with two gauge identities and one genuine constraint:

$$\varphi^{(0,1)} = -\dot{q}_1 + q_1 - q_2 + q_3\,, \qquad E_2^{(0)} + E_3^{(0)} = 0,$$
$$E_1^{(0)} + E_2^{(0)} + \frac{d}{dt}E_2^{(0)} = 0, \tag{21}$$

consequently $l = 1,\ g = 2,$ participating the gauge transformations:

$$\tilde{q}_1 = q_1 + \varepsilon\,\alpha\,, \quad \tilde{q}_2 = q_2 + \varepsilon\,(\alpha - \dot{\alpha} + \gamma)\,, \quad \tilde{q}_3 = q_3 + \varepsilon\,\gamma\,, \tag{22}$$

where $\alpha, \dot{\alpha}$ and γ are the effective gauge parameters, hence $e = 3$ and (1) implies $NPDF = 0$.

If we apply the canonical method to (20) we find the following three constraints of first-class:

$$\phi_1 = p_2\,, \quad Primary, \qquad \phi_2 = p_3\,, \quad Primary,$$
$$\phi_3 = p_1 - q_1\,, \quad Secondary, \tag{23}$$

then $M = M' = 2,\ N_1 = 3,\ N_2 = 0,\ N_1^{(p)} = 2,\ J = 3,$ and $C_{3x2} = O$; therefore (2) also gives $NPDF = 0$, and the expressions (3)-(7) are verified.

The aim of this Section was to show the use of the relations (1)-(7) with the corresponding set of values from the Lagrangian and Hamiltonian formalisms, and to exhibit the compatibility between the mentioned expressions. In the local transformations (10), (14), (18) and (22) we observe the presence of arbitrary effective gauge parameters, then in the next Section we try to float the information that they hide.

4. Lanczos approach to Noether's theorem

The essence of the Lanczos method [21-23], to obtain information from the invariance of L under an infinitesimal transformation, consists in to

consider the effective gauge parameters as new degrees of freedom for the variational problem under study. Here we apply this idea of Lanczos to the local gauge transformations indicated in Sec. 3.

A. Lagrangian (8):

In this case we have $e = 2$, then we can introduce the functions $\beta_1 = \alpha$ and $\beta_2 = \dot{\alpha}$ as new degrees of freedom; thus (10) takes the form $\tilde{q}_1 = q_1 + \varepsilon\,\beta_1$ & $\tilde{q}_2 = q_2 + \varepsilon\,(\beta_1 - \beta_2)$ producing the following change in the Lagrangian for $\varepsilon \ll 1$:

$$\tilde{L} = L + \varepsilon\left[\beta_1\dot{q}_1 + \dot{\beta}_1(q_2 + \dot{q}_1) + \beta_2(-\dot{q}_1 + q_1 - q_2)\right], \tag{24}$$

and the corresponding Euler-Lagrange equations $\frac{d}{dt}\left(\frac{\partial\tilde{L}}{\partial\dot{\beta}_r}\right) - \frac{\partial\tilde{L}}{\partial\beta_r} = 0$, $r = 1, 2$ imply the relations:

$$\varphi^{(0,1)} = 0, \qquad \frac{d}{dt}\varphi^{(0,1)} = 0, \tag{25}$$

in terms of the genuine constraint and its conservation by the time evolution. In other words, the Lanczos technique shows that the effective gauge parameters store information about the genuine constraints and their time derivative. Besides, let's remember that in [4] was exhibited the connection between the genuine constraints and the non-primary constraints (that is, secondary, tertiary,...) for the Lagrangians considered in the present work.

B. Lagrangian (12):

This system has $e = 3$, hence we employ the functions $\beta_1 = \alpha$, $\beta_2 = \dot{\alpha}$ and $\beta_3 = \ddot{\alpha}$ to implement the Lanczos process via (14) with the structure $\tilde{q}_1 = q_1 + \varepsilon\, e^{-q_1}\beta_3$, $\tilde{q}_2 = q_2 + \varepsilon\,\beta_2$ & $\tilde{q}_3 = q_3 + \varepsilon\,\beta_1$, generating thus a functional change in L:

$$\tilde{L} = L + \varepsilon\, e^{-q_1}\left[\varphi^{(0,1)}\left(\dot{\beta}_2 - \beta_3\right) - \varphi^{(1,1)}\left(\dot{\beta}_1 - \beta_2\right)\right], \tag{26}$$

and the Euler-Lagrange equations for β_r, $r = 1,2,3$ give the conditions:

$$\varphi^{(0,1)} = 0\,, \qquad \frac{d}{dt}\varphi^{(0,1)} - \dot{q}_1\,\varphi^{(0,1)} + \varphi^{(1,1)} = 0\,,$$
$$\frac{d}{dt}\varphi^{(1,1)} - \dot{q}_1\,\varphi^{(1,1)} = 0\,, \tag{27}$$

which is information about the constraints and their time evolution.

C. Lagrangian (16):

We introduce the functions β_r as in the previous case, then (18) acquires the form $\tilde{q}_1 = q_1 + \varepsilon\,\beta_2$, $\tilde{q}_2 = q_2 + \varepsilon\,(\beta_3 - \beta_1)$ & $\tilde{q}_3 = q_3$, and produces the following infinitesimal change:

$$\tilde{L} = L + \varepsilon\left[\varphi^{(0,1)}\left(\dot{\beta}_2 - \beta_3 + \beta_1\right) - \varphi^{(1,1)}\beta_2\right], \tag{28}$$

and from the Euler-Lagrange equations for β_r we obtain the information:

$$\varphi^{(0,1)} = 0\,, \qquad \frac{d}{dt}\varphi^{(0,1)} + \varphi^{(1,1)} = 0. \tag{29}$$

D. Lagrangian (20):

Here we employ (22) with the functions $\beta_1 = \alpha$, $\beta_2 = \dot{\alpha}$ and $\beta_3 = \gamma$, that is, $\tilde{q}_1 = q_1 + \varepsilon\,\beta_1$, $\tilde{q}_2 = q_2 + \varepsilon\,(\beta_1 - \beta_2 + \beta_3)$ & $\tilde{q}_3 = q_3 + \varepsilon\,\beta_3$, therefore:

$$\tilde{L} = L + \varepsilon\left[\left(q_1 - \varphi^{(0,1)}\right)\dot{\beta}_1 + \dot{q}_1\,\beta_1 + \varphi^{(0,1)}\beta_2\right], \tag{30}$$

and the Euler-Lagrange equations for the new degrees of freedom β_r imply (25) with $\varphi^{(0,1)}$ given by (21).

The invariance of L under local gauge transformations leads to constraints, then it is natural that the effective gauge parameters store information about the genuine constraints if they are considered as additional degrees of freedom for the variational problem under analysis; the Lanczos approach allows extract such information.

References

[1] B. Díaz, D. Higuita, M. Montesinos, *Lagrangian approach to the physical degree of freedom count,* J. Math. Phys. **55** (2014) 122901.

[2] H. J. Rothe, K. D. Rothe, *Classical and quantum dynamics of constrained Hamiltonian systems,* World Scientific Lecture Notes in Physics **81**, Singapore (2010).

[3] P. Lam-Estrada, J. López-Bonilla, R. López-Vázquez, G. Ovando, *Lagrangians: Symmetries, gauge identities, and first integrals,* The SciTech, J. of Sci. & Tech. **3**, No. 1 (2014) 54-66.

[4] P. Lam-Estrada, J. López-Bonilla, R. López-Vázquez, G. Ovando, *On the gauge identities and genuine constraints of certain Lagrangians,* Prespacetime Journal **6**, No. 3 (2015) 238-246.

[5] P. Lam-Estrada, J. López-Bonilla, R. López-Vázquez, G. Ovando, *Matrix method to construct point symmetries of Lagrangians,* Bull. of Kerala Mathematics Assoc. **12**, No. 1 (2015) 43-52.

[6] P. Lam-Estrada, J. López-Bonilla, R. López-Vázquez, S. Vidal-Beltrán, *Constraints and gauge relations in the Lagrangian formalism,* World Scientific News **95** (2018) 215-223.

[7] L. Rosenfeld, *On the quantization of wave fields,* Ann. der Phys. **5** (1930) 113-152.

[8] P. Hanson, T. Regge, C. Teitelboim, *Constrained Hamiltonian systems,* Accad. Naz. dei Lincei, Rome (1976).

[9] C. A. Hurst, *Dirac's theory of constraints,* in 'Proc. Recent developments in Mathematical Physics', Eds. H. Mitter, L. Pitter; Springer-Verlag, Berlin (1987) 18-52.

[10] P. Bergmann, *The canonical formulation of general-relativistic theories: The early years, 1930-1959,* in 'Einstein and the history of general relativity', Eds. D. Howard, J. Stachel; Birkhäuser, Boston (1989) 293-299.

[11] A. Wipf, *Hamilton's formalism for systems with constraints,* in 'Canonical gravity: From classical to quantum', Eds. J. Ehlers, H. Friedrich; Springer-Verlag, Berlin (1994) 22-58.

[12] M. Henneaux, C. Teitelboim, *Quantization of gauge systems,* Princeton University Press, NJ (1994).

[13] J. Earman, *Tracking down gauge: an ode to the constrained Hamiltonian formalism,* in 'Symmetries in Physics. Philosophical Reflections', Eds. Katherine Brading, Elena Castellani; Cambridge University Press (2003) 140-162.

[14] D. C. Salisbury, *Rosenfeld, Bergmann, Dirac and the invention of constrained Hamiltonian dynamics,* arXiv: physics/0701299v1 [physics.hist-ph] 25 Jan 2007.

[15] D. C. Salisbury, *Peter Bergmann and the invention of constrained Hamiltonian dynamics,* in 'Einstein and the changing worldviews of Physics', Eds. C. Lehner, J. Renn, M. Schemmel; Einstein Studies **12,** Birkhäuser, Boston (2012) 247-257.

[16] P. Dirac, *Lecture on quantum mechanics,* Yeshiva University, New York (1964).

[17] M. J. Gotay, J. M. Nester, G. Hinds, *Presympletic manifolds and the Dirac-Bergmann theory of constraints,* J. Math. Phys. **19**, No. 11 (1978) 2388-2399.

[18] E. Castellani, *Dirac on gauges and constraints,* Int. J. Theor. Phys. **43,** No. 6 (2004) 1503-1514.

[19] J. N. Goldberg, *Second-class constraints,* in 'On Einstein's path. Essays in honor of Engelbert Schucking', Ed. A. Harvey; Springer-Verlag, New York (1999) 251-256.

[20] G. R. Allcock, *The intrinsic properties of rank and nullity of the Lagrange bracket in the one dimensional calculus of variations,* Phil. Trans. Roy. Soc. London **279**, No. 1290 (1975) 487-545.

[21] C. Lanczos, *The variational principles of mechanics,* University of Toronto Press (1970).

[22] C. Lanczos, *Emmy Noether and calculus of variations,* Bull. Inst. Math. Appl. **9**, No. 8 (1973) 252-258.

[23] P. Lam, J. López-Bonilla, R. López-Vázquez, *On the Noether's theorem,* Prespacetime Journal **6**, No. 4 (2015) 322-325.

[24] R. Cawley, *Determination of the Hamiltonian in the presence of constraints,* Phys. Rev. Lett. **42**, No. 7 (1979) 413-416.

[25] X. Gracia, J. M. Pons, *Gauge generators, Dirac's conjecture, and degrees of freedom for constrained systems,* Ann. of Phys. **187**, No. 2 (1988) 355-368.

[26] M. E. V. Costa, H. O. Girotti, T. J. M. Simes, *Dynamics of gauge systems and Dirac's conjecture,* Phys. Rev. D**32**, No. 2 (1985) 405-410.
[27] A. Cabo, D. Louis-Martínez, *On Dirac's conjecture for Hamiltonian systems with first-and second-class constraints,* Phys. Rev. D**42**, No. 8 (1990) 2726-2735.
[28] S. D. Poisson, *Mémoire sur la variation des constants arbitraries dans les questions de mécanique,* Jour. de l'École Polytechnique **8** (1809) 266-344.
[29] C. Lanczos, *The Poisson bracket,* in 'Aspects of quantum theory', Eds. A. Salam, E. P. Wigner, Cambridge University Press (1972) 169-178.
[30] M. Henneaux, C. Teitelboim, J. Zanelli, *Gauge invariance and degree of freedom count,* Nucl. Phys. B**332**, No. 1 (1990) 169-188.
[31] M. Havelková, *Symmetries of a dynamical system represented by singular Lagrangians,* Comm. in Maths. **20**, No. 1 82012) 23-32.
[32] G. F. Torres del Castillo, *Point symmetries of the Euler-Lagrange equations,* Rev. Mex. Fís. **60** (2014) 129-135.

HADRONIC JOURNAL 46, 305 - 313 (2023)
DOI 10.29083/HJ.46.03.2023/SC305

ZERO-POINT ENERGY CONUNDRUM

J. J. Bevelacqua
Bevelacqua Resources
7531 Flint Crossing Circle SE
Owens Cross Roads, AL 35763 USA
bevelresou@aol.com

Received June 24, 2023
Revised July 18, 2023

Abstract

The zero-point energy concept results in an infinite energy that has not yet been fully resolved. The need for the zero-point energy is confirmed in Santilli's synthesis of the neutron from the proton and the electron in the core of a star.

A possible resolution lies in establishing a cutoff energy (e.g., at the Planck scale) that negates the singularity. This singularity is avoided by establishing a restricted energy region that precludes exceeding the cutoff energy scale except under extreme circumstances (e.g., during a big bang/big crunch event). Potential energy functions, analogous to the Higgs potential or the short range hard core nuclear interaction, are introduced as possible mechanisms to establish the cutoff energy.

Keywords: Quantum Field Theory, Virtual Particles, Zero Point Energy, Planck-scale effect

PACS Index: 11.10.-Z Field Theory, 03.70.+K Quantized Fields, 25.75.Dw Particle Production, 98.80.Cq Particle Theory Models

1.0 Introduction

The zero-point energy (ZPE) concept results in an infinite energy that has not yet been fully resolved [(1)-(2)]. The need for the zero-point energy is confirmed in Santilli's mathematical, theoretical and experimental studies on synthesis of the neutron from the proton and the electron in the core of a star [3]. Santilli [3] refers to the zero-point energy as "universal substratum" with an extremely large energy density for the characterization and propagation of electromagnetic waves at 300,000 km/s.

A possible resolution lies in establishing a cutoff energy (e.g., at the Planck scale) that negates the singularity. In this paper, the cutoff energy restriction is addressed utilizing a spin zero free field Hamiltonian. Since the free field restriction precludes interactions with other particles and antiparticles, particles cannot be created or destroyed in pairs. Therefore, the free field Hamiltonian does not measure the energy of these pairs and the 1/2 quantum energy terms can be interpreted as free fields that are not emerging from or entering into the vacuum in pairs.

Associated with the ZPE issue and the postulated physical effects are fluctuations that are typically quantified in terms of pair production and annihilation in a bubbling quantum foam, the zero-point energy of fermion fields, virtual particle vacuum bubbles and loops, and interacting virtual particles [(4)-(7)]. Although these theoretical arguments have been and continue to be made, there is no experimental basis to select if any of these proposed mechanisms occur.

A number of experiments have been proposed to validate the existence of the ZPE. These include the Casimir effect [8], Lamb shift in hydrogen ([9]-[10]), anomalous magnetic moment of the electron [11], and Fulling-Davies-Unruh effect ([12]-[15]). These theories and associated experiments provide useful information, but are not definitive. These are other possible explanations for the proposed effects including the incorporation of higher order corrections beyond the usually assumed quantum field theory (QFT) interaction terms.

This paper proposes that the ZPE singularity could be avoided by establishing a restricted energy region that precludes exceeding a cutoff energy scale except under extreme circumstances (e.g., during a big bang/big crunch event). The cutoff energy scale is established by introducing a potential energy function that restricts the accessible energy scale.

2.0 Theoretical Approach

The free field Hamiltonian for a spin zero field [16] is

$$H_0^0 = \sum_{k=0}^{\infty} \omega_k \left(N_x(\vec{k}) + 1/2 + N_y(\vec{k}) + 1/2 \right) \qquad (1)$$

where $N_x(\vec{k})$ is the number operator for field particles (x) with three-momentum $\vec{k}$ and $N_y(\vec{k})$ is the number operator for field antiparticles (y) with three-momentum $\vec{k}$. In (1), $\omega^2 - \vec{k}^2 = \mu^2$ where ω is the field quanta energy and μ is the mass of the field particle. The momentum $\vec{k}$ is an eigenstate of the field. For example, the free field, spin zero Hamiltonian operating of the particle ket $|\phi_k\rangle$ yields

$$H_0^0 |\phi_k\rangle = \sum_{k=0}^{\infty} \omega_k \left(N_x(\vec{k}) + 1/2 + N_y(\vec{k}) + 1/2 \right) |\phi_k\rangle \qquad (2)$$

If $|\phi_k\rangle$ is restricted to a single type x particles, (2) becomes

$$H_0^0 |\phi_k\rangle = \left(\omega_k + \sum_{k=0}^{\infty} \omega_k \left(1/2 + 1/2 \right) \right) |\phi_k\rangle \qquad (3)$$

The vacuum adds 1/2 quanta of energy for each $\vec{k}$ for both type x particles and type y antiparticles. These 1/2 quanta are the zero-point energy (ZPE), that is the source of the infinite energy singularity and associated conundrum. (3) illustrates the fact that every state is superimposed on the vacuum.

The infinite energy issue becomes even more obvious by considering the vacuum state $|0\rangle$

$$H_0^0 |0\rangle = \sum_{k=0}^{\infty} \omega_k \left(N_x(\vec{k}) + 1/2 + N_y(\vec{k}) + 1/2 \right) |0\rangle = \sum_{k=0}^{\infty} \omega_k \left(1/2 + 1/2 \right) |0\rangle \qquad (4)$$

Since every state is superimposed on the vacuum, every state has infinite energy. The unrestricted sum in (4) represents the perspective that the vacuum is endowed with infinite energy. Given the infinite energy singularity, the remainder of this paper addresses a possible mechanism, to impose an energy cutoff to mitigate this singularity.

3.0 Normal Ordering

The infinite sum of 1/2 quanta energy noted in (3) and (4) presents a significant challenge in QFT. This infinite energy associated with the vacuum would lead to an extreme curvature within the scope of general relativity. However, this physical effect has not been observed. From a theoretical perspective, the infinite energy singularity is eliminated if the sums of (3) and (4) are terminated at a large but finite energy (e.g., at the Planck scale).

One possibility to mitigate the effects of the infinite sum is to impose normal ordering [16]. Within the scope of normal ordering, all destruction operators in any term are relocated to the right hand side of that term. This operation is justified for operators that commute. For example, the discrete plane wave solutions of the Klein-Gordon equation can be written as [17]

$$\phi(x)=\sum_k \frac{1}{\sqrt{2V\omega_k}} a(\vec{k}) e^{-ikx} + \sum_k \frac{1}{\sqrt{2V\omega_k}} \hat{b}(\vec{k}) e^{ikx} \quad (5)$$

$$\hat{\phi}(x)=\sum_k \frac{1}{\sqrt{2V\omega_k}} b(\vec{k}) e^{-ikx} + \sum_k \frac{1}{\sqrt{2V\omega_k}} \hat{a}(\vec{k}) e^{ikx} \quad (6)$$

where $a(\vec{k})$ ($\hat{a}(\vec{k})$) is an operator that destroys (creates) an x field particle with momentum $\vec{k}$, and $b(\vec{k})$ ($\hat{b}(\vec{k})$) is an operator that destroys (creates) and a y field antiparticle with momentum $\vec{k}$. Normal ordering would have little effect for $\hat{a}(\vec{k})$ and $b(\vec{k})$ because these operators commute.

However, terms such as $\mathbf{a}\left(\vec{\mathbf{k}}\right)$ and $\hat{\mathbf{a}}\left(\vec{\mathbf{k}}\right)$ are more problematic because these operators do not commute. Although normal ordering is commonly utilized in QFT, it violates the non-commutivity property of certain operators that is a fundamental postulate of quantum field theory. Therefore it is reasonable to question the appropriateness of normal ordering to resolve the infinite energy issue.

4.0 Cutoff Potential

There is a lack of theoretical justification in addressing the vacuum infinite energy issue through normal ordering. Efforts to impose an arbitrary energy limit or explaining the ZPE in terms of the Casimir effect, Lamb shift, anomalous magnetic moment of the electron, and Fuller-Davies-Unruh effect were also not universally accepted as a complete explanation of the infinite energy issue ([1]-[2]).

In view of these approaches and their limitations, this paper postulates the existence of an energy cutoff characterized by a potential energy function that mitigates the ZPE singularity. This energy restriction eliminates the singularity and the ZPE issue. Two possible potential forms are presented. These include an analogue to the short range hard core interaction in nuclei [18] and a vacuum potential analogue of the Higgs field ([19]-[20]).

4.1 Hard Core Nuclear Potential Analogue

An energy restriction can be formally defined in terms of a potential function

$$\mathbf{V}(\phi,\omega)=\mathbf{V}_1(\phi,\omega_1)+\mathbf{V}_2(\phi,\omega_2) \qquad (7)$$

where V_1 defines an accessible energy region from $0 \leq \omega \leq \omega_1$ and V_2 represents a potential term that is sufficiently large (e.g., at the Planck scale) to preclude additional particle production from the vacuum. The use of a V_2 term to restrict the accessible parameter space is analogous to the use of a hard core nuclear potential to represent the short range repulsion between nucleons [18]. A hard core precludes the spatial interaction region of nucleons to values typically taken to be about 0.4 fm. The V_2 term effectively terminates the sum of (3) and (4)

$$H_0^0 |0\rangle = \sum_{k=0}^{k_2} \omega_k (1/2+1/2)|0\rangle \qquad (8)$$

where $\omega_2^2 = \vec{k}_2^2 + \mu^2$, ω_2 is the cutoff energy, and $\vec{k}_2$ is the associated three-momentum. Terminating the sum in (8) eliminates the ZPE issue.

4.2 Vacuum Potential Analogue of the Higgs Field

An additional approach facilitates the energy cutoff, and utilizes a potential similar to the Higgs field potential. The Higgs field incorporates an energy scale that characterizes the electroweak interaction. In a similar manner, the analogue vacuum field potential is also characterized by an energy scale (e.g., at the Planck scale) that effectively terminates the (3) and (4) sums, and eliminates the energy singularity. This potential approach is similar to the application of a potential function to characterize the Higgs field.

For specificity, the Higgs analogue potential energy function is assumed to have a form

$$V(\phi) = \mu^2 \hat{\phi}\phi + \lambda(\hat{\phi}\phi)^2 \qquad (9)$$

where μ and λ are not specifically defined, but can be selected to yield the desired energy cutoff. The Higgs field potential can be characterized by the values $\mu \approx 126$ GeV, $\upsilon \approx 246$ Gev, and $\lambda \approx 0.13$ that are derived from the parameterization

$$\mu^2 = 2\lambda\upsilon^2 \qquad (10)$$

For the Higgs field υ represents the energy scale of the electroweak interaction. In a similar manner for the ZPE interaction, υ represents the energy scale that truncates the sum of (8). In (10), μ represents the field particle mass (e.g., at the Planck scale) which has yet to be determined.

5.0 Conclusions

The use of a potential describing the particles generated from the spin zero free field Klein-Gordon Hamiltonian offers a possible resolution to the infinite energy singularity encountered with the vacuum. This singularity known as the zero point energy has not yet been fully resolved.

A possible resolution lies in establishing a cutoff energy (e.g., at the Planck scale) that negates the singularity. This singularity is avoided by establishing a restricted energy region that precludes exceeding the cutoff energy scale except under extreme circumstances (e.g., during a big bang/big crunch event). Potential energy functions, analogous to the Higgs potential or the short range hard core nuclear interaction, provide possible mechanisms to establish the cutoff energy.

References

[1] J. J. Bevelacqua, Possible Planck-scale physical production mechanisms and consequences of negative energies—Initial formulation, Physics Essays **34** (3) (2021), 342-351.
[2] J. J. Bevelacqua, Planck-Scale Quantum Field Theory –II- Evaluation of QED Analogue Amplitudes, Hadronic Journal **45**, (2022), 235-252.
[3] R. M. Santilli, Reduction of Matter in the Universe to Protons and Electrons via the Lie-isotopic Branch of Hadronic Mechanics,
Progress in Physics **19** (2023), 73-99.
https://www.ptep-online.com/2023/PP-65-09.PDF
[4] J. A. Wheeler, On the Nature of Quantum Geometrodynamics, Annal. Phys. **2**, (1967) 604-614.
[5] R. Penrose, Gravitational collapse and space-time singularities, Phys. Rev. Lett. 14, (1965) 57-59.
[6] M. S. Morris and K. S. Thorne, Wormholes in spacetime and their use for interstellar travel: A tool for teaching general relativity, Am. J. Phys. 56, (1988) 395-412.
[7] S. Weinberg, The cosmological constant problem, Rev. Mod. Phys. **61**, (1989) 1-23.
[8] M. S. Morris, K. S. Thorne, and U. Yurtsever, Wormholes, Time Machines, and the Weak Energy Condition, Phys. Rev. Lett. **61**, (1988) 1446-1449.
[9] H. A. Bethe, The Electromagnetic Shift of Energy Levels, Phys. Rev. **72**, (1947) 339-341.
[10] S. L. Bu, Negative Energy: From Lamb Shift to Entanglement, arXiv:1605.08268v1 [physics.gen-ph] 18 May 2016 (2016).
[11] R. F. O'Connell, Effect of the Anomalous Magnetic Moment of the Electron on the Nonlinear Lagrangian of the Electromagnetic Field, Phys. Rev. **176**, (1968) 1433- 1437.
[12] S. A. Fulling, Nonuniqueness of Canonical Field Quantization in Riemannian Space-Time, Phys. Rev. **D7**, (1973) 2850-2862.
[13] W. G. Unruh, Notes on black-hole evaporation, Phys. Rev. **D14**, (1976) 870-892.
[14] P. C. W Davies, Scalar production in Schwarzschild and Rindler metrics, J. Phys. A: Math. Gen. **8**, (1975) 609-616.
[15] G. E. A. Matsas and D. A. T. Vanzella, The Fulling-Davies-Unruh Effect is Mandatory: The Proton's Testimony, arXiv:gr-qc/0205078v1 17 May 2002 (2002).

[16] M. E. Peshkin and D. V. Schroeder, An Introduction to Quantum Field Theory, Boulder, CO, Westview Press (1995).
[17] R. D. Klauber, Mechanism for Vanishing Zero Point Energy, arXiv:astro-ph/0309679v3 19 Jul 2007.
[18] R. Jastrow, On the Nucleon-Nucleon Interaction, Phys. Rev. **81**, (1951) 165-170.
[19] P. W. Higgs, Broken Symmetries, Massless Particles and Gauge Fields, Phys. Lett. **12** (1964), 132-133.
[20] P. W. Higgs, Broken Symmetries and the Masses of Gauge Bosons, Phys. Rev. Lett. **13** (1964), 508-509.

HADRONIC JOURNAL 46, 315 - 338 (2023)
DOI 10.29083/HJ.46.03.2023/SC315

THE STOCHASTIC NATURE OF HIDDEN VARIABLES IN QUANTUM MECHANICS

Piero Chiarelli
National Research Council of Italy,
San Cataldo, Moruzzi 1,
56124, Pisa, Italy
and
Center "E. Piaggio", University of Pisa, Diotisalvi 2,
56122, Pisa, Italy
pchiare@ifc.cnr.it

Received July 12, 2023
Revised August 3, 2023

Abstract

In the present work the author establish the theoretical basis of the hidden variable of the IsoRedShift Mechanics by generalizing the Madelung hydrodynamic representation of the Pauli equation to its stochastic counterpart, which incorporates the noise arising from gravitational background fluctuations. The model reveals that conventional quantum mechanics is applicable only in a perfectly static universal spacetime. In the real case, due to the fluctuations of the spacetime background, originating from the Big Bang and by other cosmological source, the quantum evolution of mass densities and spin waves experience a drag force. The theory demonstrates that the hidden variable parameter, needed for the accurate description of nuclear mechanics, represents the stochastic-induced correction to the conventional quantum mechanics being the deterministic limit of the more general stochastic quantum theory.
The theory shows that the experimental measurements of the hidden variable in nuclear mechanics provide empirical evidence of the presence of dark energy of the fluctuating gravitational background that perturbs the deterministic expression of quantum mechanics resulting in quantum decoherence and giving rise to the emergence of classical mechanics in macroscopic systems.

1 Introduction

The hidden variables in quantum mechanics were introduced firstly by David Bohm [1-3] in 1952 with the theory called "pilot-wave" which incorporated the existence of hidden variables.

According to Bohm, hidden variables are additional properties of particles that exist alongside their quantum state. These variables determine the behavior of particles and provide a more complete classical-like description of their motion, in contrast to the probabilistic nature of standard quantum mechanics.

Bohm's theory sparked significant interest and debate within the scientific community [4-6]. However, it faced challenges due to the famous Bell's theorem, formulated by physicist John Bell in the 1960s. Bell's theorem suggested that hidden variables theories, such as Bohm's, would be incompatible with the predictions of quantum mechanics.

Nonetheless, the exploration of hidden variables continued. Physicists sought to develop alternative theories that could reconcile the probabilistic nature of quantum mechanics with the concept of determinism inherent in hidden variables.

In recent years, new perspectives have emerged, such as the idea of "contextuality" and the concept of "informational completeness." These approaches aim to address the fundamental questions surrounding hidden variables and provide a deeper understanding of the nature of quantum systems.

While the debate on hidden variables in quantum mechanics is ongoing, the exploration of this concepts has contributed to a deeper exploration of the foundations of quantum theory and continues to stimulate new avenues of research in the field.

Ruggero Maria Santilli has made significant contributions [7-12] to the study of hidden variables in quantum mechanics. His work has offered alternative perspectives and mathematical frameworks for understanding the behavior of particles beyond the conventional quantum formalism.

Santilli developed a theory known as "IsoRedShift Mechanics" which introduces new mathematical and conceptual tools for describing hidden variables. This theory incorporates the notion of isodual mathematics, which extends conventional mathematics to include antimatter and other previously unexplored realms.

One of the key aspects of Santilli's theory is the introduction of "hidden symmetries" that can account for the probabilistic nature of quantum mechanics while retaining a deterministic framework. These hidden symmetries provide a more comprehensive description of particle behavior, bridging the gap between

the probabilistic predictions of standard quantum mechanics and the deterministic features of hidden variables theories.
Furthermore, Santilli's contributions extend beyond the theoretical realm. He has developed experimental tests and proposed methods for detecting and observing hidden variables, offering potential avenues for experimental validation of these ideas.
While Santilli's work on hidden variables remains controversial and subject to ongoing debate within the scientific community, his research has opened up new possibilities for exploring the fundamental nature of quantum systems and expanding our understanding of the underlying principles governing their behavior.
Santilli's contributions have sparked further discussions and investigations into the nature of hidden variables and their potential implications for our understanding of quantum mechanics.
In recent works the author, while remaining within the school of thought that hidden variables represent a lack of information about the quantum mechanics, demonstrates [13-16] that, by utilizing Madelung's Hydrodynamic approach, in a spacetime with a stochastic background of gravitational waves, quantum mechanics becomes a stochastic theory, whose deterministic limit is represented by the current quantum mechanics.
Within the framework of the stochastic generalization of quantum hydrodynamics, the author shows [13-14] that it is possible to demonstrate that under suitable conditions, in the limit of a macroscopic-sized physical system, quantum mechanics transitions into a decoherent realization that manifests classical behavior. Moreover, by generalizing the principle of least action in the quantum hydrodynamic formulation, it is obtained that [16-17] quantum decoherence is necessary to obtain the classical principle of least action, and thus theoretically derive classical mechanics and the theory of general relativity.
In this work, employing the hydrodynamic representation of the Pauli equation in the presence of background fluctuations, the author calculates, at first-order of approximation, the corrective stochastic contribution generated by the background vacuum fluctuations.
By comparing the Madelung hydrodynamic representation of Pauli equation, utilizing the iso-matrices, with the stochastic generalization of the hydrodynamic Pauli's equation, the author provides a theoretical expression for the hidden variable contained into the non-unitary iso-matrices thus unveiling their stochastic origin. This output suggests that, rather than hidden variables, we are dealing with a lack of information about how the quantum mechanics realizes itself in the real vacuum owning the gravitational wrinkles originated at the big-

bang and subsequently by the cosmological dynamics, highlighting the need for further development in the field.

2 The quantum potential fluctuations induced by the background of stochastic gravitational waves

The quantum-hydrodynamic representation of the Schrodinger equation [18]

$$-i\hbar\frac{\partial}{\partial t}\psi=\left(\frac{\hbar^2}{2m}\frac{\partial^2}{\partial q_\beta \partial q_\beta}-V_{(q)}\right)\psi \tag{1}$$

for the complex wave function $\psi=|\psi|e^{-\frac{iS}{\hbar}}$, are given by the conservation equation for the mass density $|\psi|^2$

$$\frac{\partial}{\partial t}|\psi|^2+\frac{\partial}{\partial q_i}(|\psi|^2\dot{q}_i)=0 \tag{2}$$

and by the motion equation

$$\ddot{q}_{j(t)}=-\frac{1}{m}\frac{\partial\left(V_{(q)}+V_{qu(n)}\right)}{\partial q_j} \tag{3}$$

where $\dot{q}_i$ is defined, through the momentum $p_i=\frac{\partial S_{(q,t)}}{\partial q_i}$, where $S_{(q,t)}=-\frac{\hbar}{2}ln\frac{\psi}{\psi^*}$ and where

$$V_{qu}=-\frac{\hbar^2}{2m}\frac{1}{|\psi|}\frac{\partial^2|\psi|}{\partial q_i\partial q_i}. \tag{4}$$

In order to introduce the effect of the metric tensor fluctuations of the space-time background, we assume that:

1. The fluctuations of the vacuum curvature are described by the wave function ψ_{vac} with density $|\psi_{vac}|^2$;
2. The (dark) energy density E of the gravitational waves is proportional to $|\psi_{vac}|^2$;

3. The equivalent mass of vacuum fluctuations m_{dark} is defined by the identity
$E = m_{dark} c^2 |\psi_{vac}|^2$

4. The stochastic gravitaional wrinkles originated by the big-bang and the gravitational dynamics of space-time, are approximately assumed to not interact with the physical system (gravitational interaction is sufficiently weak to be disregarded).

In this case the wave function of the overall system ψ_{tot} reads

$$\psi_{tot} \cong \psi\psi_{vac} \tag{5}$$

Moreover, by assuming that, the equivalent mass m_{dark} of the dark energy of gravitational waves is much smaller than the mass of the system (i.e., $m_{tot} = m_{dark} + m \cong m$), the overall quantum potential (1.16) reads

$$\begin{aligned} V_{qu(m_{tot})} &= -\frac{\hbar^2}{2m_{tot}} |\psi|^{-1} |\psi_{vac}|^{-1} \frac{\partial^2 |\psi||\psi_{vac}|}{\partial q_i \partial q_i} \\ &= -\frac{\hbar^2}{2m}\left(|\psi|^{-1} \frac{\partial^2 |\psi|}{\partial q_i \partial q_i} + |\psi_{vac}|^{-1} \frac{\partial^2 |\psi_{vac}|}{\partial q_i \partial q_i} + |\psi|^{-1} |\psi_{vac}|^{-1} \frac{\partial |\psi_{vac}|}{\partial q_i} \frac{\partial |\psi|}{\partial q_i} \right). \end{aligned} \tag{6}$$

Moreover, given the vacuum mass density noise of wave-length λ

$$\delta\rho_{vac(\lambda)} = |\psi_{vac(\lambda)}|^2 \propto cos^2 \frac{2\pi}{\lambda} q \tag{7}$$

associated to the fluctuation wave-function

$$\psi_{vac} \propto \pm cos \frac{2\pi}{\lambda} q, \tag{8}$$

it follows that the quantum potential energy fluctuations read

$$\delta \bar{E}_{qu} = \int_V n_{tot(q,t)} \delta V_{qu(q,t)} dV, \tag{9}$$

where

$$\delta V_{qu(q,t)} = -\frac{\hbar^2}{2m}\left(|\psi_{vac}|^{-1} \frac{\partial^2 |\psi_{vac}|}{\partial q_i \partial q_i} + |\psi|^{-1} |\psi_{vac}|^{-1} \frac{\partial |\psi_{vac}|}{\partial q_i} \frac{\partial |\psi|}{\partial q_i} \right)$$

$$= \frac{\hbar^2}{2m}\left(\left(\frac{2\pi}{\lambda}\right)^2 + |\psi|^{-1} \frac{\partial |\psi|}{\partial q_i} \left(\pm cos \frac{2\pi}{\lambda} q \right)^{-1} \left(\pm sin \frac{2\pi}{\lambda} q \right) \right). \qquad (10)$$

$$= \frac{\hbar^2}{2m}\left(\left(\frac{2\pi}{\lambda}\right)^2 + |\psi|^{-1} \frac{\partial |\psi|}{\partial q_i} tan \frac{2\pi}{\lambda} q \right)$$

For $V \to \infty$, the unidimensional case leads to

$$\delta \bar{E}_{qu(\lambda)} = \frac{1}{\bar{n}_{tot} V} \frac{\hbar^2}{2m} \int_V n_{tot(q,t)} \left(\left(\frac{2\pi}{\lambda}\right)^2 + |\psi|^{-1} \frac{\partial |\psi|}{\partial q_i} tan \frac{2\pi}{\lambda} q \right) dq$$

$$= \frac{1}{\bar{n}_{tot} V} \frac{\hbar^2}{2m} \left(\left(\frac{2\pi}{\lambda}\right)^2 \int_V n_{tot(q,t)} dq + \int_V n_{tot(q,t)} \left(|\psi|^{-1} \frac{\partial |\psi|}{\partial q_i} tan \frac{2\pi}{\lambda} q \right) dq \right) \qquad (11)$$

$$\cong \frac{\hbar^2}{2m}\left(\frac{2\pi}{\lambda}\right)^2$$

In (11) it has been used the normalization condition $\int_V n_{tot(q,t)} dq = \bar{n}_{tot} V$ and, on large volume ($V \gg \lambda_c{}^3$ see (15)), it has been used the approximation

$$lim_{\lambda \to 0} \int_{-\infty}^{\infty} n_{tot(q,t)} \left(|\psi|^{-1} \frac{\partial |\psi|}{\partial q_i} tan \frac{2\pi}{\lambda} q \right) dq \ll \bar{n}_{tot} V \left(\frac{2\pi}{\lambda}\right)^2 . \qquad (12)$$

For the three-dimensional case, (11) leads to

$$\delta \bar{E}_{qu(\lambda)} \cong \frac{\hbar^2}{2m} \sum_i (k_i)^2 = \frac{\hbar^2}{2m} |k|^2 \qquad (13)$$

The result (13) shows that the energy, due to the mass/energy density fluctuations of the vacuum, increases as the inverse squared of λ . Being so, the quantum potential fluctuations, of very short wave length (i.e., $\lambda \to 0$) can lead to unlimited large energy fluctuations even for vanishing noise amplitude $T \to 0$. This

fact could prevent the realization of the deterministic, zero noise, limit (2-4) representing the quantum mechanics.

On the other hand, the convergence to the deterministic limit (2-4) of quantum mechanics for $T \to 0$ is warranted by the fact that uncorrelated fluctuations on shorter and shorted distances are energetically unilkely. Thence, the requirement of convergence to the conventional quantum mechanics for $T \to 0$ imples a supplemental condition on the spatial correlation function of the noise as $\lambda \to 0$.

The calculation of the shape of the spatial correlation function $G(\lambda)$ brings a quite heavy stochastic calculation [19]. A more simple and straight way to calculate $G(\lambda)$ can be obtained by considering the spectrum of the fluctuations.

Since each component of spatial frequency $k = \frac{2\pi}{\lambda}$ brings the quantum potential energy contribution (11), its probability of happening, reads

$$p_{(\lambda)} \propto exp\left[-\frac{\delta \bar{E}_{qu}}{kT}\right] = exp\left[-\frac{\frac{\hbar^2}{2m}\left(\frac{2\pi}{\lambda}\right)^2}{kT}\right] = exp\left[-\left(\frac{\pi\lambda_c}{\lambda}\right)^2\right] \tag{14}$$

where

$$\lambda_c = \sqrt{2}\frac{\hbar}{(mkT)^{1/2}} \tag{15}$$

is the De Broglie length.

From (14) the spectrum $S(k)$ of the spatial frequency reads

$$S(k) \propto p(\frac{2\pi}{\lambda}) = exp\left[-\left(\frac{\pi\lambda_c}{\lambda}\right)^2\right] = exp\left[-\left(\frac{k\lambda_c}{2}\right)^2\right] \tag{16}$$

From (16) we can see that the spectrum is not white and the components with wavelength λ smaller than λ_c go quickly to zero. Besides, from (16) the spatial shape $G(\lambda)$ reads

$$G_{(\lambda)} \propto \int_{-\infty}^{+\infty} exp[ik\lambda]S_{(k)}dk \propto \int_{-\infty}^{+\infty} exp[ik\lambda]\, exp\left[-\left(k\frac{\lambda_c}{2}\right)^2\right]dk$$
$$\propto \frac{\pi^{1/2}}{\lambda_c} exp\left[-\left(\frac{\lambda}{\lambda_c}\right)^2\right] \tag{17}$$

The expression (17) shows that uncorrelated mass density fluctuations on shorter and shorter distance are progressively suppressed by the quantum potential allowing the realization of the conventional "deterministic" quantum mechanics for systems whose physical length is much smaller than the De Broglie one λ_c.

For the sufficiently general case to be of practical interest, where the mass density noise correlation function can be assumed Gaussian with null correlation time, isotropic into the space and independent among different co-ordinates, it can be assumed of the form

$$<\delta n_{(q_\alpha,t)}, \delta n_{(q_\beta+\lambda,t+\tau)}> = <\delta n_{(q_\alpha)}, \delta n_{(q_\beta)}>_{(T)}\ G(\lambda)\delta(\tau)\delta_{\alpha\beta}, \tag{18}$$

that, for system whose physical length $\mathcal{L}$ is much smaller thanthe De Broglie'one (i.e., $\frac{\mathcal{L}}{\lambda_c} \ll 1$), reads

$$G_{(\lambda)} \propto \frac{1}{\lambda_c} exp\left[-\left(\frac{\lambda}{\lambda_c}\right)^2\right] \cong \frac{1}{\lambda_c}\left(1-\left(\frac{\lambda}{\lambda_c}\right)^2\right) \cong \frac{1}{\lambda_c} = \frac{1}{\hbar}\sqrt{\frac{mkT}{2}} \tag{19}$$

On this ansatz, equation (3) assumes the stochastic form [15] (see appendix)

$$\ddot{q}_{j(t)} = -\kappa\dot{q}_{j(t)} - \frac{1}{m}\frac{\partial\left(V_{(q)} + V_{qu(\rho)}\right)}{\partial q_j} + \kappa D^{1/2}\xi_{(t)}. \tag{20}$$

where the probability mass density function ρ is now defined by the Smolukowski conservation equation stemming from (20) and obeys to the

condition $lim_{T\to 0}\,\rho = |\psi|^2$ since by (17-18) the convergence to the quantum mechanics is warranted.

3 The Langevin-Schrodinger equation from the Stochastic Madelung quantum Hydrodynamic

Generally assuming for the stochastic case, the complex field

$$\psi_{(q,t)} = \rho_{(q,t)}^{1/2}\, exp\left[i\frac{S_{(q,t)}}{\hbar}\right], \tag{21}$$

where close to the deterministic limit of quantum mechanics we can utilize the identity $\rho_{(q,t)}^{1/2} \cong |\psi_{(q,t)}|$, it follows that the quantum-hydrodynamic equations (2-4) reads

$$\begin{aligned}\ddot{q}_\alpha &= \frac{1}{m}\frac{d}{dt}\frac{\partial S}{\partial q_\alpha} = \frac{\partial}{\partial t}\frac{\partial S}{\partial q_\alpha} + \frac{1}{m}\frac{\partial^2 S}{\partial q_\alpha \partial q_\beta}\frac{\partial S}{\partial q_\beta} = \frac{\partial}{\partial q_\alpha}\left(\frac{\partial S}{\partial t} + \frac{1}{m}\frac{\partial S}{\partial q_\beta}\frac{\partial S}{\partial q_\beta}\right) \\ &= -\frac{1}{m}\frac{\partial\left(V_{(q)} - \dfrac{\hbar^2}{2m}\dfrac{1}{|\psi|}\dfrac{\partial^2|\psi|}{\partial q_\beta \partial q_\beta} + \kappa S - q_\beta^{1/2} q_\beta^{1/2} m\kappa D^{1/2}\xi_{(t)}\right)}{\partial q_\alpha}\end{aligned} \tag{22}$$

leading to the partial stochastic differential equation

$$m\frac{\partial S}{\partial t} + \frac{\partial S}{\partial q_\beta}\frac{\partial S}{\partial q_\beta} = -\left(V_{(q)} - \frac{\hbar^2}{2m}\frac{1}{|\psi|}\frac{\partial^2|\psi|}{\partial q_\beta \partial q_\beta} + \kappa S - q_\beta^{1/2} q_\beta^{1/2} m\kappa D^{1/2}\xi_{(t)} + C_{(t)}\right). \tag{23}$$

Equation (23) leads to the Langevin-Schrodinger equation, by observing that, for system of physical length $\mathcal{L}$ (such as $\frac{\mathcal{L}}{\lambda_c} \ll 1$), ρ obeys to the Smolukowski conservation equation (see Equations (A.24-27) in appendix) that reads

$$\begin{aligned}&lim_{\frac{\mathcal{L}}{\lambda_c}\to 0}\left(\partial_t \rho_{(q,t)} + \frac{\partial \rho_{(q,t)} < \dot{q} >_i}{\partial q_i} + Q_{diss(q,t)}\right) \\ &\cong \left(\partial_t \rho_{(q,t)} + \frac{\partial \rho_{(q,t)}\dot{q}_i}{\partial q_i} + Q_{diss(q,t)}\right) = 0\end{aligned} \tag{24}$$

where $\rho_{(q,t)} = \int \mathcal{N}(q,p,t)d^3p$ (see (A21, A22-7) in appendix) and

$$Q_{diss(q,t)} = \int \left(\begin{array}{c} 0 \\ \frac{1}{2}\frac{\partial D\mathcal{N}_{(q,p,t)}}{\partial p_\alpha} + \ldots + \frac{1}{n!}\sum_{h=2}^{\infty} \frac{\partial^k C^{(k)}_{\alpha\chi\ldots\ldots\varepsilon}\mathcal{N}_{(q,p,t)}}{\underbrace{\partial p_\chi \ldots \partial p_\varepsilon}_{(k-terms)}} \end{array} \right) d^{3h}p. \qquad (25)$$

In fact, since close to the deterministic limit of quantum mechanics it holds that

$$lim_{\frac{\lambda_c}{\mathcal{L}}\to\infty} < \dot{q} >= \dot{q}, \qquad (26)$$

where $< .... >$ stands for the mean value, and

$$lim_{\frac{\lambda_c}{\mathcal{L}}\to\infty} \rho = |\psi|^2, \qquad (27)$$

it follows that

$$\frac{\partial|\psi|}{\partial t} = -\frac{1}{m}\frac{\partial|\psi|}{\partial q_\alpha}\frac{\partial S}{\partial q_\alpha} - \frac{1}{2m}|\psi|\frac{\partial}{\partial q_\alpha}\frac{\partial S}{\partial q_\alpha} + \frac{Q_{diss(q,t)}}{2|\psi|}. \qquad (28)$$

Equation (28) with the help of (23), leads to the generalized Langevin-Schrodinger equation (GLSE) that for time-independent systems reads

$$-i\hbar\frac{\partial}{\partial t}\psi = \frac{\hbar^2}{2m}\frac{\partial^2}{\partial q_\beta \partial q_\beta}\psi - \left(V_{(q)} + Const + \kappa S - q_\beta^{1/2} q_\beta^{1/2} m\kappa D^{1/2}\xi_{(t)} + i\frac{Q_{diss(q,t)}}{2|\psi|^2} \right)\psi \qquad (29)$$

Close to the deterministic limit of quantum mechancis (i.e., microscopic system with physical length $\mathcal{L}$ much smaller than λ_c) it is possible to characterize the ability of the system to dissipate by the semiempirical parameter α defined by the relation [15] $lim_{\frac{\mathcal{L}}{\lambda_c}\to 0} \kappa \cong lim_{T\to 0}\, \alpha\frac{2kT}{mD}$. On this ansatz, the realization of the quantum mechanics is warranted (see Equation (20)) by the condition $lim_{\frac{\mathcal{L}}{\lambda_c}\to 0} \alpha = 0$. In this case, it can be readily seen that the GLSE (29) reduces to the Schrodinger equation. It is worth mentioning that for highly dissipative systems close to the quantum mechanical limit they obey to the equation

$$\left(i\hbar\frac{\partial}{\partial t} + \frac{\hbar^2}{2m}\frac{\partial^2}{\partial q_\beta \partial q_\beta} - V_{(q)} \right)\psi = i\frac{Q_{diss(q,t)}}{2|\psi|^2}\psi > 0 \qquad (30)$$

4 The canonical Langevin-Schrödinger equation

When non-vanishing drag force is present in microscopic systems even if they are close to the quantum deterministic limit (i.e., $\frac{\mathcal{L}}{\lambda_c} = \varepsilon \ll 1$), Equation (29) does not converges to the conventional quantum mechanics.

When the parameter α remains quite high close to quantum limit such as

$$lim_{\frac{\mathcal{L}}{\lambda_c}\to 0}\ \alpha = \alpha_0 . \qquad (31)$$

Equation (29) converges to the quantum Brownian motion. In fact, under condition (31) and by utilizing dimensional considerations, the following relations apply:

I. $$lim_{\frac{\mathcal{L}}{\lambda_c}\to 0}\ D = lim_{T\to 0}\ \gamma_D\left(\frac{\mathcal{L}}{\lambda_c}\right)^2\frac{\hbar}{2m} = lim_{T\to 0}\ \gamma_D\mathcal{L}^2\frac{kT}{4\hbar} = 0 \qquad (32)$$

II. $$lim_{\frac{\mathcal{L}}{\lambda_c}\to 0}\ \kappa \cong lim_{T\to 0}\ \alpha\frac{2kT}{mD} = \alpha_0\frac{8\hbar}{m\gamma_D\mathcal{L}^2} = finite\ , \qquad (33)$$

III. $$lim_{\frac{\mathcal{L}}{\lambda_c}\to 0}\ Q_{diss(q,t)} = 0\ . \qquad (34)$$

where γ_D is a pure not-null number.

Thus, by (33,34) being $|\frac{Q_{diss(q,t)}}{2|\psi|^2}| << |\kappa S|$, the term $i\frac{Q_{diss(q,t)}}{|\psi|^2}$ can be disregarded in (29) and close to the deterministic limit we have

$$lim_{T\to 0}\ i\hbar\frac{\partial}{\partial t}\psi = -\frac{\hbar^2}{2m}\frac{\partial^2}{\partial q_\beta \partial q_\beta}\psi + \left(V_{(q)} + \kappa S - q_\beta^{1/2}q_\beta^{1/2}m\kappa D^{1/2}\xi_{(t)} + C_{(t)}\right)\psi . \qquad (35)$$

that describes the quantum Brownian motion.

It is worth noting that Equations (29,35) can be derived by the integrability of the velocity field $\dot{q}_\beta = \frac{1}{m}\frac{\partial S}{\partial q_\beta}$ that can be warranted close to the quantum behaviour, but that it may fail in macroscopic large-scale classical system since, generally speaking, the velocity field is not-integrable.

5 The stochastic quantum hydrodynamic equation for charged particles

For charged particles the Schrodinger equation [18] reads

$$i\hbar\left(\frac{\partial}{\partial t} - e\phi\right)\psi = \frac{1}{2m}\left(\frac{\hbar}{i}\frac{\partial}{\partial q_\beta} - eA_\beta\right)^2 \psi \tag{36}$$

leading to the quantum hydrodynamic equations [18]

$$\frac{\partial}{\partial t}|\psi|^2 + \frac{\partial}{\partial q_i}(|\psi|^2\,\dot{q}_i) = 0 \tag{37}$$

$$m\ddot{q}_i = \frac{e}{m}\left(E_i + \varepsilon_{kli}\dot{q}_k B_l\right) - \frac{\partial V_{qu}}{\partial q_i}, \tag{38}$$

where in this case the quantum potential reads

$$V_{qu} = -\frac{\hbar^2}{2m}\frac{1}{|\psi|}\frac{\partial^2|\psi|}{\partial q_i \partial q_i}. \tag{39}$$

Following the same procedure of section 2, equations (37-38), in presence of gravitational background fluctuations, lead to stochastic hydrodynamic motion equation

$$\ddot{q}_{j(t)} = -\kappa\dot{q}_{j(t)} + \frac{e}{m^2}\left(E_i + \varepsilon_{kli}\dot{q}_k B_l\right) - \frac{1}{m}\frac{\partial V_{qu}}{\partial q_i} + \kappa D^{1/2}\xi_{(t)} \tag{40}$$

Equation (40), in the case of constant vector potential (i.e., $\dot{A} = 0$), leads to the Langevin-Schrodinger equation for charged particles that reads

$$lim_{T\to 0}\, i\hbar\left(\frac{\partial}{\partial t} - e\phi\right)\psi = \frac{1}{2m}\left(\frac{\hbar}{i}\frac{\partial}{\partial q_\beta} - eA_\beta\right)^2 \psi + \left(\kappa S - q_\beta^{1/2} q_\beta^{1/2} m\kappa D^{1/2}\xi_{(t)} + C_{(t)}\right)\psi \tag{41}$$

6 The stochastic quantum hydrodynamic equation for charged particles with spin

For charged particles with spin the Schrodinger equation [18] leads to the Pauli's equation

$$i\hbar\left(\frac{\partial}{\partial t}-e\phi\right)\Psi=\left(\frac{1}{2m}\left(\frac{\hbar}{i}\frac{\partial}{\partial q_\beta}-eA_\beta\right)^2-\mu B_i\sigma_i\right)\Psi \tag{42}$$

where

$$\Psi=\begin{pmatrix}\psi_1\\ \psi_2\end{pmatrix}=\begin{pmatrix}\chi_1\\ \chi_2\end{pmatrix}|\Psi|^2\,e^{i\frac{S}{\hbar}}=\begin{pmatrix}cos\frac{\vartheta}{2}e^{-i\frac{\varphi}{2}}\\ sin\frac{\vartheta}{2}e^{i\frac{\varphi}{2}}\end{pmatrix}\rho e^{i\frac{S}{\hbar}} \tag{43}$$

$$|\Psi|^2=\Psi^\dagger\Psi \tag{44}$$

where the probability density of magnetic moment is identified by the vector

$$\boldsymbol{\mu}=\mu\Sigma=\mu\Psi^\dagger\sigma\Psi \tag{45}$$

whose versor n reads

$$n=\left(sin\vartheta cos\varphi, sin\vartheta sin\varphi, cos\vartheta\right)=\frac{\Psi^\dagger\sigma\Psi}{\Psi^\dagger\Psi}=\frac{\Sigma}{\rho} \tag{46}$$

leading to the quantum hydrodynamic equations [18]

$$\frac{\partial}{\partial t}|\Psi|^2+\frac{\partial}{\partial q_i}(|\Psi|^2\,\dot{q}_i)=0 \tag{47}$$

$$m\ddot{q}_i=\frac{e}{m}\left(E_i+\varepsilon_{kli}\dot{q}_k B_l\right)-\frac{1}{m}\frac{\partial V_{qu}}{\partial q_i}+\frac{\hbar^2}{4m^2}\frac{1}{|\Psi|^2}\frac{\partial}{\partial q_j}\left(\frac{\partial n_k}{\partial q_i}\right)\left(\frac{\partial n_k}{\partial q_j}\right) \tag{48}$$

$$\dot{n}_i=\frac{2\mu}{\hbar}\left(n\times B\right)_i+\frac{\hbar}{2m}\frac{\varepsilon_{ilm}}{|\Psi|^2}\frac{\partial}{\partial q_j}\left(|\Psi|^2\,n_l\frac{\partial}{\partial q_j}n_m\right) \tag{49}$$

where

$$V_{qu}=-\frac{\hbar^2}{2m}\frac{1}{|\Psi|}\frac{\partial^2|\Psi|}{\partial q_i\partial q_i}, \tag{50}$$

For the stochastic problem, the deterministic variables transform into the corresponding probabilistic distributions following the association $|\psi|^2 \rightarrow \rho$ and

$$n \rightarrow P(n). \tag{51}$$

In the deterministic limit when $\delta n \rightarrow 0$, since the noise correlation function (18) warrants the convergence to the quantum mechanics, we have that

$$lim_{\,\delta n \rightarrow 0} < P(n) > = n \tag{52}$$

and, for the stationary eigenstates (i.e., $\dot{n} = 0$ and $\dot{q} = 0$),

$$lim_{\,\delta n \rightarrow 0} < \dot{P}(n) > = \dot{n} = 0 \tag{53}$$

$$lim_{\,\delta n \rightarrow 0} < \dot{q} > = \dot{q} = 0. \tag{54}$$

where $< .... >$ stands for the mean value.

Therefore, the difference between the pseudo potential of the deterministic spin motion equation (49),

$$\frac{\hbar}{2m} \frac{\varepsilon_{ilm}}{|\Psi|^2} \frac{\partial}{\partial q_j} \left(|\Psi|^2 \, n_l \frac{\partial}{\partial q_j} n_m \right) = \frac{1}{|\Psi|^2} \frac{\partial}{\partial q_j} N_{ij}(|\Psi|^2, n), \tag{55}$$

and its stochastic counterpart $\frac{1}{\rho} \frac{\partial}{\partial q_j} N_{ij}(\rho, P(n))$, at first order as a function of $\dot{P}(n)$ and $\dot{q}$ (close to the deterministic limit and near stationary condition (53)) can be developed in series expansion as

$$\begin{aligned} &\frac{1}{\rho} \frac{\partial}{\partial q_j} N_{ij}(\rho, P(n)) - \frac{1}{|\Psi|^2} \frac{\partial}{\partial q_j} N_{ij}(|\Psi|^2, n) \\ &\cong C + A\dot{P}(n) + B\dot{q} \cong C_i + A_{ij} \dot{n}_j - \kappa_{s\rho_{ij}} \dot{q}_{j(t)} \end{aligned} \tag{56}$$

Moreover, by generally posing

$$A_{ij} \dot{n}_j = -\left(\frac{\Psi^\dagger \kappa_{ss_{ij}} \sigma_j \Psi}{\Psi^\dagger \Psi} \right) \tag{57}$$

and, since from (53) $lim_{\,\delta n \rightarrow 0} < C > = 0$,

$$C_i = \kappa_{s\rho ij} D^{1/2}_{\rho s_j} \xi_{(t)}, \tag{58}$$

the stochastic spin motion equation (49) reads

$$\begin{aligned} \dot{n}_i = \left(\frac{\Psi^\dagger \sigma_i \Psi}{\Psi^\dagger \Psi} \right)^{\cdot} = \frac{2\mu}{\hbar}(n \times B) + \frac{\hbar}{2m} \frac{\varepsilon_{ilm}}{|\Psi|^2} \frac{\partial}{\partial q_j} \left(n_l \frac{\partial}{\partial q_j} n_m \right) \\ - \left(\frac{\Psi^\dagger \kappa_{ss_{ij}} \sigma_j \Psi}{\Psi^\dagger \Psi} \right)^{\cdot} - \kappa_{s\rho_{ij}} \dot{q}_{j(t)} + \kappa_{s\rho ij} D^{1/2}_{s\rho_j} \xi_{(t)} \end{aligned} \tag{59}$$

Furthermore, if we consider the more simplified situation of stationary mass density distribution with only spin waves noisy oscillations, equation (59) reduces to

$$\dot{n}_i = \frac{2\mu}{\hbar}(n \times B) + \frac{\hbar}{2m} \frac{\varepsilon_{ilm}}{|\Psi|^2} \frac{\partial}{\partial q_j} \left(n_l \frac{\partial}{\partial q_j} n_m \right) - \left(\frac{\Psi^\dagger \kappa_{ss_{ij}} \sigma_j \Psi}{\Psi^\dagger \Psi} \right)^{\cdot} + \kappa_{s\rho ij} D^{1/2}_{s\rho_j} \xi_{(t)} \tag{60}$$

7 The quantum hydrodynamic equation for charged particles with Santilli spin iso-matrices

By utilizing the iso-matrices [12] in the form

$$\hat{\sigma}_i = \sigma_i + \Delta\sigma_i, \tag{61}$$

where

$$\Delta\sigma_1 = \begin{pmatrix} 0 & \lambda - 1 \\ \lambda^{-1} - 1 & 0 \end{pmatrix} \tag{62}$$

$$\Delta\sigma_2 = \begin{pmatrix} 0 & -i(\lambda - 1) \\ i(\lambda^{-1} - 1) & 0 \end{pmatrix} \tag{63}$$

$$\Delta\sigma_3 = \begin{pmatrix} \lambda^{-1} - 1 & 0 \\ 0 & -(\lambda - 1) \end{pmatrix} \tag{64}$$

the iso-spin versor of the Madelung quantum hydrodynamic description reads

$$\hat{n} = \frac{\Psi^\dagger \hat{\sigma} \Psi}{\Psi^\dagger \Psi} = \frac{\Psi^\dagger \sigma \Psi}{\Psi^\dagger \Psi} + \frac{\Psi^\dagger \Delta\sigma \Psi}{\Psi^\dagger \Psi} = n + \frac{\Psi^\dagger \Delta\sigma \Psi}{\Psi^\dagger \Psi} \tag{65}$$

and the spin motion equation (49, 55) reads

$$\dot{\hat{n}} = \frac{2\mu}{\hbar}(n \times B) + \frac{1}{\rho}\partial_j N_{ij} + \left(\frac{\Psi^\dagger \Delta\sigma \Psi}{\Psi^\dagger \Psi} \right)^{\bullet} \tag{66}$$

By comparing (59) with (66), that is to assume that the iso-spin reproduces the stochastic perturbation of the gravitational background onto the quantum mechanics, it follows that

$$\begin{aligned} \dot{\hat{n}}_i &= \frac{2\mu}{\hbar}(n \times B) + \frac{1}{\rho}\partial_j N_{ij} + \left(\frac{\Psi^\dagger \Delta\sigma_i \Psi}{\Psi^\dagger \Psi} \right)^{\bullet} = \dot{n}_i \\ &= \frac{2\mu}{\hbar}(n \times B)_i + \frac{1}{\rho}\partial_j N_{ij} - \left(\frac{\Psi^\dagger \left(\kappa_{(i)ss}\sigma_i\right)\Psi}{\Psi^\dagger \Psi} \right)^{\bullet} + \kappa_{s\rho} D_{s\rho}^{1/2} \xi_{(t)} \end{aligned} \tag{67}$$

and, therefore, that

$$\left(\frac{\Psi^\dagger \Delta\sigma_i \Psi}{\Psi^\dagger \Psi} \right)^{\bullet} = -\left(\frac{\Psi^\dagger \kappa_{ss_{ij}} \sigma_j \Psi}{\Psi^\dagger \Psi} \right)^{\bullet} + \kappa_{s\rho} D_{s\rho}^{1/2} \xi_{(t)} \tag{68}$$

Moreover, since the fluctuations $\kappa_{s\rho} D_{\rho s}^{1/2} \xi_{(t)}$ due to the gravitational background are quite small respect the drag term $\left(\frac{\Psi^\dagger \kappa_{ss_{ij}} \sigma_j \Psi}{\Psi^\dagger \Psi} \right)^{\bullet}$ (that is to say that we experience or measure a sort of mean value of the hidden variables), it follows that

$$\Delta\sigma_i = -\kappa_{ss_{ij}} \sigma_j, \tag{69}$$

that, for $\lambda = 1 - \varepsilon$ with $\varepsilon \ll 1$, leads to

$$\Delta\sigma_1 = \begin{pmatrix} 0 & \lambda - 1 \\ \lambda^{-1} - 1 & 0 \end{pmatrix} = \begin{pmatrix} 0 & -\varepsilon \\ \varepsilon & 0 \end{pmatrix} = -\kappa_{ss_{1j}} \sigma_j = -\kappa_{ss_{11}} \begin{pmatrix} 0 & 1 \\ 1 & 0 \end{pmatrix} \tag{70}$$

$$\Delta\sigma_2 = \begin{pmatrix} 0 & -i(\lambda - 1) \\ i\left(\lambda^{-1} - 1\right) & 0 \end{pmatrix} \cong \begin{pmatrix} 0 & i\varepsilon \\ i\varepsilon & 0 \end{pmatrix} = -\kappa_{ss_{2j}} \sigma_j = -\kappa_{ss_{22}} \begin{pmatrix} 0 & -i \\ i & 0 \end{pmatrix} \tag{71}$$

$$\Delta\sigma_3 = \begin{pmatrix} \lambda^{-1}-1 & 0 \\ 0 & -(\lambda-1) \end{pmatrix} \cong \begin{pmatrix} \varepsilon & 0 \\ 0 & \varepsilon \end{pmatrix} = -\kappa_{ss_{3j}}\sigma_j = -\kappa_{ss_{33}}\begin{pmatrix} 1 & 0 \\ 0 & -1 \end{pmatrix} \tag{72}$$

and therefore,

$$\kappa_{ss_{ij}} = (1-\lambda)\begin{pmatrix} \begin{pmatrix} 1 & 0 \\ 0 & -1 \end{pmatrix} & 0 & 0 \\ 0 & \begin{pmatrix} 1 & 0 \\ 0 & -1 \end{pmatrix} & 0 \\ 0 & 0 & \begin{pmatrix} -1 & 0 \\ 0 & 1 \end{pmatrix} \end{pmatrix} \tag{73}$$

From (73) it is worth noting that in the deterministic limit of standard quantum mechanics, for $\lambda = 1$, we have that $\kappa_{(i)ss} = 0$.

Under the light of the stochastic quantum hydrodynamic theory, the standard quantum mechanics represents the particular case that is realized in static space-time without the fluctuating background of gravitational dark-energy.

The evolution of quantum mechanical densities, within spacetime containing a gravitational noisy background, perceive the presence of such noisy dark energy as a field that generates a drag force on spin waves oscillations as well as on the motion of the mass density. This phenomenon bears resemblance to the effect of the Higgs Boson, whose field imparts inertia to elementary particles traversing through it.

It is worth noting that such gravitational induced drag force generates the quantum decoherence on macroscopic system and potentially leads to the appearance of the classical behavior on large sized systems [13-17, 19].

8 Conclusion

By extending the Madelung hydrodynamic representation of the Pauli equation to its stochastic counterpart, which incorporates the noise arising from gravitational background fluctuations, it becomes feasible to establish the theoretical basis about the hidden variable of the IsoRedShift Mechanics model. The model reveals that canonical quantum mechanics is applicable only in a perfectly static universal spacetime. In the real case, due to the fluctuations of the spacetime background, originating from the Big Bang and by other cosmological source, the quantum evolution of mass densities and spin waves experience a drag force. The theory demonstrates that the hidden variable

parameter, needed for the accurate description of nuclear mechanics, represents the stochastic-induced correction to the conventional quantum mechanics representing the deterministic limit of the stochastic quantum theory.
The experimental measurements of the hidden variable in nuclear mechanics provide empirical evidence of the presence of dark energy of the fluctuating gravitational background that perturbs the deterministic expression of quantum mechanics. Generally speaking, the quantum mechanics realizes itself in a stochastic form, possibly resulting in quantum decoherence and giving rise to the emergence of classical mechanics in macroscopic systems.

References

1. D. Bohm, "A Suggested Interpretation of the Quantum Theory in Terms of 'Hidden Variables' I and II." Physical Review, Vol. 85, Issue 2, pp. 166-179 (1952).
2. D. Bohm, B. J. Hiley, "The Undivided Universe: An Ontological Interpretation of Quantum Theory." Routledge, New York (1993).
3. D. Bohm, "Causality and Chance in Modern Physics." Routledge, New York (2007).
4. J. S. Bell, "On the Einstein Podolsky Rosen Paradox." Physics Physique Физика, Vol. 1, No. 3, pp. 195-200 (1964).
5. A. Aspect, P. Grangier, and G. Roger, "Experimental Tests of Realistic Local Theories via Bell's Theorem." Physical Review Letters, Vol. 47, Issue 7, pp. 460-463 (1981).
6. A. Peres, "Quantum Theory: Concepts and Methods." Kluwer Academic Publishers, Dordrecht (1993).
7. R. M. Santilli, "Foundations of Theoretical Mechanics: The Inverse Problem in Newtonian Mechanics." Springer, New York (1978).
8. R. M. Santilli, "Hadronic Mechanics and Nonpotential Interactions." Hadronic Press, Palm Harbor (1995).
9. R. M. Santilli, "Isodual Theory of Antimatter: with Applications to Antigravity, Grand Unification and Cosmology." Springer, New York (2006).
10. R. M. Santilli. "A Quantitative Representation of Particle Entanglements via Bohm's Hidden Variable According to Hadronic Mechanics." Progress in Physics, Vol. 1, pp. 150-159 (2002).
11. R.M., Santilli, Sobczyk, G. Representation of nuclear magnetic moments via a Clifford algebra formulation of Bohm's hidden variables. *Sci Rep* **12**, 20674 (2022). https://doi.org/10.1038/s41598-022-24970-4 .

12. R. M. Santilli. "Apparent Resolution of the Coulomb Barrier for Nuclear Fusions Via the Irreversible Lie-admissible Branch of Hadronic Mechanics." Progress in Physics, Vol. 1, pp. 61-78 (2002).
13. Chiarelli, P., Quantum to Classical Transition in the Stochastic Hydrodynamic Analogy: The Explanation of the Lindemann Relation and the Analogies Between the Maximum of Density at He Lambda Point and that One at Water-Ice Phase Transition, Physical Review & Research International, 3(4): 348-366, 2013.
14. Chiarelli, P., The quantum potential: the missing interaction in the density maximum of He^4 at the lambda point?, Am. J. Phys. Chem.. **2**(6) (2014) 122-131.
15. Chiarelli, S., Chiarelli, P., Stochastic Quantum Hydrodynamic Model from the Dark Matter of Vacuum Fluctuations: The Langevin-Schrödinger Equation and the Large-Scale Classical Limit, Open Access Library Journal 2020, Volume 7, e6659, DOI: 10.4236/oalib.1106659.
16. Chiarelli, P., Beyond General Relativity: Exploring Quantum Geometrization of Spacetime, BP International, 2023, in Press.
17. Chiarelli, P., The Spinor-Tensor Gravity of the Classical Dirac Field, Symmetry 2020, 12, 1124; doi:10.3390/sym12071124 .
18. Birula, I.B.; Cieplak, M.; Kaminski, J. *Theory of Quanta*; Oxford University Press: New York, NY, USA, 1992, pp 80-111;
19. Chiarelli, P. Can fluctuating quantum states acquire the classical behavior on large scale? *J. Adv. Phys.* **2013**, *2*, 139–163.
20. Y.B., Rumer, M.S., Ryvkin Thermodynamics, Statistical Physics, and Kinetics. Moscow: Mir Publishers; 1980; 269.

Appendix

In presence of curvature fluctuations, the mass distribution density (MDD) $|\psi|^2 = \tilde{n}$ becomes a stochastic function that we can ideally pose $\tilde{n} = \overline{n} + \delta n$ where δn is the fluctuating part and $\overline{n}$ is the regular one that obeys to the limit condition

$$lim_{T\to 0}\, \tilde{n} = lim_{T\to 0}\, \overline{n} = |\psi|^2 . \qquad \text{(A1)}$$

The characteristics of the Madelung quantum potential that, in presence of stochastic noise, fluctuates, can be derived by generally posing that is composed by the regular part $\overline{V_{qu(n)}}$ (to be defined) plus the fluctuating one V_{st} such as

$$V_{qu(\tilde{n})} = -\frac{\hbar^2}{2m}\tilde{n}^{-1/2}\frac{\partial^2\tilde{n}^{1/2}}{\partial q_\beta \partial q_\beta} = \overline{V_{qu(\tilde{n})}} + V_{st}\,. \tag{A2}$$

where the stochastic part of the quantum potential V_{st} leads to the force noise

$$-\frac{\partial V_{st}}{\partial q_i} = m\varpi_{(q,t,T)}\,. \tag{A3}$$

where the noise correlation function reads

$$\begin{aligned}\lim_{T\to 0} <\varpi_{(q_\alpha,t)},\varpi_{(q_\beta+\lambda,t+\tau)}> &= \lim_{T\to 0} <\varpi_{(q_\alpha)},\varpi_{(q_\beta)}>_{(T)}\; G(\lambda)\delta(\tau)\delta_{\alpha\beta} \\ &\approx \frac{<\varpi_{(q_\alpha)},\varpi_{(q_\beta)}>_{(T)}}{\lambda_c}\cdot\delta(\tau)\delta_{\alpha\beta}\end{aligned} \tag{A4}$$

with

$$\lim_{T\to 0} <\varpi_{(q_\alpha)},\varpi_{(q_\beta)}>_{(T)} = 0 \tag{A5}$$

Besides, the regular part $\overline{V_{qu(\tilde{n})}}$, for microscopic systems ($\frac{\mathcal{L}}{\lambda_c} \ll 1$), without loss of generality, can be rearranged as

$$\overline{V_{qu(\tilde{n})}} = -\frac{\hbar^2}{2m}\overline{\left(\tilde{n}^{-1/2}\frac{\partial^2\tilde{n}^{1/2}}{\partial q_\beta \partial q_\beta}\right)} = -\frac{\hbar^2}{2m}\frac{1}{\rho^{1/2}}\frac{\partial^2\rho^{1/2}}{\partial q_\beta \partial q_\beta} + \overline{\Delta V} = V_{qu(\rho)} + \overline{\Delta V} \tag{A6}$$

where $\rho_{(q,t)}$ is the probability mass density function (PMD) associated to the stochastic process we are going to define that in the deterministic limit obeys to the condition $lim_{T\to 0}\,\rho_{(q,t)} = lim_{T\to 0}\,\tilde{n} = lim_{T\to 0}\,\overline{n} = |\psi|^2$.

Given the quantum hydrodynamic equation of motion (3) for the fluctuating MDD $\tilde{n} = \overline{n} + \delta n$,

$$\ddot{q}_\alpha = -\frac{1}{m}\frac{\partial\left(V_{(q)} + V_{qu(\tilde{n})}\right)}{\partial q_\alpha} \tag{A7}$$

we can rearrange it as

$$\ddot{q}_\alpha = -\frac{1}{m}\frac{\partial\left(V_{(q)} + V_{qu(\rho)} + \frac{\hbar^2}{2m}\left(\frac{1}{\rho^{1/2}}\frac{\partial^2\rho^{1/2}}{\partial q_\beta \partial q_\beta} - \frac{1}{\tilde{n}^{1/2}}\frac{\partial^2\tilde{n}^{1/2}}{\partial q_\beta \partial q_\beta}\right)\right)}{\partial q_\alpha}, \tag{A8}$$

The term

$$\frac{\partial}{\partial q_\alpha}\left(\frac{1}{\rho^{1/2}}\frac{\partial^2\rho^{1/2}}{\partial q_\beta \partial q_\beta} - \frac{1}{\tilde{n}^{1/2}}\frac{\partial^2\tilde{n}^{1/2}}{\partial q_\beta \partial q_\beta}\right) \tag{A9}$$

that in the deterministic case is null since

$$\lim_{\frac{\mathcal{L}}{\lambda_c}\to 0 \text{ or } T\to 0} \tilde{n} = \lim_{\frac{\mathcal{L}}{\lambda_c}\to 0 \text{ or } T\to 0} \left(\bar{n} + \delta n\right) = \bar{n} \equiv \rho, \tag{A10}$$

generates an additional acceleration in the motion equation (A8), which close to the stationary condition (i.e., $\dot{q}=0$), can be developed in the series approximation and reads

$$\frac{\partial}{\partial q_\alpha}\left(\frac{1}{\rho^{1/2}}\frac{\partial^2\rho^{1/2}}{\partial q_\beta \partial q_\beta} - \frac{1}{\tilde{n}^{1/2}}\frac{\partial^2\tilde{n}^{1/2}}{\partial q_\beta \partial q_\beta}\right) \cong A_0 + A_1\dot{q} + ... + A_n\dot{q}^n + O(\tfrac{\mathcal{L}}{\lambda_c}). \tag{A11}$$

Moreover, since near the limiting condition (A10) we can pose

$$\lim_{\frac{\mathcal{L}}{\lambda_c}\to 0} \tilde{n}_{(q)} = \lim_{\frac{\mathcal{L}}{\lambda_c}\to 0} \bar{n}_{(q)} + \delta n_{(q,t)} \cong \rho_{(q)} + \varepsilon_{(q)}\delta n_{(t)}, \tag{A12}$$

with $\lim_{\frac{\mathcal{L}}{\lambda_c}\to 0} \varepsilon_{(q)} = 1$ and where $\varepsilon_{(q)}$ is smooth with $\frac{\partial^2\varepsilon^{1/2}}{\partial q_\beta \partial q_\beta}$ finite (since $\lambda_c \gg \mathcal{L} \neq 0$), it follows that

$$\lim_{\frac{\mathcal{L}}{\lambda_c}\to 0}\left(\frac{\partial}{\partial q_\alpha}\frac{1}{\rho^{1/2}}\frac{\partial^2\rho^{1/2}}{\partial q_\beta\partial q_\beta}-\frac{\partial}{\partial q_\alpha}\frac{1}{\tilde{n}^{1/2}}\frac{\partial^2\tilde{n}^{1/2}}{\partial q_\beta\partial q_\beta}\right)$$

$$\cong \lim_{\frac{\mathcal{L}}{\lambda_c}\to 0}\frac{\partial}{\partial q_\alpha}\left(\frac{1}{\rho^{1/2}}\frac{\partial^2\rho^{1/2}}{\partial q_\beta\partial q_\beta}-\frac{1}{\rho^{1/2}}\frac{\partial^2\rho^{1/2}\left(1+\frac{\varepsilon_{(q)}\delta n_{(t)}}{2\rho}\right)}{\partial q_\beta\partial q_\beta}\right), \tag{A13}$$

$$\cong \delta n_{(t)}\frac{\partial}{\partial q_\alpha}\left(-\frac{1}{\rho^{1/2}}\frac{\partial^2\frac{\varepsilon_{(q)}}{2\rho^{1/2}}}{\partial q_\beta\partial q_\beta}\right)$$

,

Moreover, given that at the stationary condition (i.e., $<\dot{q}>=\lim_{\Delta t\to\infty}\frac{1}{\Delta t}\int_{t-\frac{\Delta t}{2}}^{t\frac{\Delta t}{2}}\dot{q}_{(q,\tau)}d\tau=0$) it holds

$$\bar{n}_{(q)(T=0)}=\lim_{T\to 0}<\tilde{n}_{(q)}>=\lim_{T\to 0}\lim_{\Delta t\to\infty}\frac{1}{\Delta t}\int_{t-\frac{\Delta t}{2}}^{t\frac{\Delta t}{2}}\tilde{n}_{(q,\tau)}d\tau$$

$$=\tilde{n}_{(q)(T=0)}+\lim_{T\to 0}\lim_{\Delta t\to\infty}\frac{1}{\Delta t}\int_{t-\frac{\Delta t}{2}}^{t\frac{\Delta t}{2}}\delta n_{(t)}d\tau \quad , \tag{A14}$$

$$\cong\bar{n}_{(q)(T=0)}+\lim_{T\to 0}<\delta n_{(t)}>_{(T)}$$

and thus

$$\lim_{T\to 0 or\frac{\mathcal{L}}{\lambda_c}\to 0}<\delta n_{(t)}>_{(T)}=0, \tag{A15}$$

the mean $<A_0>$, by (A13) reads

$$\lim_{\frac{\mathcal{L}}{\lambda_c}\to 0} < A_0 >= \lim_{\frac{\mathcal{L}}{\lambda_c}\to 0} \lim_{\dot{q}\to 0} < \frac{\partial}{\partial q_\alpha}\left(\frac{1}{\rho^{1/2}}\frac{\partial^2\rho^{1/2}}{\partial q_\beta \partial q_\beta} - \frac{1}{\tilde{n}^{1/2}}\frac{\partial^2\tilde{n}^{1/2}}{\partial q_\beta \partial q_\beta}\right) >$$

$$\cong \lim_{\frac{\mathcal{L}}{\lambda_c}\to 0} < \delta n_{(t)} > \frac{\partial}{\partial q_\alpha}\left(-\frac{1}{\rho^{1/2}}\frac{\partial^2 \frac{\varepsilon_{(q)}}{2\rho^{1/2}}}{\partial q_\beta \partial q_\beta}\right) = 0 \tag{A16}$$

Therefore, the general form of the stochastic term A_0 as the zero-mean noise, with null correlation time (see (A4)), reads

$$A_0 = m\kappa D^{1/2}\xi_{(t)}. \tag{A17}$$

Thence, at leading order in $\dot{q}$, sufficiently close to the deterministic limit of quantum mechanics ($\frac{\mathcal{L}}{\lambda_c} \ll 1$), we obtain that

$$\begin{aligned}\frac{\hbar^2}{2m}\frac{\partial}{\partial q_\alpha}\left(\frac{1}{\rho^{1/2}}\frac{\partial^2\rho^{1/2}}{\partial q_\beta \partial q_\beta} - \frac{1}{\tilde{n}^{1/2}}\frac{\partial^2\tilde{n}^{1/2}}{\partial q_\beta \partial q_\beta}\right) &\cong m\kappa D^{1/2}\xi_{(t)} + A_1\dot{q} + O\left((\frac{\mathcal{L}}{\lambda_c})^2\right) \\ &\cong \frac{\partial}{\partial q_\alpha}\left(m\kappa D^{1/2}\xi_{(t)}q_\alpha + \kappa S\right) + O\left((\frac{\mathcal{L}}{\lambda_c})^2\right)\end{aligned} \tag{A18}$$

The first order approximation (A18) allows to write (A7) as the Marcovian process

$$\ddot{q}_{j(t)} = -\kappa\dot{q}_{j(t)} - \frac{1}{m}\frac{\partial\left(V_{(q)} + V_{qu(\rho)}\right)}{\partial q_j} + \kappa D^{1/2}\xi_{(t)}. \tag{A19}$$

where

$$\rho_{(q,t)} = \int_{-\infty}^{+\infty} \mathcal{N}_{(q,p,t)} d^3p \ , \tag{A20}$$

where

$$\mathcal{N}(q,\dot{q},t) = \int P(q,\dot{q},z,\dot{z},|\,t,0)\mathcal{N}_{(z,\dot{z},0)} d^3z d^3\dot{z} \tag{A21}$$

where $P(q,\dot{q},z,\dot{z},|\,t,0)$ is the probability transition function of the Smolukowski conservation equation [20]

$$P(q,p,q_0,p_0|(t'+\tau-t_0),t_0)=\int_{-\infty}^{\infty}P(q,p,q',p'|\tau,t')P(q',p',q_0,p_0|t'-t_0,t_0)d^3q'd^3p' \tag{A22}$$

of the Marcovian process (A19).
Moreover, by comparing (A7) in the form

$$\ddot{q}_\alpha=-\frac{1}{m}\frac{\partial\left(V_{(q)}+\overline{V_{qu(\tilde{n})}}+V_{st}\right)}{\partial q_\alpha}=-\frac{1}{m}\frac{\partial\left(V_{(q)}+V_{qu(\rho)}+\overline{\Delta V}+V_{st}\right)}{\partial q_\alpha} \tag{A23}$$

with (A18), it follows that

$$\overline{\Delta V}=\frac{\hbar^2}{2m}\left(\frac{1}{\rho^{1/2}}\frac{\partial^2\rho^{1/2}}{\partial q_\beta\partial q_\beta}-\overline{\left(\tilde{n}^{-1/2}\frac{\partial^2\tilde{n}^{1/2}}{\partial q_\beta\partial q_\beta}\right)}\right)\cong\kappa S \tag{A24}$$

and that

$$V_{st}=q_\beta^{1/2}q_\beta^{1/2}\kappa D^{1/2}\xi_{\alpha(t)}. \tag{A25}$$

HADRONIC JOURNAL 46, 339 - 358 (2023)
DOI 10.29083/HJ.46.03.2023/SC339

QUANTUM HEAT ENGINES AND THE GENERALIZED UNCERTAINTY PRINCIPLE

Gardo Blado, Jonathan Nguyen, Giovani Renteria,
Sklylar Gay, Bryce Mortimer
Physics Discipline
College of Science and Engineering
Houston Christian University
7502 Fondren Rd.
Houston, TX 77074 USA
gblado@hbu.edu

Received July 1, 2023
Revised August 3, 2023

Abstract

We study the effects of the generalized uncertainty principle (GUP) on the efficiency of quantum heat engines based on a particle in an infinite square well using the partition function approach. In particular, we study the Carnot and Otto heat engines. For the system we used, the GUP-corrected efficiencies turned out to be lower than efficiencies without the GUP effects. However, as expected, GUP effects increase as the temperature of the cold heat bath decreases and as the width of the potential well decreases.

Key words: generalized uncertainty principle, quantum Carnot engine, quantum Otto engine, quantum engine, infinite square well

1. Introduction

The efforts to unify the two pillars of modern physics namely general relativity and quantum mechanics, to a theory of quantum gravity (QG), continue to this day. QG effects are expected to be strong at the Planck scale. Unfortunately, this scale is beyond the reach of experiments. Hence, physicists focus on predictions which are independent of QG models (such as string theory, asymptotically safe QG and loop QG). One such prediction is the emergence of a minimal length. The presence of a minimal length leads to the modification of the Heisenberg uncertainty principle[1] to a Generalized uncertainty principle (GUP). The GUP has led to numerous phenomenological studies [4-10, 15-22]. The present paper will explore the application of the GUP to quantum thermodynamics by studying GUP-effects on the efficiency of Carnot and Otto engines. We will consider a particle subjected to an infinite square well potential (ISW) in thermal equilibrium with a heat bath [11].

The paper is organized as follows. A general discussion on how to calculate the efficiency of a quantum heat engine using the partition function of a particle in an infinite square well is done in section 2. The general formula derived in section 2 to calculate the heat involved in the processes is then applied to the quantum Carnot and quantum Otto cycles in sections 3 and 4 respectively to derive known results. Section 5 derives a corresponding general formula to compute the GUP-corrected heat energy. This general formula is applied to get the GUP-corrected efficiencies of the quantum Carnot and Otto cycles in sections 6 and 7 respectively. Finally, some conclusions are discussed in the last section.

2. Quantum Heat Engine

Let us first outline the approach we will take in calculating the efficiency. Our approach follows [11] and [12]. We will calculate the efficiency as.

$$\eta = \frac{W}{Q_{in}} = \frac{Q_{in} - |Q_{out}|}{Q_{in}} = 1 - \frac{|Q_{out}|}{Q_{in}}. \tag{1}$$

The heat involved is calculated using the entropy,

$$\Delta S = \oint \frac{dQ}{T}. \tag{2}$$

[1] Some of the first studies on the modification of the Heisenberg Uncertainty Principle and the associated algebra were done by Santilli [1-3].

To calculate the entropy, we use the partition function Z.

$$Z \equiv \sum_{n=1}^{\infty} e^{-\beta E_n} \tag{3}$$

with the β parameter defined by

$$\beta \equiv \frac{1}{kT} \tag{4}$$

where k is the Boltzmann's constant. From Z, we calculate the free energy

$$F = -\frac{1}{\beta} ln\, Z \tag{5}$$

and internal energy

$$U = -\frac{\partial}{\partial \beta} ln\, Z. \tag{6}$$

From F and U, we get the entropy [13, 12]

$$S = k\beta(U - F). \tag{7}$$

As mentioned above, we consider a quantum heat engine based on a particle confined in an infinite square well (ISW) potential in thermal equilibrium with a heat bath. The energy of a particle in an ISW [14] is

$$E_n = \gamma n^2 \tag{8}$$

where we define

$$\gamma \equiv \frac{\pi^2 \hbar^2}{2mL^2} \tag{9}$$

with m the mass of the particle in the well of width L and $n = 1,2,3, \ldots$. From (3), for the infinite square well, we have $Z = \sum_{n=1}^{\infty} e^{-\beta \gamma n^2}$. For sufficiently large mass m of the particle in the well, the energy levels can be very close together to make the approximation [11, 13],

$$Z = \sum_{n=1}^{\infty} e^{-\beta \gamma n^2} \approx \int_0^{\infty} dn\, e^{-\beta \gamma n^2} = \frac{1}{2}\sqrt{\frac{\pi}{\beta \gamma}}\,. \tag{10}$$

Using this partition function, we get from (3), (5), (6) and (7), the entropy

$$S = \frac{k}{2} + k\, ln\left(\frac{1}{2}\sqrt{\frac{\pi}{\beta \gamma}}\right) = S_0 - \frac{1}{2} k\, ln(\beta \gamma) == \frac{k}{2} + k\, ln\left(\frac{1}{2}\sqrt{\frac{\pi}{\beta \gamma}}\right) \tag{11}$$

with the constant, $S_0 \equiv \frac{k}{2} + k \ln\left(\frac{\sqrt{\pi}}{2}\right)$. From (2) and (11), let us calculate the heat involved when a particle in an infinite square well goes from an initial state i to a final state f. From (2), we have

$$dQ = \frac{dS}{k\beta} \tag{12}$$

where the entropy is a function of β and γ, $S(\beta,\gamma)$. Hence $dS = \frac{\partial S}{\partial \beta}d\beta + \frac{\partial S}{\partial \gamma}d\gamma$ and from (11), we get $dS = -\frac{k}{2\beta}d\beta - \frac{k}{2\gamma}d\gamma$. Hence (12) becomes $dQ = -\frac{d\beta}{2\beta^2} - \frac{d\gamma}{2\beta\gamma}$. Integrating the preceding equation from an initial state i to a final state f, we get

$$Q_{if} = \frac{1}{2}\left(\frac{1}{\beta_f} - \frac{1}{\beta_i}\right) - \frac{1}{2}\int_i^f \frac{d\gamma}{\beta\gamma} \tag{13}$$

Let us next use (13) to find the efficiencies of the quantum Carnot and quantum Otto engines involving a particle in an infinite square well. For future reference, we note that we impose a condition [12, 11].

$$\beta\gamma = k_0 = \text{constant} \tag{14}$$

in the adiabatic process, which is apparently consistent with (11) ($\Delta S = 0$). Physically, adiabatic processes are possible when we vary both L and T together such that $\beta\gamma$ is constant for a particular mass of the working substance.

3. Quantum Carnot Cycle

The classical Carnot cycle is illustrated in Figure 1. Processes AB and CD are isothermal processes at temperatures T_h and T_l respectively with $T_h > T_l$. The heat Q_h enters the system at the process AB while the heat loss of Q_l occurs in the process CD.

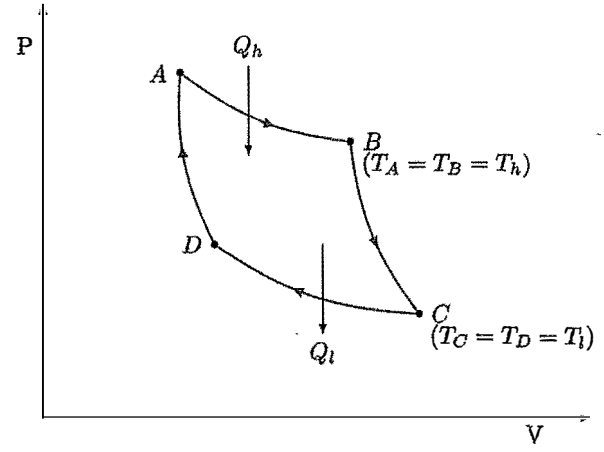

Figure 1: Classical Carnot Cycle

Processes BC and DA are adiabatic expansion and compression processes respectively. In introductory physics classes the Carnot cycle is discussed as the most efficient heat engine with an efficiency of $\eta_{\substack{classical\\Carnot}} = 1 - \frac{T_l}{T_h}$. In transitioning to the quantum Carnot cycle, we use the equivalent isothermal and adiabatic processes as in the classical Carnot cycle [11].

For the Carnot cycle, (1) becomes $\eta = 1 - \frac{|Q_{out}|}{Q_{in}} = 1 - \frac{|Q_l|}{Q_h}$. Let us calculate Q_l and Q_h for the Carnot cycle. For an isothermal process, we get from (13)

$$Q_{isothermal} = -\frac{1}{2\beta}\int_i^f \frac{d\gamma}{\gamma} = -\frac{1}{2\beta} ln\left(\frac{\gamma_f}{\gamma_i}\right). \tag{15}$$

Hence for AB and CD:

$$Q_{AB} = -\frac{1}{2\beta_h} ln\left(\frac{\gamma_B}{\gamma_A}\right) = -\frac{1}{\beta_h} ln\left(\frac{L_A}{L_B}\right) = \frac{1}{\beta_h} ln\left(\frac{L_B}{L_A}\right) \tag{16}$$

and

$$Q_{CD} = -\frac{1}{2\beta_l} ln\left(\frac{\gamma_D}{\gamma_C}\right) = -\frac{1}{\beta_l} ln\left(\frac{L_C}{L_D}\right) \tag{17}$$

where we used (9). For the adiabatic process Q_{BC}, (13) gives

$$Q_{BC} = \frac{1}{2}\left(\frac{1}{\beta_l} - \frac{1}{\beta_h}\right) - \frac{1}{2}\int_B^C \frac{d\gamma}{\beta\gamma} \tag{18}$$

Evaluating the integral using (14), $\frac{1}{2}\int_B^C \frac{d\gamma}{\beta\gamma} = \frac{1}{2k_0}(\gamma_C - \gamma_B) = \frac{\gamma_C}{2k_0} - \frac{\gamma_B}{2k_0}$. But $k_0 = \beta_C\gamma_C = \beta_B\gamma_B$ so we can write $\frac{1}{2}\int_B^C \frac{d\gamma}{\beta\gamma} = \frac{\gamma_C}{2\beta_C\gamma_C} - \frac{\gamma_B}{2\beta_B\gamma_B} = \frac{1}{2}\left(\frac{1}{\beta_C} - \frac{1}{\beta_B}\right) = \frac{1}{2}\left(\frac{1}{\beta_l} - \frac{1}{\beta_h}\right)$. Hence, (18) yields

$$Q_{BC} = 0. \tag{19}$$

Similarly, we can show

$$Q_{DA} = 0. \tag{20}$$

Note that from (16) and (17) $Q_{AB} = Q_h > 0$ since there is an expansion from $A \rightarrow B$ while $Q_{CD} = Q_l < 0$ since there is a compression from $C \rightarrow D$. Hence from (1), (16) and (17) we get

$$\eta = 1 - \frac{|Q_l|}{Q_h} = 1 - \frac{|Q_{CD}|}{Q_{AB}} = 1 - \frac{\frac{1}{\beta_l} ln\left(\frac{L_C}{L_D}\right)}{\frac{1}{\beta_h} ln\left(\frac{L_B}{L_A}\right)} = 1 - \frac{T_l}{T_h}\frac{ln\left(\frac{L_C}{L_D}\right)}{ln\left(\frac{L_B}{L_A}\right)}. \tag{21}$$

Note for the adiabatic processes $\beta_C\gamma_C = \beta_B\gamma_B$ and $\beta_D\gamma_D = \beta_A\gamma_A$ and for the isothermal processes, $\beta_A = \beta_B$ and $\beta_C = \beta_D$. Hence, $\frac{\gamma_D}{\gamma_C} = \frac{\gamma_A}{\gamma_B}$. With (9), we get $\frac{L_C}{L_D} = \frac{L_B}{L_A}$. This yields from (21), the quantum Carnot efficiency

$$\eta_C = 1 - \frac{T_l}{T_h} = 1 - \frac{\beta_h}{\beta_l} \tag{22}$$

which is also the classical Carnot cycle efficiency [11].

4. Quantum Otto Cycle

The classical Otto cycle is illustrated in
Figure 2 with $T_B > T_A > T_C > T_D$. Processes AB and CD are isochoric (constant volume) processes at volumes V_h and V_l respectively with $V_l > V_h$. The heat Q_h enters the system at the process AB while the heat loss of Q_l occurs in the process CD. Processes BC and DA are adiabatic expansion and compression processes respectively.

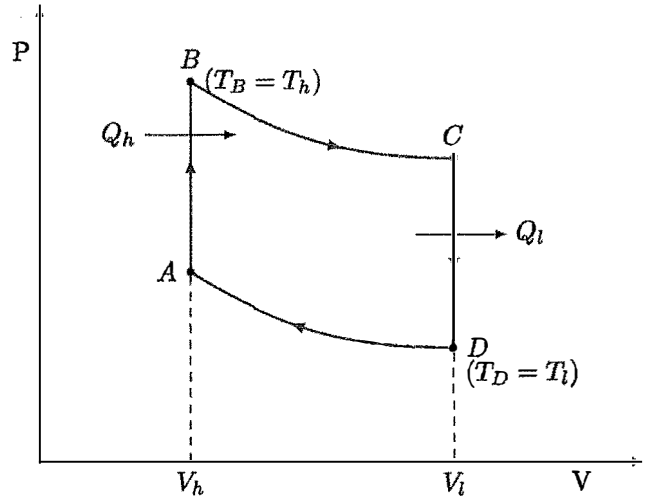

Figure 2: Classical Otto Cycle with $T_B > T_A > T_C > T_D$

The efficiency of a classical Otto engine is $\eta_{\substack{classical \\ Otto}} = 1 - \left(\frac{V_h}{V_l}\right)^{\gamma_A - 1}$ with γ_A is the adiabatic exponent of the ideal gas working substance. In transitioning to the

quantum Otto cycle, we use the equivalent isothermal and adiabatic processes as in the classical Carnot cycle [11].

From (13), let us calculate the efficiency of a quantum Otto cycle involving a particle in an infinite square well. For the isochoric process as in Figure 2, $A \rightarrow B$ (constant length of the ISW), we have (with $\beta_B = \beta_h$, $\beta_D = \beta_l$, $\gamma_B = \gamma_h$ and $\gamma_D = \gamma_l$ as in [11]),

$$Q_{AB} = \frac{1}{2}\left(\frac{1}{\beta_B} - \frac{1}{\beta_A}\right) = \frac{1}{2}\left(\frac{1}{\beta_h} - \frac{1}{\beta_A}\right). \tag{23}$$

With (14),

$$\beta_A\gamma_A = \beta_D\gamma_D = \beta_l\gamma_l. \tag{24}$$

Hence $\beta_A = \frac{\beta_l\gamma_l}{\gamma_A} = \frac{\beta_l\gamma_l}{\gamma_h}$ and (23) becomes $Q_{AB} = \frac{1}{2}\left(\frac{1}{\beta_h} - \frac{\gamma_h}{\beta_l\gamma_l}\right)$ or

$$Q_{AB} = \frac{\gamma_h}{2}\left(\frac{1}{\beta_h\gamma_h} - \frac{1}{\beta_l\gamma_l}\right). \tag{25}$$

Similarly, we can show that for the other isochoric process,

$$Q_{CD} = \frac{\gamma_l}{2}\left(\frac{1}{\beta_l\gamma_l} - \frac{1}{\beta_h\gamma_h}\right). \tag{26}$$

For the adiabatic process $B \rightarrow C$, from (13) and (14), we get $Q_{BC} = \frac{1}{2}\left(\frac{1}{\beta_C} - \frac{1}{\beta_B}\right) - \frac{1}{2k_0}\int_B^C d\gamma = \frac{1}{2}\left(\frac{1}{\beta_C} - \frac{1}{\beta_B}\right) - \frac{1}{2k_0}(\gamma_C - \gamma_B)$. From (14) we can write $\frac{1}{2k_0}(\gamma_C - \gamma_B) = \frac{\gamma_C}{2k_0} - \frac{\gamma_B}{2k_0}$. But for the process $B \rightarrow C$,

$$k_0 = \beta_C\gamma_C = \beta_B\gamma_B = \beta_h\gamma_h. \tag{27}$$

So, $\frac{1}{2k_0}(\gamma_C - \gamma_B) = \frac{\gamma_C}{2\beta_C\gamma_C} - \frac{\gamma_B}{2\beta_B\gamma_B} = \frac{1}{2}\left(\frac{1}{\beta_C} - \frac{1}{\beta_B}\right)$. Hence,

$$Q_{BC} = 0. \tag{28}$$

Similarly, we can show that for the other adiabatic process $D \rightarrow A$, with $\beta_A\gamma_A = \beta_D\gamma_D$

$$Q_{DA} = 0. \tag{29}$$

(25) to (29), agree with [11] with $Q_{AB} = Q_{in}$ and $Q_{CD} = Q_{out}$. Hence from (1), (25) and (26), we get $\eta_O = 1 - \frac{|Q_{out}|}{Q_{in}} = 1 - \frac{|Q_{CD}|}{Q_{AB}} = 1 - \frac{\gamma_l}{\gamma_h}$ and with (9), we get the quantum Otto efficiency

$$\eta_O = 1 - \frac{\gamma_l}{\gamma_h} = 1 - \frac{L_h^2}{L_l^2} \tag{30}$$

as also derived in [11]. We next turn to the calculation of the GUP-corrected efficiencies of the quantum Carnot and Otto cycles using a similar method.

5. GUP-corrected Quantum Heat Engine

The generalized uncertainty principles has been discussed widely in the literature [15-22]. Quantum gravity theories lead to a minimal length scale which can result from a modification of the Heisenberg uncertainty principle $\Delta x \Delta p \geq \frac{\hbar}{2}$ to a generalized uncertainty principle (GUP)

$$\Delta x \Delta p \geq \frac{\hbar}{2} F(\beta_G, \Delta p) \tag{31}$$

[15, 23-26] where $F(\beta_G, \Delta p)$ is some function of the the GUP parameter β_G and the uncertainty in momentum Δp. In [4], we employ a first order approximation of (31)

$$\Delta x \Delta p \geq \frac{\hbar}{2}(1 + \beta_G(\Delta p)^2). \tag{32}$$

A modified momentum-position commutation relations given by $[x, p] = i\hbar(1 + \beta_G p^2)$ replaces $[x_0, p_0] = i\hbar$. The modified commutation relation can be shown to be satisfied by $x = x_0$ and $p = p_0(1 + \beta_G p_0^2)$ with $p_0 = \frac{\hbar}{i}\frac{d}{dx}$. The new operators lead to a GUP-corrected Schrodinger equation, $\left(\frac{p_0^2}{2m} + \frac{\beta_G}{m} p_0^4 + V\right)\psi = E\psi$. From this modified Schrodinger equation the energy eigenvalues of a particle in an infinite square well can be derived and is given by

$$E_n^G = \frac{n^2\pi^2\hbar^2}{2mL^2} + \frac{n^4}{L^4}\frac{\beta_G \pi^4 \hbar^4}{m} \tag{33}$$

for a potential well of width L [4, 16].

In this section, we derive the GUP-corrected Q_{if}^G version of (13). Similar to (3), we can write the GUP-corrected partition function as $Z^G \equiv \sum_{n=1}^{\infty} e^{-\beta E_n^G}$. From (33) the GUP-corrected energy is given by $E_n^G = E_n + \frac{n^4}{L^4}\frac{\beta_G \pi^4 \hbar^4}{m} = E_n(1 + \delta n^2)$ with (using also (9))

$$\delta = \delta(\beta_G, L) = \frac{2\beta_G \pi^2 \hbar^2}{L^2} = 4m\beta_G \gamma \ll 1 \tag{34}$$

with a small GUP parameter β_G. We have $Z^G \equiv \sum_{n=1}^{\infty} e^{-\beta E_n} e^{-\beta E_n \delta n^2} \approx \sum_{n=1}^{\infty} e^{-\beta E_n}(1 - \delta\beta E_n n^2) = \sum_{n=1}^{\infty} e^{-\beta E_n} - \delta\beta \sum_{n=1}^{\infty} E_n n^2 e^{-\beta E_n}$. $Z^G \approx Z - \delta\beta \sum_{n=1}^{\infty} E_n n^2 e^{-\beta E_n}$. From (8) and (9), we have $Z^G \approx Z -$

$\delta\beta\sum_{n=1}^{\infty}\gamma n^2 n^2 e^{-\beta E_n} = Z - \delta\beta\gamma\underbrace{\sum_{n=1}^{\infty} n^4 e^{-\beta\gamma n^2}}_{\approx\int_0^{\infty} dn\, n^4 e^{-\beta\gamma n^2}} \approx Z - \delta\beta\gamma\left(\frac{3\sqrt{\pi}}{8}(\beta\gamma)^{-5/2}\right)$. We used the approximation in (10). With (34), we get

$Z^G \approx Z - 4m\beta_G\gamma\beta\gamma\left(\frac{3\sqrt{\pi}}{8}(\beta\gamma)^{-5/2}\right)$ or

$$Z^G \approx Z - K(\beta^3\gamma)^{-1/2} \tag{35}$$

where

$$K \equiv \frac{3\sqrt{\pi}}{2}\beta_G m. \tag{36}$$

Since $K\sim\beta_G$ and is hence small, we can make the approximation (using also (10)),

$$ln\, Z^G = ln\left(Z\left[1 - \frac{K(\beta^3\gamma)^{-1/2}}{Z}\right]\right) \approx ln\, Z - \frac{2K}{\sqrt{\pi}\beta}. \tag{37}$$

Similar to the calculations in Section 2 above, we then calculate the GUP-corrected free energy F^G, internal energy U^G, entropy S^G and finally the heat Q_{if}^G. We just list them next. Note that the quantities without the superscript "G" are the values without the GUP correction.

$F^G = -\frac{1}{\beta} ln\, Z^G = F + \frac{2K}{\sqrt{\pi}\beta^2}$

$U^G = -\frac{\partial}{\partial\beta} ln\, Z^G = U - \frac{2K}{\sqrt{\pi}\beta^2}$

$S^G = k\beta(U^G - F^G) = S - \frac{4kK}{\sqrt{\pi}\beta}$

What is notable about (37) is that the GUP correction terms are independent of the width of the square well, in agreement to the analogous independence from the volume of an ideal gas in the GUP-corrected thermodynamic quantities in [27]. Similar to (12), we have $dQ^G = \frac{dS^G}{k\beta} = \frac{dS}{k\beta} - \frac{1}{k\beta}d\left(\frac{4kK}{\sqrt{\pi}\beta}\right) = \frac{dS}{k\beta} - \frac{1}{k\beta}d\left(\frac{6\beta_G mk}{\beta}\right)$ so integrating from an initial state i to a final state f, we get $Q_{if}^G = Q_{if} - 6\beta_G m\int_i^f \frac{d(\beta^{-1})}{\beta}$. This yields

$$Q_{if}^G = Q_{if} - \frac{\lambda}{2}\left(\frac{1}{\beta_f^2} - \frac{1}{\beta_i^2}\right),\ \lambda \equiv 6\beta_G m. \tag{38}$$

With Q_{if} given in (13).

6. GUP-corrected Quantum Carnot Cycle

Recall the processes in a Carnot engine: $A \to B$, an isothermal expansion at temperature T_h, $B \to C$, an adiabatic expansion, $C \to D$, an isothermal compression at a lower temperature T_l, and an adiabatic compression, $D \to A$. From (38), for the isothermal processes (equal initial and final temperatures), $Q^G_{AB} = Q_{AB} > 0$ and $Q^G_{CD} = Q_{CD} < 0$. For the corresponding processes, $Q^G_{BC} = -\frac{\lambda}{2}\left(\frac{1}{\beta_C^2} - \frac{1}{\beta_B^2}\right) = \frac{\lambda}{2}\left(\frac{1}{\beta_B^2} - \frac{1}{\beta_C^2}\right) > 0$ since $T_B = T_h > T_C = T_l$. Similarly $Q^G_{DA} = -\frac{\lambda}{2}\left(\frac{1}{\beta_A^2} - \frac{1}{\beta_D^2}\right) < 0$ since $T_A = T_h > T_D = T_l$. With the GUP correction the processes $B \to C$ and $D \to A$ have some heat involved. Hence,

$$Q^G_{in} = Q^G_{AB} + Q^G_{BC} = Q_{AB} + \frac{\lambda}{2}\left(\frac{1}{\beta_h^2} - \frac{1}{\beta_l^2}\right) \tag{39}$$

and

$$Q^G_{out} = Q^G_{CD} + Q^G_{DA} = Q_{CD} - \frac{\lambda}{2}\left(\frac{1}{\beta_h^2} - \frac{1}{\beta_l^2}\right) = -|Q_{CD}| - \frac{\lambda}{2}\left(\frac{1}{\beta_h^2} - \frac{1}{\beta_l^2}\right). \tag{40}$$

From (1),

$$\eta^G_C = 1 - \frac{|Q^G_{out}|}{Q^G_{in}} = 1 - \frac{|Q_{CD}| + \Delta Q}{Q_{AB} + \Delta Q} \tag{41}$$

where we define

$$\Delta Q \equiv \frac{\lambda}{2}\left(\frac{1}{\beta_h^2} - \frac{1}{\beta_l^2}\right) \tag{42}$$

Note that $\Delta Q \ll Q_{if}$ in (38) since $\lambda \sim \beta_G$. In addition, $\Delta Q > 0$ due to (14). Let us manipulate the second term in (41) which has the relatively small quantity ΔQ. $\frac{|Q_{CD}|+\Delta Q}{Q_{AB}+\Delta Q} = \frac{|Q_{CD}|}{Q_{AB}} \frac{\left(1+\frac{\Delta Q}{|Q_{CD}|}\right)}{\left(1+\frac{\Delta Q}{Q_{AB}}\right)} \approx \frac{|Q_{CD}|}{Q_{AB}}\left(1 + \frac{\Delta Q}{|Q_{CD}|}\right)\left(1 - \frac{\Delta Q}{Q_{AB}}\right)$. Expanding this expression to the first order of ΔQ (with $\Delta Q \sim \lambda \sim \beta_G$, (41) becomes $\eta^G_C = 1 - \frac{|Q_{CD}|}{Q_{AB}} - \Delta Q\left(\frac{Q_{AB}-|Q_{CD}|}{Q_{AB}^2}\right)$. With (21), we finally get

$$\eta^G_C = \eta_C - \Delta\eta, \Delta\eta \equiv \frac{\Delta Q}{Q_{AB}}\eta_C. \tag{43}$$

Note that the GUP correction term $\Delta\eta > 0$ since ΔQ and Q_{AB} are both positive as pointed out above. Hence the GUP-corrected quantum Carnot efficiency is less than the non-GUP quantum Carnot efficiency. Let us rewrite (43) in terms of the ratios

of the higher and lower temperatures and highest and lowest lengths. Remember that Q_{AB} is from the non-GUP corrected quantum Carnot process. From (42) and (16), we get

$$\Delta\eta \equiv \frac{\Delta Q}{Q_{AB}}\eta_C = \frac{\frac{\lambda}{2}\left(\frac{1}{\beta_h^2}-\frac{1}{\beta_l^2}\right)}{\frac{1}{2\beta_h}ln\left(\frac{\gamma_A}{\gamma_B}\right)}\eta_C = \frac{\lambda\beta_h\left(\frac{1}{\beta_h^2}-\frac{1}{\beta_l^2}\right)}{ln\left(\frac{\gamma_A}{\gamma_B}\right)}\eta_C. \tag{44}$$

Hence we get

$$\frac{\Delta\eta}{\eta_C} = \frac{\lambda\beta_h\left(\frac{1}{\beta_h^2}-\frac{1}{\beta_l^2}\right)}{ln\left(\frac{\gamma_A}{\gamma_B}\right)} = \lambda k T_h \frac{1-(\beta_h/\beta_l)^2}{ln\left(\frac{\gamma_A}{\gamma_B}\right)} \tag{45}$$

From our discussion in section 3, we have $\beta_C\gamma_C = \beta_B\gamma_B$. Hence we can write $\frac{\gamma_A}{\gamma_B} = \frac{\beta_h}{\beta_l}\frac{\gamma_A}{\gamma_C}$ and (45) becomes

$$\frac{\Delta\eta}{\eta_C} = \lambda k T_h \frac{(1-r^2)}{ln(r\cdot r_L)} \tag{46}$$

with $r \equiv \frac{\beta_h}{\beta_l} = \frac{T_l}{T_h}$ and $r_L \equiv \frac{L_C^2}{L_A^2}$ with $0 < r < 1$ and $r_L > 1$. Note that we wrote the GUP correction term $\frac{\Delta\eta}{\eta_C}$ in (46) in terms of the highest temperature and width (T_h and L_C) and the lowest temperature and width (T_l and L_A). From (46), we plot $f \equiv \frac{\Delta\eta}{\eta_C}\left(\frac{1}{\lambda k T_h}\right)$ in Figure 3 and Figure 4. We only consider the parts in both figures where $f > 0$ since as mentioned above, we expect $\Delta\eta > 0$. In Figure 3 we plot $f(r)$ with $r_L = 2$. As r increases $T_l \to T_h$, $\Delta\eta \to 0$ while decreasing r, or lower T_l, the GUP correction $\Delta\eta$ increases. Since thermal energy decreases, we expect gravitational effects to predominate. In Figure 4, we plot $f(r_L)$ with $r = 0.5$. As r_L increases (maximum width L_C increases), $\Delta\eta \to 0$ while as r_L decreases (maximum width L_C decreases), $\Delta\eta$ increases. This is expected since the effect of the minimal length is more pronounced for decreasing length dimensions. Choosing different values of r_L to plot and $f(r)$ and different values of r to plot $f(r_L)$ give the same behavior as in Figure 3 and Figure 4 respectively.

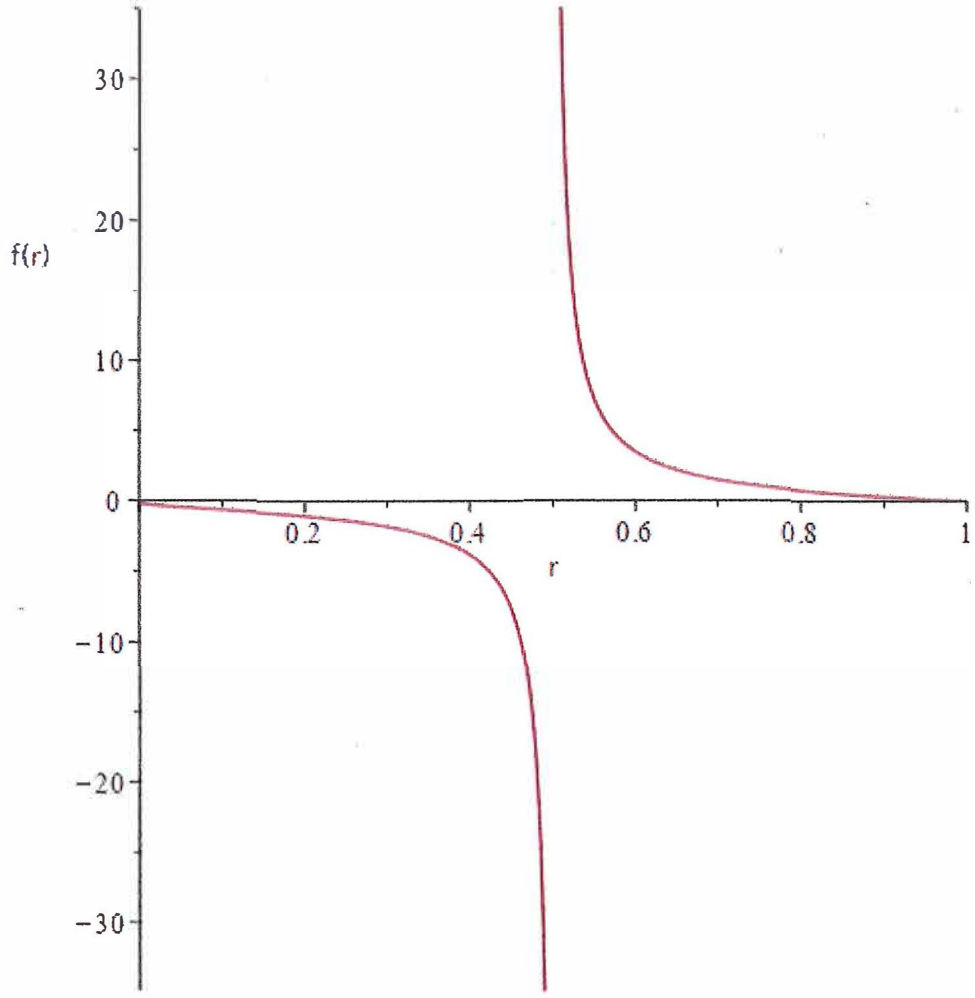

Figure 3 Plot of $f(r)$ with $r_L = 2$.

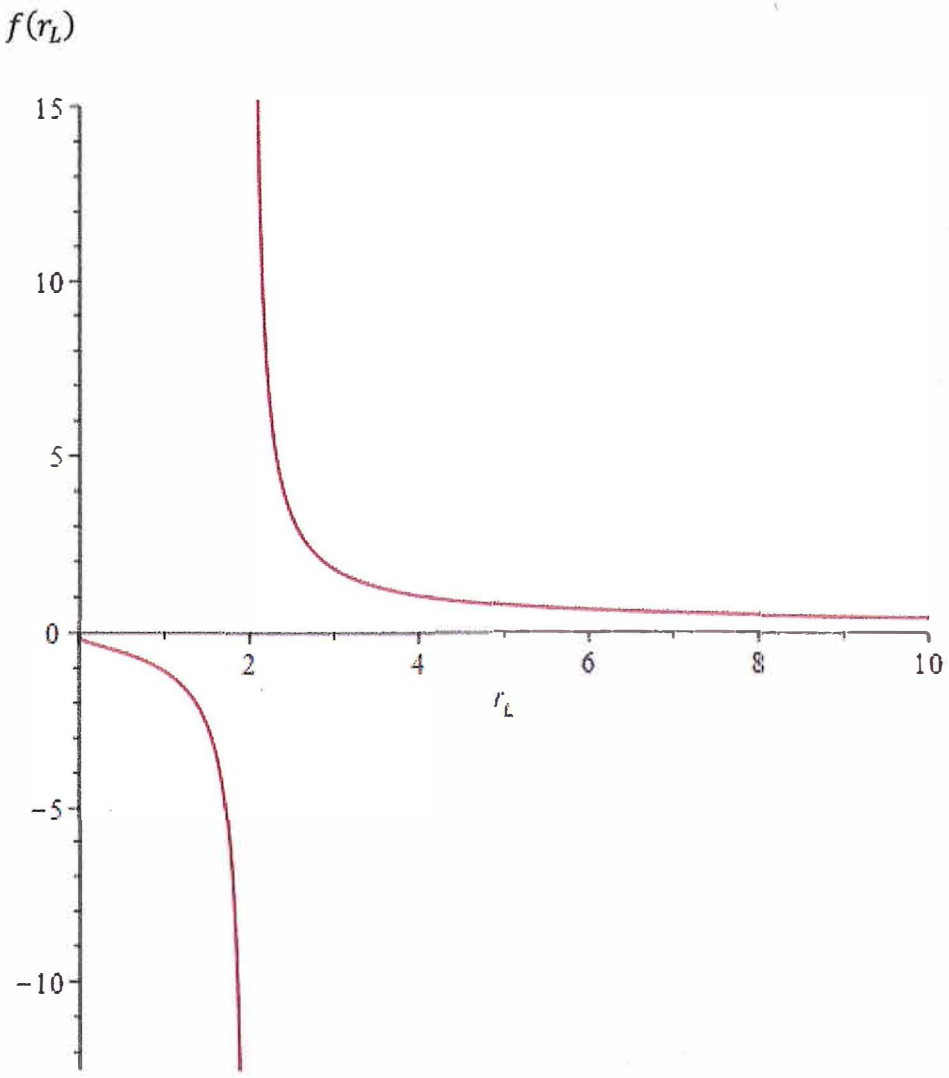

Figure 4 Plot of $f(r_L)$ with $r = 0.5$.

7. GUP-corrected Quantum Otto Cycle

Recall the process in an Otto engine: $A \to B$, an isochoric (constant volume) process, $B \to C$, an adiabatic expansion, $C \to D$, an isochoric (constant volume) process and $D \to A$, an adiabatic compression. As before we use (38) to write down the heat involved. For the isochoric processes $A \to B$, and $C \to D$,

$$Q_{AB}^{G} = Q_{AB} - \frac{\lambda}{2}\left(\frac{1}{\beta_B^2} - \frac{1}{\beta_A^2}\right) \text{ and } Q_{CD}^{G} = Q_{CD} - \frac{\lambda}{2}\left(\frac{1}{\beta_D^2} - \frac{1}{\beta_C^2}\right) \tag{47}$$

respectively. For the corresponding processes $B \to C$ and $D \to A$ yield

$$Q_{BC}^{G} = -\frac{\lambda}{2}\left(\frac{1}{\beta_C^2} - \frac{1}{\beta_B^2}\right) = \frac{\lambda}{2}\left(\frac{1}{\beta_B^2} - \frac{1}{\beta_C^2}\right) \text{ and } Q_{DA}^{G} = -\frac{\lambda}{2}\left(\frac{1}{\beta_A^2} - \frac{1}{\beta_D^2}\right). \tag{48}$$

With the GUP correction the processes $B \to C$ and $D \to A$ have some heat involved. Since $Q_{AB} > 0$ and $Q_{CD} < 0$, we expect $Q_{AB}^{G} > 0$ and $Q_{CD}^{G} < 0$ since the GUP-correction is $\frac{\lambda}{2}\left(\frac{1}{\beta_f^2} - \frac{1}{\beta_i^2}\right)$ is smaller than Q_{if}. $Q_{BC}^{G} > 0$ and $Q_{DA}^{G} < 0$ since $T_B > T_C$ and $T_A > T_D$ respectively as noted in Figure 2. Hence from (47) and (48)

$$\begin{aligned} Q_{in}^{G} = Q_{AB}^{G} + Q_{BC}^{G} &= Q_{AB} - \frac{\lambda}{2}\left(\frac{1}{\beta_B^2} - \frac{1}{\beta_A^2}\right) + \frac{\lambda}{2}\left(\frac{1}{\beta_B^2} - \frac{1}{\beta_C^2}\right) \\ &= Q_{AB} + \frac{\lambda}{2}\left(\frac{1}{\beta_A^2} - \frac{1}{\beta_C^2}\right) \end{aligned} \tag{49}$$

and

$$\begin{aligned} Q_{out}^{G} = Q_{CD}^{G} + Q_{DA}^{G} &= Q_{CD} - \frac{\lambda}{2}\left(\frac{1}{\beta_D^2} - \frac{1}{\beta_C^2}\right) - \frac{\lambda}{2}\left(\frac{1}{\beta_A^2} - \frac{1}{\beta_D^2}\right) \\ &= Q_{CD} + \frac{\lambda}{2}\left(\frac{1}{\beta_C^2} - \frac{1}{\beta_A^2}\right) = -|Q_{CD}| + \frac{\lambda}{2}\left(\frac{1}{\beta_C^2} - \frac{1}{\beta_A^2}\right). \end{aligned} \tag{50}$$

Putting (49) and (50) into (1), we get $\eta_O^G = \frac{Q_{AB} + \frac{\lambda}{2}\left(\frac{1}{\beta_A^2} - \frac{1}{\beta_C^2}\right) - \left(|Q_{CD}| - \frac{\lambda}{2}\left(\frac{1}{\beta_C^2} - \frac{1}{\beta_A^2}\right)\right)}{Q_{in}^{G}} = \frac{W}{Q_{in}^{G}}$ with W as the non-GUP work involved. Manipulating η_O^G with (49), we get $\eta_O^G = \frac{W}{Q_{AB} + \Delta Q_{AB}} = \frac{W}{Q_{AB}} \frac{1}{1 + \frac{\Delta Q_{AB}}{Q_{AB}}} \approx \frac{W}{Q_{AB}}\left(1 - \frac{\Delta Q_{AB}}{Q_{AB}}\right)$ where

$$\Delta Q_{AB} \equiv \frac{\lambda}{2}\left(\frac{1}{\beta_A^2} - \frac{1}{\beta_C^2}\right). \tag{51}$$

Finally, $\eta_O^G = \eta_O - \frac{W \Delta Q_{AB}}{Q_{AB}^2}$ or

$$\eta_O^G = \eta_O - \Delta\eta_O,\ \Delta\eta_O \equiv \frac{W\Delta Q_{AB}}{Q_{AB}^2} \tag{52}$$

with $\Delta\eta_O$ as the GUP correction. It is clear that $\Delta\eta_O > 0$ since W and ΔQ_{AB} are both positive. Hence the GUP-corrected quantum Otto efficiency is less than the non-GUP quantum Otto efficiency.

Similar to the GUP-corrected Carnot cycle let us look at $\frac{\Delta\eta_O}{\eta_O}$. From (25) and (26),

$$W = Q_{AB} - |Q_{CD}| = \left(\frac{\gamma_h - \gamma_l}{2}\right)\left(\frac{1}{\beta_h\gamma_h} - \frac{1}{\beta_l\gamma_l}\right). \tag{53}$$

Putting (53), (51), and (25) into $\Delta\eta_O$ of (52), and with (30), we get

$$\frac{\Delta\eta_O}{\eta_O} = \lambda\beta_h\left(\frac{1}{\beta_A^2} - \frac{1}{\beta_C^2}\right)\frac{1}{1-r_L^O r} \text{ where } r_L^O \equiv \frac{\gamma_h}{\gamma_l} = \frac{L_l^2}{L_h^2} \text{ and } r \equiv \frac{\beta_h}{\beta_l} = \frac{T_l}{T_h} \tag{54}$$

with $r_L^O > 1$ and $0 < r < 1$. Since processes BC and DA are not adiabatic when we put in the GUP correction (see (48)), (9) does not apply and we cannot relate β_A to $\beta_D = \beta_l$ and β_C to $\beta_B = \beta_h$. To facilitate an analysis like section 0 above, let us assume that similar to the relations in (24) and (27), we can write generally

$$\beta_A = f_{AD}\beta_D = f_{AD}\beta_l \text{ and } \beta_C = f_{CB}\beta_B = f_{CB}\beta_h \tag{55}$$

With $f_{AD} < 1$ and $f_{CB} > 1$ since $T_D < T_A$ and $T_B > T_C$ as noted in Figure 2. For the non-GUP case in (24) and (27), $f_{AD} = \frac{\gamma_l}{\gamma_h}$ since $\gamma_A = \gamma_B = \gamma_h$, $f_{CB} = \frac{\gamma_h}{\gamma_l}$ since $\gamma_C = \gamma_D = \gamma_l$ for the isochoric processes AB and CD. Putting (55) into (54), we get

$$\frac{\Delta\eta_O}{\eta_O} = \lambda\frac{\beta_h}{\beta_A^2}\left(1 - \frac{f_{AD}^2}{f_{CB}^2}\cdot\frac{1}{r}\right)\left(\frac{1}{1-r_L^O r}\right). \tag{56}$$

In Figure 5, we plot (56) $f_{GUP}^O(r) \equiv \frac{\Delta\eta_O}{\eta_O}\cdot\frac{\beta_A^2}{\lambda\beta_h}$, with $f_{AD} = 0.5, f_{CB} = 2$, and $r_L^O = 5$. We only consider the region where $f_{GUP}^O(r) > 0$ since as noted above $\Delta\eta_O > 0$. We consider the region $0.2 < r < 0.25$. The lower the value of $r \equiv \frac{T_l}{T_h}$, (lower value of T_l) the higher the value of $\frac{\Delta\eta_O}{\eta_O}$. In Figure 6 we plot $f_{GUP}^O(r_L^O)$ with $f_{AD} = 0.5, f_{CB} = 2$, and $r = 0.1$. Just as before we only consider the region where $f_{GUP}^O(r_L^O) > 0$ since as noted above $\Delta\eta_O > 0$. We consider the region $r_L^O > 10$. As r_L^O increases (maximum width L_C increases), $\Delta\eta_O \to 0$ while as r_L^O decreases (maximum width L_C decreases), $\Delta\eta_O$ increases. Both cases exhibit a similar behavior as the GUP-corrected Carnot engine. One can show generally that these behavior in Figure 5 and Figure 6 occur when $\frac{1}{r_L^O} < r < \frac{f_{AD}}{f_{CB}}$.

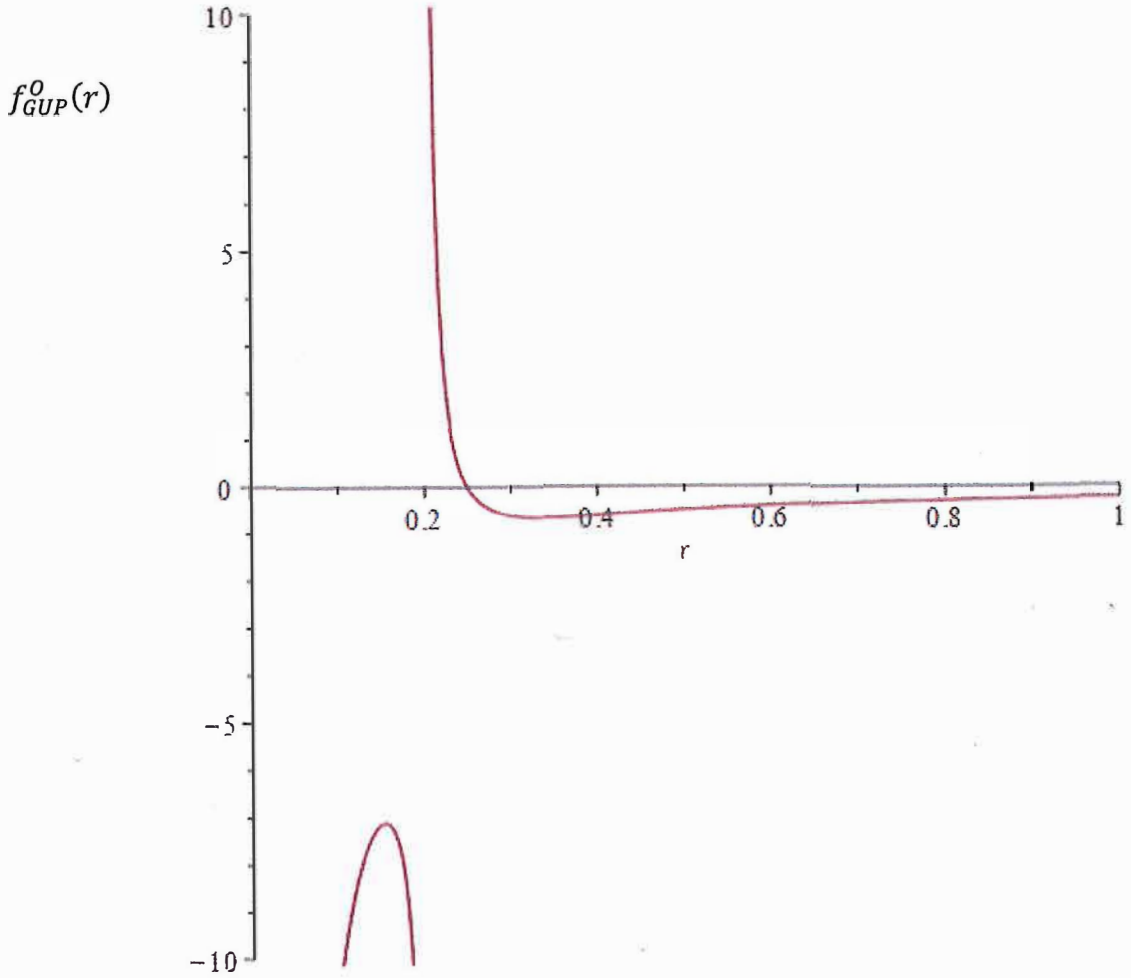

Figure 5 Plot of $f_{GUP}^{O}(r)$, with $f_{AD} = 0.5, f_{CB} = 2$, and $r_L^O = 5$.

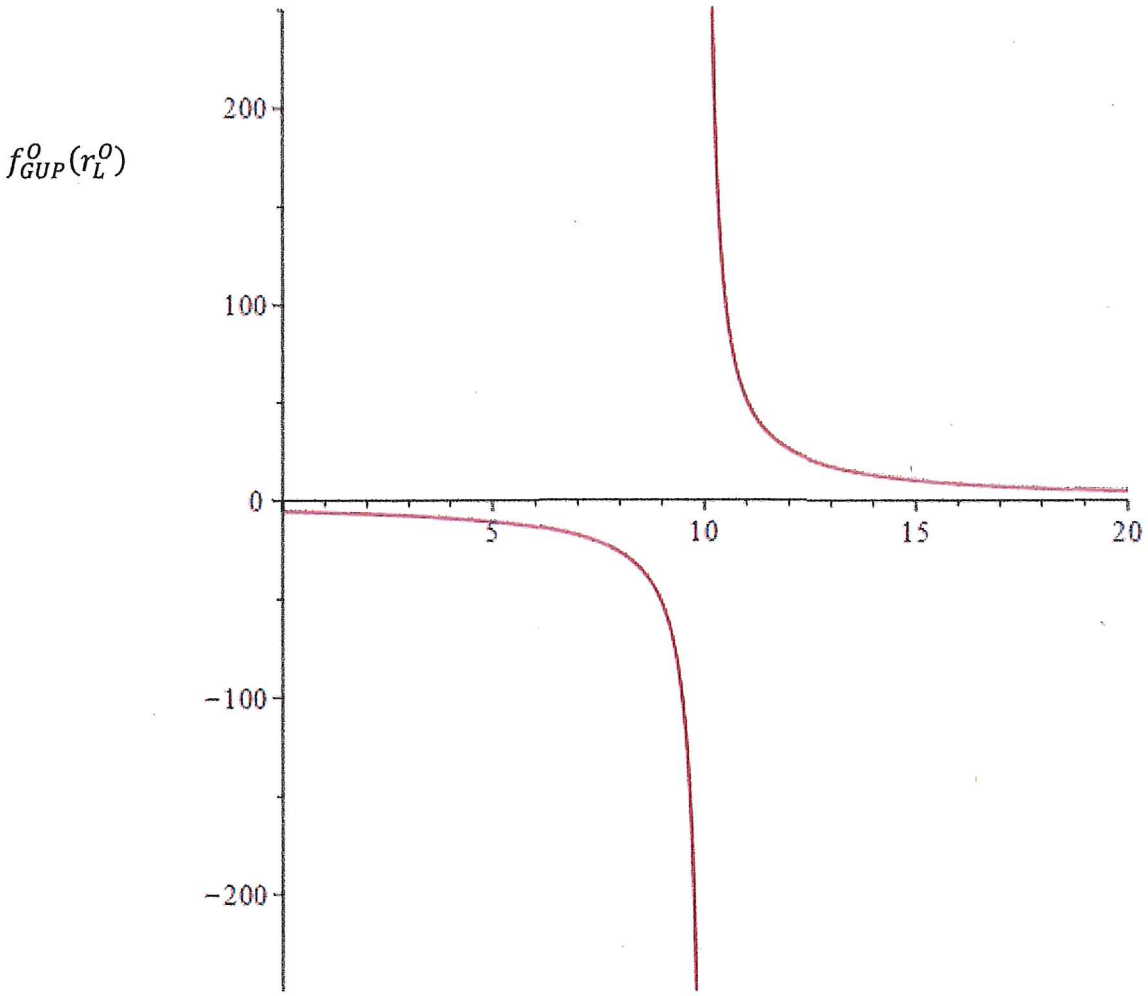

Figure 6 Plot of $f_{GUP}^{O}(r_L^O)$ with $f_{AD} = 0.5, f_{CB} = 2$, and $r = 0.1$

8. Conclusions

We analyzed the two most commonly studied heat engines in physics namely the Carnot and Otto engines. Following the approach of [11] and [12], we calculated the heats involved in the quantum Carnot and Otto cycles and the corresponding GUP-corrected quantum cycles using the partition function of the working substance namely a particle in an infinite square well in thermal equilibrium with a heat bath. Similar to the results of [27], the GUP correction to the entropy (and consequently to the heat energy) is independent of the dimension of the container (in our case the dimension of the well). In both cases the work = heat input minus |heat output| do not change with the GUP correction since the GUP-corrected heat is independent of the width of the well (see (38)). The adiabatic processes in both the Carnot and Otto cycles cease to be adiabatic in the GUP-corrected cases. This behavior is expected since the introduction of the GUP correction term in the Hamiltonian of the Schrodinger equation alters the energy of the working substance. A similar behavior is observed in [12] where an additional interaction term was introduced in the Hamiltonian. The GUP correction lowers the efficiency of the quantum heat engines discussed. In this paper (due to a GUP correction) and in [12], (due to an interaction term) we have an additive correction term in the Hamiltonian of the Schrodinger equation. In both cases the correction term resulted in a decrease in the efficiency. For both the Carnot and Otto engines, the GUP effects increase as the temperature of the cold heat bath decreases and as the width of the potential well decreases.

With the general GUP-corrected heat energy calculated in (38) with a particle in an infinite square well as the working substance, we can explore the GUP-correction in other heat engines such as the Szilard engine. It will also be interesting to study the GUP-correction using different working substances such as a two-level system and a harmonic oscillator.

Acknowledgements:

The authors would like to thank Jonathan Marcel and Sydney Carr for their participation at the beginning of this research project.

References:

[1] R. M. Santilli, Generalization of Heisenberg's uncertainty principle for strong interactions. Hadronic Journal 4 (1981) 642-663 (1981)
[2] R. M. Santilli, Isorepresentation of the Lie-isotopic SU(2) Algebra with Application to Nuclear Physics and Local Realism. Acta Applicandae Mathematicae 50 (1998) 177-190
[3] R. M. Santilli, Studies on the classical determinism predicted by A. Einstein, B. Podolsky and N.Rosen. Ratio Mathematica 37 (2019) 5-23
[4] G. Blado, C. Owens and V. Meyers, Quantum wells and the generalized uncertainty Principle. Eur. J. Phys. 35 (2014) 065011
[5] G. Blado, T. Prescott, J. Jennings, J. Ceyanes and R Sepulveda, Effects of the Generalized Uncertainty Principle on Quantum Tunneling. Eur. J. Phys. 37 (2016) 025401
[6] M. Sprenger, P. Nicolini and M. Bleicher, An Introduction to Minimal Length Phenomenology. Eur. J. Phys. 33 (2012) 853-862
[7] A. F. Ali, S. Das and E. C. Vagenas, A Proposal for Testing Quantum Gravity in the Lab. Phys. Rev. D 84 (2011) 044013
[8] M. F. Gusson, A. O. O. Gonçalves, R. O. Francisco, R. G. Furtado, J. C. Fabris and J. A. Nogueira, Dirac δ-function potential in quasiposition representation of a minimal-length scenario. Eur. Phys. J. C 78 (2018), 179
[9] S. Benczik, L. N. Chang, D. Minic and T. Tekeuchi, Hydrogen-atom spectrum under a minimal-length hypothesis. Phys. Rev. A 72 (2005) 012104
[10] F. Brau, Minimal length uncertainty relation and the hydrogen atom. J. Phys. A: Math. Gen. 32 (1999) 7691
[11] H. T. Quan, Yu-Xi Liu, C. P. Sun and F. Nori, Quantum Thermodynamic Cycles and Quantum Heat Engines. Phys. Rev. E 76 (2007) 031105
[12] M. Ramezani and M. Golshani, On the Efficiency of a Quantum Heat Engine. arXiv: 1708.00263v1 [quant-ph] (2017)
M. Ramezani, S. Marcantoni, F. Benatti, R. Floreanini, F. Petiziol, A. T. Rezakhani and M. Golshani, Impact of nonideal cycles on the efficiency of quantum heat engines. Eur. Phys. J. D 73 (2019) 144
[13] D. V. Schroeder, *An Introduction to Thermal Physics,* Addison Wesley Longman (2000)
[14] D. J. Griffiths, *Introduction to Quantum Mechanics,* Prentice-Hall, Englewood Cliffs, NJ (2005)

[15] A. Kempf, G. Mangano and R. B. Mann, Hilbert space representation of the minimal length uncertainty relations. Phys. Rev. D 52 (1995) 1108-1118
[16] K. Nozari and T. Azizi, Some aspects of minimal length quantum mechanics. Gen. Relativ. Gravit. 38 (2006) 735–742
[17] S. Hossenfelder, Minimal length scale scenarios for quantum gravity. Living Rev. Relativ. 16 (2013) 2-90
[18] L. J. Garay, Quantum gravity and minimal length. Int. J. Mod. Phys. A. 10 (1995) 145-165
[19] A. F. Ali, S. Das and E. C. Vagenas, Discreteness of space from the generalized uncertainty principle. Phys. Lett. B 678 (2009) 497– 499
[20] L. Petruzziello, Generalized uncertainty principle with maximal observable momentum and no minimal length indeterminacy. Class. Quantum Grav. 38 (2021) 135005
[21] A. N. Tawfik and A. M. Diab, A review of the generalized uncertainty principle. Rep. Prog. Phys. 78 (2015) 126001
[22] S. Das, E. C. Vagenas, Phenomenological implications of the generalized uncertainty principle. Can. J. Phys. 87 (2009) 233–240
[23] K. Nouicer, Quantum-corrected black hole thermodynamics to all orders in the Planck length. Phys. Lett. B 646 (2007) 63-71
[24] P. Pedram, A higher order GUP with minimal length uncertainty and maximal momentum. Phys. Lett. B 714 (2012) 317-323
P. Pedram, A higher order GUP with minimal length uncertainty and maximal momentum II: Applications. Phys. Lett. B 718 (2012) 638-645
[25] W. S. Chung and H. Hassanabadi, A new higher order GUP: one dimensional quantum system. Eur. Phys. J. C 79 (2019) 213
H. Hassanabadi, E. Maghsoodi and W. S. Chung, Analysis of black hole thermodynamics with a new higher order generalized uncertainty principle. Eur. Phys. J. C 79 (2019) 358
[26] H. Shababi and W. S. Chung, A new type of GUP with commuting coordinates. Mod. Phys. Lett. A 35 (2019) 2050018
[27] A. F. Ali and M. Moussa, Towards Thermodynamics with Generalized Uncertainty Principle. Advances in High Energy Physics 2014 (2014) 629148